Device physics of white polymer light-emitting diodes

Nicolai, Herman Theunis

Device Physics of White Polymer Light-Emitting Diodes

Herman Theunis Nicolai

Device Physics of White Polymer Light-Emitting Diodes

Herman Theunis Nicolai
PhD. thesis
University of Groningen

Zernike Institute PhD thesis series 2012-07
ISSN: 1570-1530
ISBN: 978-90-367-5397-5 (Printed version)
978-90-367-5398-2 (Electronic version)

The research presented in this thesis was performed in the research group Molecular Electronics of the Zernike Institute for Advanced Materials at the University of Groningen, The Netherlands. This work was funded by the European Commission under project IST-004607 (OLLA) and FP7-213708 (AEVIOM).

university of groningen / faculty of mathematics and natural sciences / zernike institute for advanced materials

RIJKSUNIVERSITEIT GRONINGEN

Device Physics of White Polymer Light-Emitting Diodes

Proefschrift

ter verkrijging van het doctoraat in de
Wiskunde en Natuurwetenschappen
aan de Rijksuniversiteit Groningen
op gezag van de
Rector Magnificus, dr. E. Sterken,
in het openbaar te verdedigen op
vrijdag 30 maart 2012
om 16.15 uur

door

Herman Theunis Nicolai

geboren op 21 juli 1980
te Meppel

Promotor:	Prof. dr. ir. P. W. M. Blom
Beoordelingscommissie:	Prof. dr. R. Coehoorn
	Prof. dr. D. M. de Leeuw
	Prof. dr. D. Neher

Dedicated to

My parents

and to the memory of

Bert de Boer

Contents

1 | Motivation

The availability of artificial light is an acquired convenience that has become essential for modern society. The increased awareness of our energy consumption and its environmental impact incites the study of more energy efficient light sources. This thesis describes the operation of a potential future light source: the white polymer light-emitting diode. This chapter serves as a motivation for the research presented in this thesis. First a brief history of artificial lighting is presented. Subsequently, the drawbacks and upcoming challenges associated with energy consumption are discussed. Finally an overview of emerging lighting technologies will be provided.

1.1 Artificial Lighting

> "*Viewed from the standpoint of civilization, the discovery of fire was one of the greatest strides along the highway of human progress. The activities of man were no longer bounded by sunrise and sunset. The march of civilization had begun.*" [1]

Nowadays, we take the ability to light up a room with the single press of a button for granted. The obviousness of lighting makes it easy to forget the profound impact of lighting on our society. Lighting has freed mankind from the constraints of nature and extended our usable time beyond sunrise and sunset. The availability of lighting promotes literacy and education and is therefore a key component in the progress of mankind.[1,2]

After primitive light sources which relied on fire, such as candles, oil lamps and gas lamps, the first form of electric lighting was the carbon arc light developed in the 19th century. The arc light relies on the ionization of air between two carbon electrodes, producing a very bright plasma. This principle was already demonstrated by Sir Humphry David and Vasilii Petrov in the early 19th century,[3] however, due to a lack of suitable power sources, carbon arc lights were only generally used at the end of the 19th century, and due to their high brightness mainly used for street lighting and projectors. A more convenient light source arrived in the form of the now ubiquitous light bulb. Although commonly attributed to Thomas Edison, the light bulb was actually developed stepwise by multiple inventors, each building on the work of others. At the time the first patent was awarded to Edison, Joseph Swan had already demonstrated a working light bulb with a carbonized filament and a partial vacuum and he had obtained a patent in the U.K.[4,5] Edison is generally credited with improving the design of the light bulb and with the subsequent commercialization.

The working principle of the light bulb is that of incandescence; the emission of light due to its elevated temperature. In a light bulb a thin filament is heated till the point of incandescence by passing an electric current through it. Although the light bulb is now in use for more than a century, its potential was not immediately apparent. Prof. Silvanus P. Thompson reportedly stated after the demonstration of the first light bulb: "*I think that any system of electric lighting depending on incandescence will utterly fail from an economic point of view (...).*"[2,6] Quite the reverse, the incandescent light bulb is now in use for more than 125 years, in which only few improvements were made. The most important modifications were the utilization of a tungsten filament and the replacement of the vacuum with an inert gas. The basic design of the light bulb remained the same over the years, as can be observed, for example, in Figure 1.1. Also the efficiency of the light bulb hardly improved in the past century as demonstrated in Table 1.1. Although relatively cheap to fabricate, the incandescent light bulb has a rather poor efficiency. Approximately 95% of the consumed energy is not converted into light but into heat,[5] which is in most cases an energy loss. It is hard to think of any other technology still in use today which exhibits such a poor efficiency.

Figure 1.1. An employee of the U.S. National Bureau of Standards tests an incandescent light bulb in an integrating sphere (1938). Obtained from Ref. 7.

1.2 The Energy Crisis

There is a by now a broad scientific consensus that energy consumption by the burning of fossil fuels affects the global climate.[8] Already more than 100 years ago Svante Arrhenius proposed that changes in the CO_2 concentration in the atmosphere could have an influence on the temperature at the surface of the Earth.[9] He also predicted that the emissions from burning fossil fuels would be substantial enough to influence the climate on Earth. Although, in a later publication Arrhenius speculated that a warming planet might actually be beneficial for mankind as it might prevent or delay a possible new ice age and would allow for a higher food production required to feed a growing population.[10] Arrhenius predicted that a doubling of the CO_2 concentration in the air would result in a temperature increase of 5 °C to 6 °C. More than a century later, the Intergovernmental Panel on Climate Change (IPCC) reported in its 2007 assessment report an estimate for the temperature increase of approximately 3 °C for a doubling of the CO_2 concentration.[8] Figure 1.2 shows the CO_2 concentration in the atmosphere over a period of more than 1000 years. A dramatic increase is observed from 1800, approximately the onset of the industrial revolution. To limit the harmful effects of the consequential temperature increase, a severe reduction of CO_2 emission would be required. Energy generation by the burning of fossil fuels accounts for three quarters of the global emission of CO_2 and other greenhouse gasses.[11]

If the threat of global warming alone would not be enough, there are other negative consequences associated with our dependence on fossil fuels. Most of the proven oil and gas reserves are located in countries that have a poor state of democracy.[12,13] and it has even been proposed that high oil exports hamper the development of democracy in those nations.[14,15] Furthermore, the dependence on a few resource rich countries, jeopardizes the security of supply of the importing

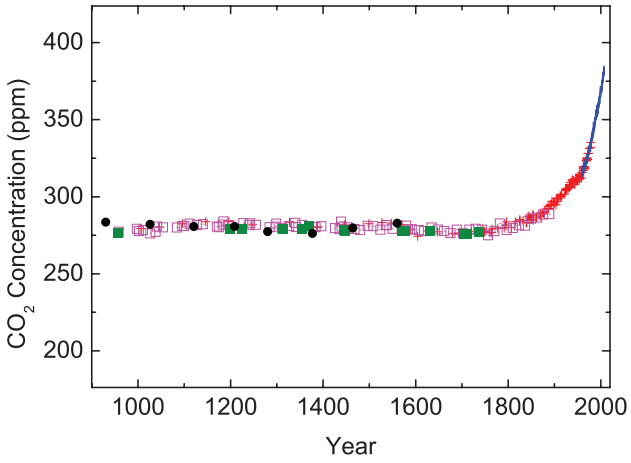

Figure 1.2. The CO_2 concentration in the Earth's atmosphere spanning a period of more than 1000 years. Adapted from Ref. 11.

countries. This makes the dependence on fossil fuels not only an environmental issue, but also an issue with strategic implications.

Finally, next to the adverse consequences of using fossil fuels, they are simply a finite resource and the amount of easy accessible fossil fuels may well become depleted in our lifetime.[16] There is therefore sufficient motivation to reduce our dependence on fossil fuels and move towards sustainable energy sources. However, as a large part of the world population aspires to improve its standard of living, the global energy demand is more likely to increase than to decrease. The global energy demand is projected to increase by 1.4% per year till 2035.[17] It will be a formidable challenge to fulfill the global energy demand with renewable energy sources.[11] If we would have any hope of becoming independent of fossil fuels, it would also require a drastic reduction of our energy consumption. Grid-based electric lighting accounts for approximately 19% of the global electricity consumption and 30% of that energy is consumed by conventional incandescent light bulbs.[18] Considering the low efficiency of incandescent light bulbs, it is evident that there is the potential for a substantial energy saving by switching to more energy efficient lighting solutions.

1.3 Solid State Lighting

Alternatives to the light bulb have already been available for many years. In 1937 General Electric demonstrated the first fluorescent tube. The operation mechanism of a fluorescent tube is actually similar to that of the carbon arc. In a fluorescent tube an electric current is passed through an inert gas containing a small amount of mercury. The electric current excites the mercury which consequently emits ultraviolet light. This light is then converted to light in the visible spectrum by phosphors that are coated on the surface of the fluorescent tube. The emission from

the phosphors is typically very narrow and accordingly the mixture of phosphors has to be selected with care so that the output spectrum appears as white. The quality of a light source is specified by the color rendering index (CRI) which is a measure of how well a light source reproduces the colors of objects. Especially cheap fluorescent tubes exhibit a poor CRI due to the narrow emission of the phosphors. The efficiency of fluorescent tubes is very high compared to incandescent light and they are therefore widely adopted in the workplace, but due to their size restraints, and the typical low CRI, they are rarely used in residential settings. Since a few decades compact fluorescent lamps (CFL) are marketed, which are essentially fluorescent tubes in the form factor of a light bulb. Their efficiency is typically lower than that of the fluorescent tube, albeit still much higher than that of the light bulb. Only due to the higher initial purchase price, it still has not been able to fully replace the incandescent light bulb. Finally, fluorescent lamps have a very important environmental drawback; the mercury contained in the lamps is very toxic which is released in the environment if it is not properly disposed of.

A new research field has emerged in the past decades; called solid-state lighting (SSL).[5,19] In this field light is generated by semiconductor light-emitting diodes (LEDs) through the process of electroluminescence. The first LED emitting visible light was demonstrated in 1962,[20] and since then the technology has evolved rapidly. LEDs have long been used as indicator lights in electronic circuits. However, the lack of an efficient blue emitting material impeded the development of white emitting LEDs. Only in 1993 the first practical blue emitting LED was demonstrated by Shuji Nakamura,[21,22] paving the way for the development of white emitting LEDs. Nowadays, the efficiencies of white inorganic LEDs have matched the efficiency of fluorescent lighting although the initial purchase cost of inorganic LEDs is still higher than that of a CFL. The lifetime of inorganic LEDs though

Year	Type of light source	Luminous efficacy (lm/W)	Ref.
∼1900	Carbon arc	8	1
1880	Carbon filament (vacuum) light bulb	3	1
1906	Tungsten filament (vacuum) light bulb	8	1
1926	Tungsten (gas) bulb	11	2
2007	Tungsten (gas) Light bulb	15	5
2007	Fluorescent tube	80	5
2007	Compact Fluorescent lamp	60	5
2007	Inorganic LED	100–150	5
2009	Organic Small Molecule LED (OLED)	90	30
2009	Polymer light-emitting diode (PLED)	11	31

Table 1.1. Comparison of the luminous efficacy of different light sources from past and present. The values reported here should only be considered as an indication. For a full evaluation of the device performance also the driving condition, brightness, CRI and lifetime should be considered. It should also be noted that the reported values of OLEDs and PLEDs concern lab efficacies and are not those of final products. For a more comprehensive review of OLED efficacies, see Ref. 27.

is far superior to that of fluorescent lighting, without being accompanied with the drawback of the hazardous mercury. LEDs are therefore often promoted as the next generation lighting solution.

A special class of LEDs is the organic LED (OLED). In these devices the active layer consists of an organic material with semiconducting properties.[23–27] Whereas inorganic semiconductors such as silicon and gallium arsenide are crystalline materials, organic semiconductors have a disordered structure. OLEDs are therefore relatively easy to fabricate and hold the promise of enabling inexpensive large area devices. The research field of OLEDs is relatively new, and so far OLEDs have not been able to match the efficiencies of inorganic LEDs. They hold, however, an important advantage over inorganic LEDs. Inorganic LEDs are fabricated from single crystal semiconductors, which are difficult to fabricate on a large area. Thus, like the light bulb and compact fluorescent lamps, inorganic LEDs are point light sources and they require luminaires to diffuse the light, which greatly reduces the effective efficiency. In contrast, OLEDs are fabricated by thermal evaporation or solution processing which enables the fabrication of large area devices. Accordingly, OLEDs are envisaged as large area light sources that should be compared with complete luminaires rather than with the constituent light source. Furthermore, since OLEDs are broadband emitters, they generally exhibit a very good CRI, which is not the case for cheap inorganic LEDs.

Organic LEDs can be divided in two categories, based on the material used in the active layer. The highest efficiencies of OLEDs so far have been achieved with low molecular weight materials. These small molecule OLEDs are fabricated via evaporation under high vacuum. This thesis deals with the device operation of white polymer light-emitting diodes (PLEDs).[28,29] In these devices the active layer consists of a semiconducting polymer. These materials cannot be evaporated, but instead they can be tuned to be soluble, which enables solution processing techniques.

White OLEDs require the simultaneous emission of two or three colors so that the output is observed as white. In evaporated OLEDs this can be achieved by the fabrication of multilayer devices where each layer emits a specific color. However, multilayer devices are difficult to process from solution and white PLEDs are therefore generally fabricated differently. This thesis describes the device operation of white PLEDs that are based on a single layer of a white-emitting copolymer. In such a PLED the emission of several colors takes place in a single layer, which severely complicates the understanding of the device operation. In the following chapters a description of the white PLED is developed by the stepwise investigation of the blue backbone polymer, and the influence of the green and red dyes. As a start, the next chapter provides an introduction to organic semiconductors and polymer light-emitting diodes. The charge transport in disordered organic semiconductors is treated and the details of the fabrication of the devices discussed in this work are presented. Finally, the different approaches to achieve white light emission will be discussed.

References

1. M. Luckiesh, *Artificial Light, Its Influence upon Civilization* (The Century Co., New York, 1920).
2. M. Luckiesh, *Ind. Eng. Chem.* **18**, 920 (1926).
3. A. Anders, *IEEE Trans. Plasma Sci.* **31**, 1060 (2003).
4. J. W. Swan, *Nature* **21**, 202 (1880).
5. C. J. Humphreys, *MRS Bull.* **33**, 459 (2008).
6. F. W. Smith, *Electrical World* **80**, 555 (1922).
7. `http://www.shorpy.com/node/7960`.
8. Intergovernmental Panel on Climate Change, *Climate Change 2007: The Physical Science Basis* (Cambridge University Press, Cambridge, 2007).
9. S. Arrhenius, *Philos. Mag. S. 5* **41**, 237 (1896).
10. S. Arrhenius, *Worlds in the Making: The Evolution of the Universe* (Harper, New York, 1908).
11. D. J. C. MacKay, *Sustainable Energy - Without the Hot Air* (UIT, Cambridge, 2008).
12. World Energy Council, *2010 Survey of Energy Resources* (WEC, London, 2010).
13. Economist Intelligence Unit, *Democracy Index 2010* (EIU 2010).
14. M. L. Ross, *World Politics* **53**, 325 (2001).
15. T. L. Friedman, *Foreign Policy* **154**, 28 (2006).
16. J. Murray and D. King, *Nature* **481**, 433 (2012).
17. International Energy Agency, *World Energy Outlook 2010* (OECD Publishing 2010).
18. International Energy Agency, *Light's Labour's Lost: Policies for Energy-efficient Lighting* (OECD Publishing, 2006).
19. R. Stevenson, *IEEE Spectrum* **46**, 26 (2009).
20. N. Holonyak and S. F. Bevacqua, *Appl. Phys. Lett.* **1**, 82 (1962).
21. S. Nakamura, T. Mukai, and M. Senoh, *Appl. Phys. Lett.* **64**, 1687 (1994).
22. F. A. Ponce and D. P. Bour, *Nature* **386**, 351 (1997).
23. J. R. Sheats, H. Antoniadis, M. Hueschen, W. Leonard, J. Miller, R. Moon, D. Roitman, and A. Stocking, *Science* **273**, 884 (1996).

24. B. W. D'Andrade and S. R. Forrest, *Adv. Mater.* **16**, 1585 (2004).

25. A. Misra, P. Kumar, M. N. Kamalasanan, and S. Chandra, *Semicond. Sci. Technol.* **21**, R35 (2006).

26. K. T. Kamtekar, A. P. Monkman, and M. R. Bryce, *Adv. Mater.* **22**, 572 (2010).

27. M. C. Gather, A. Köhnen, and K. Meerholz, *Adv. Mater.* **23**, 233 (2011).

28. R. H. Friend, R. W. Gymer, A. B. Holmes, J. H. Burroughes, R. N. Marks, C. Taliani, D. D. C. Bradley, D. A. Dos Santos, J. L. Brédas, M. Lögdlund, and W. R. Salaneck, *Nature* **397**, 121 (1999).

29. I. U. H. Raja, J. Y. Lee, I. T. Kim, and S. H. Lee, *Monatsh. Chem.* **139**, 725 (2008).

30. S. Reineke, F. Lindner, G. Schwartz, N. Seidler, K. Walzer, B. Lüssem, and K. Leo, *Nature* **459**, 234 (2009).

31. B. Zhang, C. Qin, J. Ding, L. Chen, Z. Xie, Y. Cheng, and L. Wang, *Adv. Funct. Mater.* **20**, 2951 (2010).

2 | Introduction

This chapter provides an introduction into the device physics of polymer light-emitting diodes. The physics of organic semiconductors will be described and the difference between organic and inorganic semiconductors will be highlighted. The device fabrication of polymer light-emitting diodes is presented and subsequently, the theory of charge transport in organic semiconductors is treated. Finally the development of white polymer light-emitting diodes will be discussed.

2.1 Organic Semiconductors

Polymers (*plastics*) are widely used for inexpensive, disposable products, due to their ease of manufacture, versatility and low cost. Their resistance to electrical conductance makes them excellent materials for the insulation of electrical components. Since a few decades, it is realized that a special class of polymers may be used as active electronic elements. The special property of these materials is that of (semi)conductance. The discovery that marks the inception of the research field of *plastic electronics*[1] was the observation of high electrical conduction in polyacetylene (Figure 2.1) after doping with the halogen iodine in 1977.[2–4] This discovery was awarded with the 2000 Nobel Prize in chemistry. It should be noted, however, that electrical conductance in organic compounds after doping with halogens had been observed earlier.[5,6] For instance, in 1954 conductance in a perylene-bromine complex was reported[7] and in 1963 in polypyrrole doped with iodine.[8] Furthermore, the semiconducting properties of the organic molecule anthracene were widely studied in the 1950s and 1960s[9–11] and it was one of the first examples of electroluminescence in an organic material.[12,13] Finally, the charge transport in the polymer poly(*N*-vinyl carbazole) (PVK) was studied intensively in the 1960s and early 1970s due to its potential use in xerography.[14–16]

The common feature that hands these materials their unique property is that of conjugation: the alternation of single and double bonds between carbon atoms. In organic semiconductors, three of the four electrons in the outer shell of carbon form sp^2 hybridized orbitals, combining in the in-plane σ bonds that hold the polymer together. The remaining electron forms a p_z orbital which is perpendicular to the plane of the σ bonds and overlaps with the p_z orbital of the neighboring carbon atom. This overlap forms a π bond in which the electrons are delocalized over the polymer backbone. This process is demonstrated in Figure 2.2 for the case of ethene which contains one double bond. The π bond may be excited to a π^* anti-bond while the polymer is held together by the σ bonds. The energy of the π bond, which is occupied in the ground state, is called the highest occupied molecular orbital (HOMO) while the π^* bond equals the lowest unoccupied molecular orbital (LUMO). The HOMO and LUMO levels can be compared to the valence and conduction band of inorganic semiconductors, while the π-π^* energy difference corresponds to the band gap. In organic semiconductors, the band gap is typically between 1 and 4 eV, covering the entire visible spectrum. This makes organic semiconductors suitable materials for optoelectronic devices.

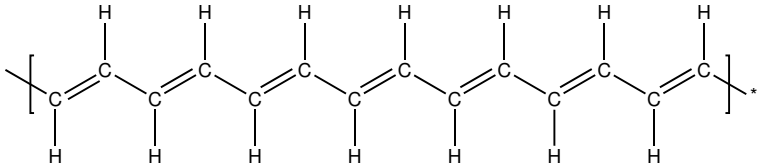

Figure 2.1. The chemical structure of polyacetylene, showing an alternation of single and double bonds between carbon atoms.

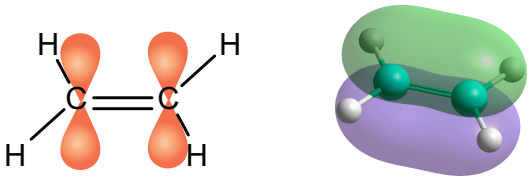

(a) (b)

Figure 2.2. (a) The chemical structure of ethane, with the p_z orbitals indicated, and (b) a 3D representation of the molecule, with the π orbital shown. The green and purple lobes represent the phase of the wave function.

2.2 Materials & Device Fabrication

The fact that the semiconducting behavior of conjugated materials originates from their molecular structure allows for the chemical tailoring of the material properties. The emission color, solubility, and charge transport properties may be tuned by modifying the conjugated backbone or the side groups.[17] As a result, the range of emission colors of polymer semiconductors covers the entire visible spectrum.

Figure 2.3 shows four examples of semiconducting polymers. PVK (Figure 2.3(a)) has been intensively investigated in the past for their use as organic photoreceptor in xerography.[18–20] Nowadays, it is used as a host material in PLEDs. PVK is not a fully conjugated polymer, since the conjugated carbazole moieties are attached as pendant-groups to an insulting polymer chain. The prototypical conjugated polymer is poly(*p*-phenylene vinylene) (PPV) of which the general structure is depicted in Figure 2.3(b). This polymer functioned as the emissive material in the first demonstrated PLED and exhibits a greenish-yellow emission.[21] The solubility of unsubstituted PPV is very poor, but it can be improved by substitution with appropriate alkyl side groups. This substitution also leads to a lowering of the band gap, causing a red shift of the emission. Examples of well-studied PPV-derivatives are poly[2-methoxy-5-(2′-ethylhexyloxy)-*p*-phenylene vinylene] (MEH-PPV), poly[2-methoxy-5-(3′,7′-dimethyloctyloxy)-*p*-phenylene vinylene] (OC_1C_{10}-PPV) and poly[{2-(4-(3′,7′-dimethyloctyloxyphenyl))}-*co*-{2-methoxy-5-(3′,7′-dimethyloctyloxy)}-1,4-phenylene vinylene] (NRS-PPV). These materials differ only in their side-chains and have a band gap of approximately 2.2 eV, yielding a red/orange emission.

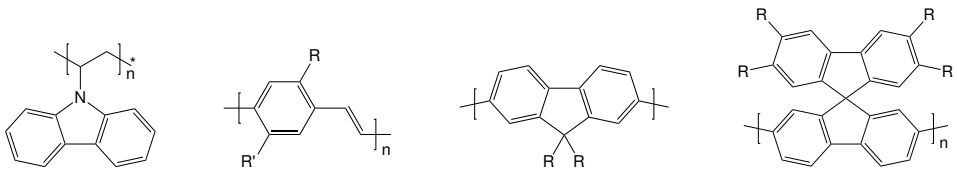

(a) (b) (c) (d)

Figure 2.3. The chemical structures of (a) poly(*N*-vinyl carbazole) (PVK), (b) poly(*p*-phenylene vinylene) (PPV), (c) polyfluorene and (d) polyspirobifluorene.

(a) (b) (c)

Figure 2.4. (a) An illustration of the device architecture of a PLED, (b) the top view and (c) an white PLED under operation.

For the realization of white light emitting PLEDs, an efficient blue emitter is a prerequisite. Polyfluorenes (Figure 2.3(c)) are attractive blue emitters due to their high photoluminescence efficiency and wide band gap.[22,23] They can be considered as a type of polyphenylene where pairs of phenylene rings are connected by an additional carbon atom, named the C-9 atom, keeping the phenyl rings in plane, resulting in an improved conjugation. Additionally, the C-9 atom allows for facile substitution of side chains to tune the solubility and interchain interactions without affecting the electronic structure.[24–26] The first polyfluorene PLED was reported by Yoshino *et al.* in 1989.[27,28] The material suffered from a low molecular weight and a poor device performance. Since then, considerable progress has been made in the synthesis of polyfluorene derivatives and the performance of polyfluorene devices. High efficient PLEDs were reported by copolymerizing fluorene with suitable units to tailor the electric and optical properties.[29–33] Salbeck *et al.* introduced spiro centers in fluorene compounds[34–36] and in fluorene polymers.[37] The spiro center links two fluorene units by connecting them at the C-9 atom while the planes of the fluorene units are oriented perpendicular to each other. This spiro linkage significantly increases the glass transition temperature (T_g) and thus improves the morphological stability while also minimizing unwanted long wavelength emission.[38] The general structure of polyspirobifluorene is shown in Figure 2.3(d).

The device configuration of a typical PLED consists of a thin emissive layer sandwiched between a cathode and an anode. Figure 2.4(a) shows an illustration of the architecture of a PLED. Due to the typical low conduction of organic materials, the layers are required to be very thin, of the order of 100 nm. Since dust particles are typically μm sized, they can be catastrophic for the operation of organic devices and PLEDs are therefore generally fabricated in a cleanroom environment. The devices demonstrated in this thesis are fabricated on 3×3 cm glass substrates with a patterned indium tin oxide (ITO) layer. ITO is a transparent conductor allowing the generated light to escape the device through the bottom contact. The substrates are ultrasonically cleaned in consecutively acetone and propanol. After drying, the substrates receive an UV ozone treatment. To reduce the roughness of the ITO layer and improve the work function, a layer of poly(3,4-ethylene dioxythiophene):poly(styrene sulfonate) (PEDOT:PSS) (Clevios P VP AI 4083, supplied by H.C. Starck) was spincoated from solution and subsequently baked (140 °C). The typical thickness of the PEDOT:PSS layer was

60 nm. After the annealing step, the substrates are transferred to a nitrogen-filled glovebox. The light-emitting polymer layers were deposited by spincoating from solution, typically in toluene. The devices are finished by the deposition of the cathode by thermal evaporation (chamber pressure ca. 10^{-6} mbar). The cathode consists of a 5 nm barium layer and a 100 nm aluminum capping layer.

By replacing the anode or cathode with an appropriate electrode, so-called single-carrier devices were fabricated. To measure the hole transport, hole-only devices were fabricated in which the cathode consists of a 20 nm palladium layer followed by a 80 nm gold layer. The high work function of palladium (~ 5.0 eV[39]) ensures that there is no electron injection so that the device current is dominated by the hole transport. Similarly, electron-only devices were fabricated by replacing the bottom contact with an oxidized aluminum layer (work function ~ 3.2 eV) preventing hole injection into the HOMO level of most materials. Table 2.1 lists the resulting device structures for the PLEDs and single-carrier devices. Unless stated otherwise, these device structures were used for the devices presented in this work. The devices were characterized in a nitrogen atmosphere using a computer controlled Keithley 2400 SourceMeter. Emission spectra measurements where performed with an Ocean Optics USB2000 spectrometer.

Figure 2.4(b) shows an illustration of the top-view of a completed device. The overlap of the bottom contact with the cathode on top defines the active area of the device. The bottom contacts and top contacts are patterned in such a way that each substrate contains four devices with active areas ranging from $\sim 1 \times 10^{-5}\,\mathrm{m}^2$ to $\sim 1 \times 10^{-4}\,\mathrm{m}^2$. The range of active areas provides a simple but powerful test of the device reliability by examining the agreement between the current densities of different device areas.

2.3 Material Characterization

An effective method to study the charge transport in organic semiconductors is by means of so-called single-carrier devices, since these devices allow for the measurement of either only the electron or only the hole current. Figure 2.5(a) shows an example of a typical current-density – voltage (J–V) plot of a hole-only device. In the J–V plot three different regimes can be discerned. At low bias, the current is dominated by the leakage current which scales linearly with the applied voltage and is symmetric around 0 V. At approximately 1 V, the device current surpasses the leakage current and the current follows an exponential behavior with voltage. Finally, at ~ 1.5 V the device current bends away from the exponential part. The

Device	Structure
HO	ITO/PEDOT:PSS ($\sim$ 60 nm)/LEP (x nm)/Pd (20 nm)/Au (80 nm)
PLED	ITO/PEDOT:PSS ($\sim$ 60 nm)/LEP (x nm)/Ba (5 nm)/Al (100 nm)
EO	Al (30 nm)/LEP (x nm)/Ba (5 nm)/Al (100 nm)

Table 2.1. The device structures for hole-only (HO) devices, PLEDs, and electron-only (EO devices).

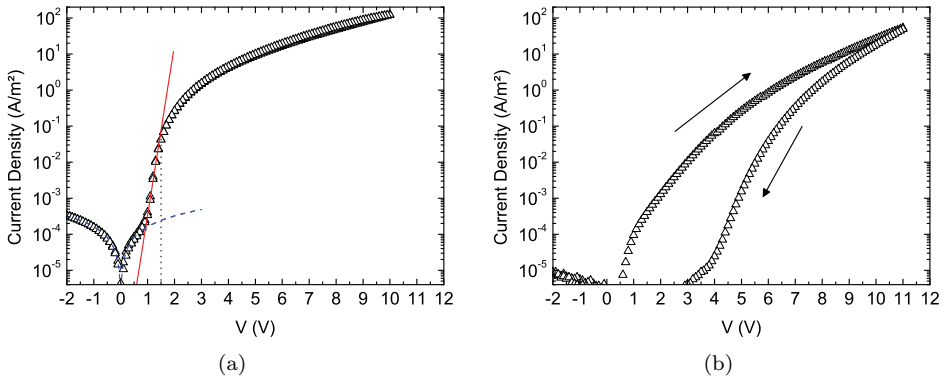

Figure 2.5. Examples of typical J–V curves of (a) a hole-only device and (b) electron-only device.

transition from an exponential dependence to a quadratic dependence stems from the built-in voltage of the device. Due to the different work functions of the contact materials, as the device is connected at 0 V, electrons will flow through the external circuit from the cathode towards the anode to equalize their Fermi levels. This leads to the formation of a built-in electric field which opposes the drift current. Below the built-in voltage the current is dominated by diffusion leading to an exponential dependence of the device current on voltage. A straightforward method to estimate the built-in voltage V_{bi} is therefore to find the voltage at which the current starts to deviate from the exponential behavior,[40] as illustrated in Figure 2.5(a). Due to band bending at the contacts, the built-in voltage can lie slightly below the potential difference of the contacts.[41,42] This is demonstrated in Figure 2.6 for the case of a double carrier device with two Ohmic contacts. Figure 2.6(a) shows the band diagram at $V = 0$ V. The alignment of the Fermi levels induces an internal electric field which opposes the drift current. Figure 2.6(c) shows the

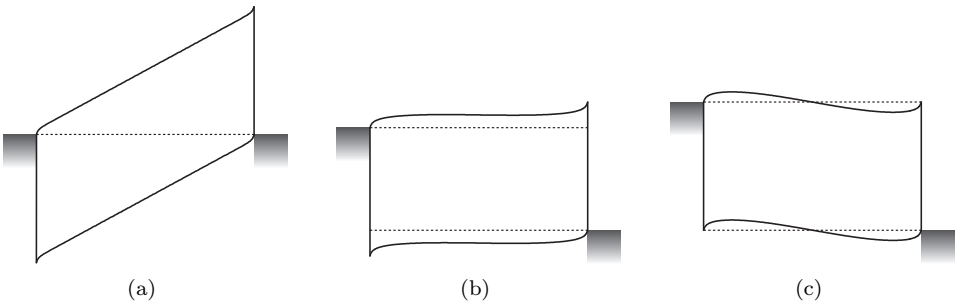

Figure 2.6. Schematic illustration of the band diagram of a PLED with Ohmic contacts at (a) no applied bias ($V = 0$ V), (b) $V = V_{\mathrm{bi}}$ and (c) at an voltage equal to the work function difference of the contact materials.

situation at the application of a voltage equal to the work function difference of the contacts. In this situation the built-in field is fully surmounted. However, already a few tenths eV below this voltage a flat band situation in the bulk of the material is achieved as illustrated in Figure 2.6(b).

Figure 2.5(b) shows a typical J–V of an electron-only device. A striking difference with the hole-only device is the appearance of hysteresis in the J–V plot. As the voltage is swept from 11 V back to 0 V, the device current is considerably lower than during the up-scan. This behavior is commonly observed in electron-only devices and is related to the presence of deep electron traps. As the voltage is increased, both the free electron density and the trapped electron density increase, while the trapped and free electron density remain in equilibrium. However, as the voltage is reduced during the down-sweep, a fraction of the trapped electrons is not released, so that the device is not anymore in equilibrium. The total electron density that is electrostatically allowed remains the same, which requires a drastic reduction of the free electron density and thus a lower electron current than during the up-scan.[43] A consequence of this hysteresis is that only the first up-scan of an electron-only device can be used for modeling purposes. Therefore, for the remainder of this thesis, only the up-scans of fresh electron-only J–V will be shown. Furthermore, due to the trap-limited nature of the electron transport, an exponential regime is generally not observed. Consequently, the built-in voltage cannot be simply deduced from the electron-only J–V curve and it is therefore left as a free fit parameter.

2.4 Charge Transport

Figure 2.7 shows a schematic picture of the energy diagram of a PLED under operation. The three processes that govern the device operation of a PLED are indicated; charge injection, transport and recombination.[44,45] The magnitude of the injection barrier φ determines whether the device current is limited by charge injection or by the bulk transport. For sufficiently small injection barriers the device current is limited by the bulk transport and the contact is defined as an Ohmic contact.[46] It has been established that for practical device thicknesses an Ohmic contact is formed if the injection barrier $\varphi \lesssim 0.3$ eV.[45,47–49] For PPV derivatives this condition is readily achieved using common contact materials such as barium and PEDOT:PSS. For wide band gap materials such as polyfluorene however, this is less straightforward. This will be discussed in more detail in Chapter 3.

On the condition of an Ohmic contact, the device current is limited by the mobility μ. In this limit, an approximation of the unipolar current density can be obtained by neglecting the contribution of diffusion current and assuming a constant mobility. This leads to the well-known Mott-Gurney law describing the space-charge limited (SCL) current:[50]

$$J_{\mathrm{SCL}} = \frac{9}{8}\varepsilon_0\varepsilon_r\mu\frac{V^2}{L^3}, \tag{2.1}$$

with $\varepsilon_0\varepsilon_{\mathrm{r}}$ the dielectric constant of the material, V the applied voltage, and L the

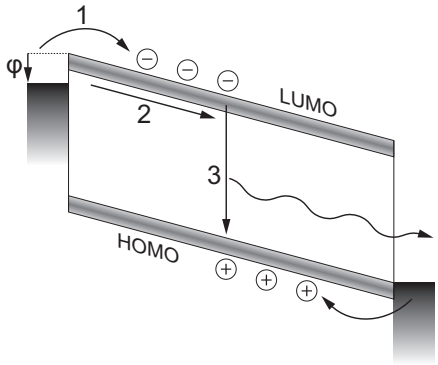

Figure 2.7. Schematic energy diagram of a PLED under operation. The three processes governing the operation of the PLED are indicated: (1) injection, (2) transport and (3) recombination.

layer thickness. Applying Equation 2.1, the mobility can be easily extracted from single-carrier SCL measurements. The mobility is a key material parameter, since it directly determines device properties such as the response time and the power efficiency. The mobility is also the origin of one of the most important differences between organic and inorganic semiconductors. It may therefore be instructive to consider the microscopic origin of the mobility μ.[51]

The mobility defines the average drift velocity v that a charge carrier obtains under the influence of an electric field E: $v = \mu E$. The mobility is therefore a measure of the conductivity of a material. Inorganic semiconductors are highly ordered materials with a periodic lattice leading to a delocalization of charge carriers. The mean free path of charge carriers in these materials is high, and limited by scattering of carriers with phonons. As a result, the charge carrier mobility in inorganic semiconductors decreases with increasing temperature. In contrast, the charge carrier mobility in organic semiconductors is observed to be strongly thermally activated. This behavior is known from impurity conduction in inorganic semiconductors[52–54] and from molecularly doped polymers, in which organic pigments are dispersed in an insulating polymer matrix.[19] In these materials charge transport takes place via 'hopping' between localized states. Although semiconducting polymers feature a delocalization of charges, this delocalization extends only in one dimension along the conjugated backbone. Additionally, the conjugated is broken in many places due to impurities and kinks in the polymer backbone. What results is a structure consisting of conjugated polymer segments on which charges are localized and need to 'hop' to other conjugated segments, similar as in molecularly doped polymers. As a consequence, the mobility in organic semiconductors is typically orders of magnitude lower than in their inorganic counterpart.

The localized states in organic semiconductors are subject to spatial and energetic disorder. For jumps upwards in energy, the carriers may be thermally assisted by phonons to overcome the energy difference, leading to the strong temperature dependence of the mobility. The resulting mobility that is measured with, for

instance, single-carrier devices, thus originates from the aggregate of many microscopic hopping events. The nature of hopping transport is also the reason that the description of charge transport in molecularly doped polymers is applicable to both semiconducting polymers and small molecule devices are similar, despite their dissimilar molecular structure.

From time-of-flight (TOF) studies and single-carrier SCL measurements, it has been observed that the charge carrier mobility increases with electric field.[55,56] The dependence of the mobility on electric field was found to have the form of a stretched exponential, as described by the Poole-Frenkel relation.[57] The temperature dependence was observed to obey an Arrhenius temperature dependence. Combined with a Poole-Frenkel dependence this lead to the following empirical equation for the charge carrier mobility

$$\mu_{\mathrm{PF}}(T,E) = \mu_0^* \exp\!\left[-\frac{\Delta}{k_{\mathrm{B}}T}\right] \exp\!\left[\gamma\sqrt{E}\right], \tag{2.2}$$

with μ_0^* the zero-field mobility in the limit of infinite temperature, Δ the activation energy, k_{B} Boltzmann's constant, T the absolute temperature, E the electric field, and γ the field activation parameter. Equation 2.2 has been used to describe the charge transport in PVK[15,16] and a variety of molecularly doped polymers, however it lacks theoretical justification. The origin of the stretched exponential term in the Poole-Frenkel theory lies in the description of how a coulomb potential near a charged localized state is modified by an electric field. For the charge transport in organic semiconductors the Poole-Frenkel theory requires a charged coulomb trap at every hopping site, which would lead to unrealistic high trap densities.

To explain the observed temperature and field dependence of the mobility Monte Carlo simulations of the charge transport were performed by Bässler. In these calculations the charge transport is thought to take place by hopping in a distribution of states (DOS) which is assumed to be Gaussianly shaped, with a width of σ. The transition rates between hopping sites were given by Miller and Abrahams.[54] The mobility dependence that was proposed based on these calculations is known as the Gaussian disorder model (GDM).[58]

$$\mu_{\mathrm{GDM}}(T,E) = \mu_0^* \exp\!\left[-\left(\frac{2}{3}\hat{\sigma}\right)^2 + C\left(\hat{\sigma}^2 - \Sigma^2\right)\sqrt{E}\right], \tag{2.3}$$

with $\hat{\sigma} \equiv \sigma/k_{\mathrm{B}}T$, Σ a parameter describing the off-diagonal disorder, and C an empirical constant depending on the site spacing. The GDM exhibits a $\ln(\mu) \propto 1/T^2$ dependence in contrast to Equation 2.2. However, in the temperature range that is typically measured the difference between a $1/T$ and a $1/T^2$ dependence is difficult to discriminate experimentally. Within the GDM, the field dependence according to Equation 2.2 is only reproduced in a limited electric field range, while such field dependence is experimentally observed over a much wider range of electric fields. An improvement to this model was made by taking into account spatial correlation between the energies of neighboring sites. This resulted in the correlated disorder

model (CDM). In this model the stretched exponential field dependence is extended to lower electric fields.[59–61]

$$\mu_{\mathrm{CDM}}(T,E) = \mu_0^* \exp\left[-\left(\frac{3}{5}\hat{\sigma}\right)^2 + 0.78\left(\hat{\sigma}^{3/2} - 2\right)\sqrt{\frac{qaE}{\sigma}}\right], \tag{2.4}$$

with q the elementary charge and a the intersite spacing.

While the dependence of the mobility on electric field has been investigated intensively, it was realized much later that an additional factor influences the mobility; the dependence of the mobility on the charge carrier density. The carrier density dependence of the mobility was difficult to determine from diode measurements, since in diodes an increase of the electric field is simultaneously accompanied by an increase of the charge carrier density. The key in disentangling the density- and electric field dependence of the mobility was the unification of diode and field-effect transistor (FET) measurements.[62] In FETs the electric field between source and drain is much smaller than that in diodes, while the charge carrier density in the conductive channel is considerably larger than typically achieved in diodes.[63] The measured mobilities in FETs are orders of magnitude larger than those in diodes. Additionally, a dependence of the mobility on the gate voltage is generally observed.[64,65] Since the charge carrier density in the channel is controlled by the gate voltage, the gate-voltage dependence of the mobility can be explained by a charge carrier density dependence.[64,66,67] The explanation for this density dependence is deep state filling. Within the framework of hopping, charge transport is thought to take place in the tail of the DOS, in which only few hopping sites are available when the charge carrier density is low. As the density of charge carriers increases, more states become accessible by hopping which is reflected in a higher mobility.

Vissenberg and Matters obtained an analytical expression for the density dependence of the mobility based on variable range hopping in an exponential DOS. The resulting density dependence has the form of a power law according to[68]

$$\mu_{\mathrm{VM}}(p) = \frac{\sigma_0}{q}\left(\frac{(T_0/T)^4 \sin(\pi T/T_0)}{(2\alpha)^3 B_{\mathrm{c}}}\right)^{T_0/T} p^{T_0/T-1}, \tag{2.5}$$

where σ_0 is a prefactor for the conductivity, α^{-1} is the effective overlap parameter between localized states, B_{c} the critical number for the onset of percolation and T_0 the characteristic temperature describing the decay of the exponential distribution. Taking into account a density dependent mobility, it could be shown that the difference between the mobilities in diodes and FETs is the direct result of the difference in the typical charge carrier densities.[62] Moreover, it was demonstrated that at room temperature, the dependence of the mobility on the charge carrier density is dominant over the field dependence of the mobility.[69] With the realization that the mobility depends on both electric field and charge carrier density, it also became apparent that the mobility is not purely a material property, but also dependent on the device architecture and measurement conditions. Only recently, a

full description of the mobility taking into account both the field and charge carrier density dependence was obtained by Pasveer *et al.* in the form of the extended Gaussian disorder model (EGDM).[70] In this expression the dependencies of the mobility on electric field and charge carrier density are factored in field- and density enhancement functions.

$$\mu_{\mathrm{EGDM}}(T,p,E) = \mu_0^* \exp\left[-C\hat{\sigma}^2\right] f(T,E) g(T,p), \tag{2.6a}$$

$$f(T,E) = \exp\left[0.44\left(\hat{\sigma}^{3/2} - 2.2\right)\left(\sqrt{1 + 0.8\left(\frac{qaE}{\sigma}\right)^2} - 1\right)\right], \tag{2.6b}$$

$$g(T,p) = \exp\left[\frac{1}{2}\left(\hat{\sigma}^2 - \hat{\sigma}\right)\left(2\frac{p}{N_{\mathrm{s}}}\right)^{\delta}\right], \tag{2.6c}$$

$$\delta \equiv 2\frac{\ln\left(\hat{\sigma}^2 - \hat{\sigma}\right) - \ln(\ln(4))}{\hat{\sigma}^2}, \tag{2.6d}$$

with $C = 0.42$ and N_{s} the transport site density with $a = N_{\mathrm{s}}^{-1/3}$ the intersite distance and μ_0^* the mobility in the limit of zero field, zero carrier density, and infinite temperature.

It should be noted that both mobility models describing the density dependence of the mobility assume a different shape of the DOS. The Vissenberg-Matters (VM) equation was obtained for an exponential DOS, while the EGDM is based on a Gaussian DOS. The fundamental difference between an exponential DOS and a Gaussian DOS is that while in the former system the average energy of the hopping carriers relaxes to $-\infty$, it relaxes to $-\sigma^2/k_{\mathrm{B}}T$ in the latter system. During a voltage sweep only a small part of the DOS is filled. Consequently, the segment of a Gaussian that is being filled during a voltage sweep may be approximated by an exponential. However, they reverse may also be true. There are only a few reports on experimental measurements of the shape of the DOS in organic semiconductors. Hulea *et al.* measured a complex DOS in PPV consisting of a Gaussian core, and a tail that contains both features of a Gaussian as well as an exponential distribution,[71] while Tal *et al.* found an exponential tail for the DOS of the organic molecule α-NPD.[72] Finally, from a computational study it was predicted that the tail of the DOS of poly(3-hexylthiophene) is exponential rather than Gaussian.[73] The experimental studies both find a complex shaped DOS and thus the assumption of either an exponential of Gaussian distribution will always be a simplification. Moreover, the shape of the distributions is not necessarily the same for all organic semiconductors. The various mobility models used to describe the charge transport in organic semiconductors depend critically on the assumed shape of the DOS. The actual shape of the DOS is therefore a major source of uncertainty, and should be regarded as an assumption only.

The underlying difference between the VM model and the EGDM is reflected in a different density dependence of the mobility. However, the difference between both models is difficult to discriminate from a *J*–*V* curve, since only a limited range of charge carrier densities is reached in a diode. The unique advantage of the

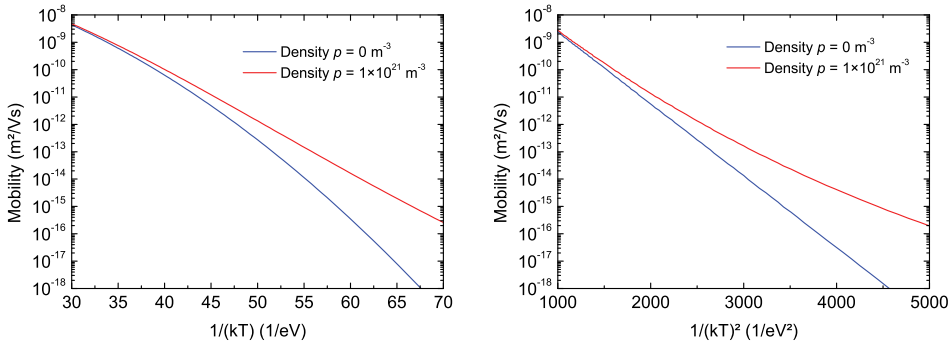

(a) (b)

Figure 2.8. Temperature dependence of the mobility in the limit of zero carrier density and at a finite carrier density of $p = 1 \times 10^{23}\,\mathrm{m}^{-3}$ (a) on an Arrhenius scale and (b) on a $1/T^2$ scale.

VM model is that the mobility parameters can be determined independently from FET measurements. However, the VM model does not take into account the field dependence of the mobility. This has been addressed empirically by implementing an additional Poole-Frenkel (PF) type field dependence. The EGDM includes both the density and field dependence of the mobility from the outset. Additionally it requires only three (temperature independent) parameters, greatly facilitating the fitting of experimental data.

Although the PF mobility model lacks a sound theoretical basis, it is still commonly used, mainly due to its simplicity.[74] In that case the enhancement of the mobility due to the charge carrier density is comprised in the field activation factor γ. It should be reckoned with that the disregard of the charge carrier density of the mobility will lead to an incorrect prediction of the thickness scaling of the device current. In a thinner device the average carrier density is higher due to diffusion of charge carriers from the contacts. As a result, the apparent mobility in a thin device is higher.[75,76] A correct quantitative description should preferably be based on a model which takes into account the field and charge carrier density from the outset and with a proper theoretical basis, such as the EGDM. However, if not enough experimental data is available to accurately determine the mobility parameters, the use of a more simple model such as the PF model may suffice, provided that the concerning thicknesses are similar.

The EGDM predicts a temperature dependence of the mobility in the limit of zero field and zero charge carrier density of $\ln(\mu) \propto 1/T^2$. However, by comparing the temperature dependence of a wide range of organic semiconductors a universal Arrhenius behavior was observed.[77] This would be in contradiction to the temperature dependence as predicted by the EGDM. However, while the field and charge carrier density dependence are factored in Equation 2.6, all factors exhibit a temperature dependence via the scaled disorder parameter $\hat{\sigma}$. To assess the temperature scaling of the EGDM, the complete equation should therefore be con-

sidered. Figure 2.8 shows the temperature dependence of the mobility $\mu(T, p, E)$ with $\mu_0^* = 1.0 \times 10^{-6}\,\mathrm{m^2/Vs}$, $\sigma = 0.12$ eV, $N_\mathrm{s} = 1 \times 10^{27}\,\mathrm{m^{-3}}$, and in the limit of zero electric field: $E = 0$ V/m. Two cases are considered; the mobility in the limit of zero charge carrier density ($p = 0$) and at a finite charge carrier density of $p = 1 \times 10^{21}\,\mathrm{m^{-3}}$. For typical device thicknesses, the average charge carrier density in a device at zero bias exceeds $1 \times 10^{21}\,\mathrm{m^{-3}}$ due to the diffusion of charges from the contacts.[76] In the limit of zero carrier density Equation 2.6c reduces to 1, and the mobility follows a $\ln(\mu) \propto 1/T^2$ temperature dependence according to Equation 2.6a. The mobility at finite carrier density however, follows a $\ln(\mu) \propto 1/T$ temperature dependence over the temperature range where J–V measurements are usually carried out. The additional temperature dependence of the density enhancement causes an Arrhenius-like temperature dependence of the mobility at finite carrier density. The apparent discrepancy between a $1/T$ and $1/T^2$ dependence thus lies in the ambiguity in the use of the term 'mobility'. The mobility extrapolated to zero charge carrier density according to the EGDM (Equation 2.6a) follows a $1/T^2$ scaling, while the *effective* mobility that is obtained from, for instance, single carrier SCL measurements is predicted to follow an Arrhenius behavior.[78,79] To conclude this section, the density dependence of the mobility complicates the accurate measurement and comparison of mobility values, since its value depends on the operating conditions. A full determination of the mobility function should therefore involve a series of measurements within which the carrier density, electric field and temperature can be varied quite independently over large parameter ranges. When the carrier density is insufficiently varied during a measurement, at best an *effective* mobility can be obtained.

2.5 Trap-Limited Transport

The hole transport in semiconducting polymers is usually observed to be trap-free which allows for the relatively straightforward measurement of the hole mobility. The electron transport often exhibits a markedly different behavior. For instance, in PPV derivatives it is found that the electron current is orders of magnitude lower than the hole transport and that it is characterized by a stronger voltage- and thickness dependence.[80] Such behavior is characteristic for trap-limited conduction, where charge carriers are trapped in localized states in the band gap. An analytical description for the trap-limited current in the presence of a discrete trap level was obtained by Lampert.[81] He found that the current density has the same dependence as the trap-free SCL current, only scaled with a factor θ,

$$J_\mathrm{TLC} = \frac{9}{8}\theta\varepsilon_0\varepsilon_r\mu\frac{V^2}{L^3}, \tag{2.7a}$$

$$\theta = \frac{N_\mathrm{c}}{N_\mathrm{t}}\exp\left[-\frac{E_\mathrm{t}}{k_\mathrm{B}T}\right], \tag{2.7b}$$

with N_c the effective density of states in the LUMO, N_t the trap density and E_t the trap depth. For the derivation of Equation 2.7 it was assumed that the density of trapped electrons is larger than the density of free electrons: $n_\mathrm{t} \gg n$. As a

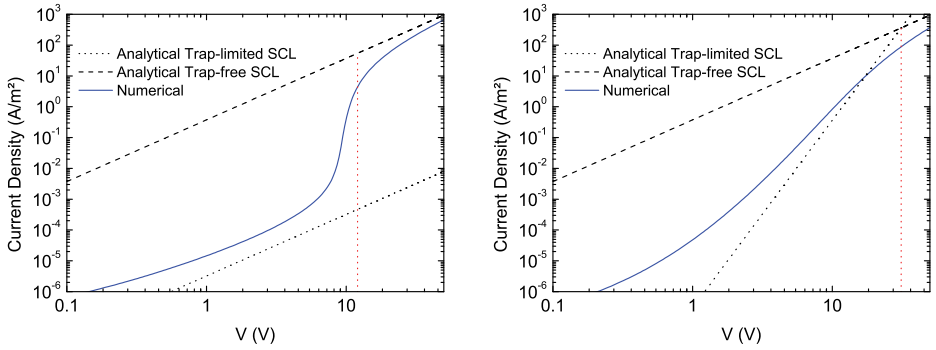

Figure 2.9. Numerical calculation of the trap-limited transport in the case of (a) a discrete trap level and (b) and exponential trap distribution, and their analytical approximations. The thickness of the layer is $L = 200$ nm, and a constant mobility of $\mu = 1 \times 10^{-10}\,\mathrm{m^2/Vs}$ was used. For the case of a discrete trap level the trap parameters are $N_\mathrm{t} = 1 \times 10^{23}\,\mathrm{m^{-3}}$ and $E_\mathrm{t} = 0.5$ eV. For the case of an exponential trap distribution the trap parameters are $N_\mathrm{t} = 1 \times 10^{24}\,\mathrm{m^{-3}}$ and $T_\mathrm{t} = 1500$ K.

result, Equation 2.7 is only valid in the regime where the trap is not fully filled. As the voltage is increased, the electron density is raised, so that at a certain voltage the trap is completely filled. At this voltage, all additional injected charges will contribute to the transport, leading to a rapid increase of the current, as demonstrated in Figure 2.9(a). At voltages above the trap-filled limit, the amount of trap charges is smaller than the concentration of free charges, and the current approaches the trap-free SCL. The voltage at which the trap becomes completely filled can be calculated by assuming that at this point the total charge density is completely determined by the trap density N_t. Solving the Poisson equation then leads to the following expression for the trap-filled limit:

$$V_\mathrm{TFL} = \frac{qN_\mathrm{t}L^2}{2\varepsilon_0\varepsilon_r}. \tag{2.8}$$

A sharp increase of the electron current as shown in Figure 2.9(a) is rarely observed in organic semiconductors. This suggests that in organic semiconductors the trap states exhibit a broad distribution, which may be expected in a disordered system. It is often assumed that the trap states are exponentially distributed in the forbidden band gap, as illustrated in the inset of Figure 2.9(b). For this case, an analytical expression was obtained by Mark and Helfrich.[82]

$$J_\mathrm{TLC} = N_\mathrm{c} q\mu \left(\frac{\varepsilon_0\varepsilon_r}{qN_\mathrm{t}}\right)^{r+1} \left(\frac{2r+1}{r+1}\right)^{r+1} \left(\frac{r}{r+1}\right)^{r} \frac{V^{r+1}}{L^{2r+1}}, \tag{2.9}$$

with $r = T_\mathrm{t}/T$, where T_t is a characteristic temperature describing the exponential

decay of the trap distribution. Analogous to Equation 2.8, the trap-filled limit in the case of an exponential can be calculated as

$$V_{\mathrm{TFL}} = \frac{qL^2}{\varepsilon_0 \varepsilon_r} \left[\frac{9}{8} \frac{N_{\mathrm{t}}^r}{N_{\mathrm{c}}} \left(\frac{r+1}{r} \right)^r \left(\frac{r+1}{2r+1} \right)^{r+1} \right]^{1/(r-1)} . \tag{2.10}$$

In the derivations of Equations 2.7 and 2.9 several approximations are made. The density of trapped charges is assumed to be large as compared to the free charge carrier density and as a result the approximations are only valid below the trap-filled limit. Additionally, diffusion of charge carriers is neglected so that traps filled at zero bias are not taken into account. A more accurate result is therefore obtained using a numerical device model, which includes these effects.[83] Figure 2.9 shows the calculated trap-limited current for the case of a discrete trap level and an exponential trap level, together with their respective approximations, Equation 2.7 and Equation 2.9. For both trap distributions the value of the trap-filled limit is indicated. It is observed that the approximations only yield a crude agreement with the more accurate numerical model. One may therefore wonder what the usefulness of these approximations is, considering their inaccuracy. The answer is that approximations like Equations 2.7 and Equation 2.9 offer direct insight in how the trap-limited current depends on the values of the trap parameters. For instance, using Equation 2.9 the trap temperature T_{t} can be directly estimated from the thickness dependence of the trap-limited transport.

From Equation 2.7 and Equation 2.9, it can also be observed that both the mobility and the trap density appear in the prefactor of the trap-limited current. Consequently, it is difficult to determine the trap density when the mobility is unknown. In FET measurements by Chua *et al.* it was observed that the electron transport of a wide range of semiconducting polymers is similar to the hole transport.[84] This lead to the notion that the electron mobility is equal to the hole mobility. Indeed, it was recently shown by Zhang *et al.* that for the case of MEH-PPV the intrinsic electron mobility is equal to the hole mobility.[85] In that study, MEH-PPV was molecularly doped with the n-type dopant decamethylcobaltocene (DMC). The HOMO level of DMC is not high enough to dope the LUMO of MEH-PPV, but it was able to fill the traps in the band gap of MEH-PPV. It was observed that after doping, the magnitude of the electron current and the temperature dependence were equal to the hole current. This result proved additionally that the traps that govern the trap-limited transport in MEH-PPV are energetically located at least 0.4 eV below the LUMO of MEH-PPV.

Taking into account equal mobilities for electrons and holes, and adopting an exponential distribution of trap states, the voltage and thickness dependence of the electron transport in PPV could be consistently described.[86,87] The uncertainty of the shape of the DOS also applies to the trap distribution. On the assumption of a Gaussian LUMO, it may be more obvious to also consider a Gaussian distribution of trap states. However, the mathematics involved and the behavior of a Gaussian trap distribution are less straightforward. This will be dealt with in more detail in Chapter 6.

2.6 White Polymer Light-Emitting Diodes

After initial demonstrations of electroluminescence from anthracene,[12,13] the first report of an efficient OLED was by Tang and VanSlyke, who fabricated an OLED from vacuum fabricated small molecule tris(8-hydroxyquinoline)-aluminum (Alq_3).[88] A few years later the Cambridge group demonstrated an OLED employing a polymeric emissive layer of PPV.[21] The importance of this discovery was that it demonstrated the potential for the fabrication of large area applications with simple coating techniques. OLEDs based on small molecules are nowadays used as pixels in mobile phone displays and prototypes of televisions employing OLEDs have been presented by several display manufacturers. The progress of polymer light-emitting diodes (PLEDs) is lagging behind which can be understood from the different techniques used for the fabrication. In small molecule based OLEDs, the active layers are generally deposited by thermal evaporation. With this technique it is relatively straightforward to fabricate multilayer devices, so that for all the processes that govern the device operation a separate layer can be used which is individually optimized for that specific task. Polymers, on the other hand, are generally deposited using technologies based on solution processing, such as spincoating or printing. Consequently it is more difficult to manufacture polymeric multilayer devices and PLEDs have not been able to match the efficiencies of small molecule OLEDs.

Thermal evaporation requires relative expensive vacuum technology while solution processing holds the promise of cost efficient fabrication of large area devices. Solution processed PLEDs may therefore hold a competitive edge over small molecule OLEDs for large area applications, such as lighting. The latter requires a broad emission over the full visible spectrum, which can be achieved in a number of ways,[89] as illustrated in Figure 2.10. One approach is the fabrication of multi-layer devices, where each layer emits light with a specific color so that the combined output is perceived as white.[90–92] As mentioned above, multilayer devices are difficult to process from solution due to the required solvent incompatibilities, which negates the advantage of simple and low-cost solution processed fabrication. Another approach is to use a blend of materials each emitting in a different color,[93–97] which however requires absolute control over the morphology and suffers from phase segregation. An attractive way to avoid these complications is the use of a copolymer, in which red and green dyes are incorporated into a blue backbone.[33,98–100] In such a copolymer a small concentration of narrow band gap dyes are copolymerized in a wide band gap host polymer. The current is then carried by the polymer backbone, while the recombination originates from both the blue-emitting backbone as the dyes. The main advantage of using such a copolymer is that white light emission can be obtained using only one emissive layer that can be spincoated or printed. This layer is then responsible for the injection of charges, the transport and recombination.

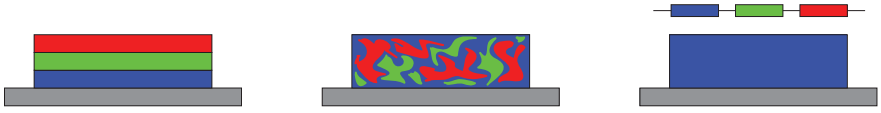

Figure 2.10. Schematic representation of the different methods to generate white light.

2.7 Scope of this Thesis

This thesis deals with the device physics of white polymer light-emitting diodes that are based on a single layer of a white-emitting copolymer. The final objective of this work is to develop a description of the device operation of a white-emitting PLED based on a copolymer in which green and red dyes are incorporated in a blue backbone. The fact that in such a copolymer, the emission of several colors takes place in a single layer severely complicates the understanding of the device operation. In the following chapters, the device operation of the white-emitting PLED is unraveled by first studying the device operation of the blue-emitting PLED and subsequently by stepwise investigating the influence of the green and red dye.

For white-emitting copolymers, an efficient blue emitter is a prerequisite. However, due to the wide band gap associated with blue emission, it is challenging to find suitable injection materials. For this purpose two different approaches to resolve this issue are investigated. First, in Chapter 3 a novel hole injection material, MoO_3, is discussed. It is shown that MoO_3 forms an Ohmic hole injecting contact on poly(9,9-dioctylfluorene) (PFO), which was not possible using the common hole injecting material poly(3,4-ethylenedioxythiophene)/poly(styrenesulphonic acid) (PEDOT:PSS). Another approach to improve the injection and transport of holes in wide band gap materials is the incorporation of arylamine units. In Chapter 4 the hole transport in a series of blue-emitting polymers with varying arylamine content is investigated. It is shown that the arylamine units act as traps for the hole transport at low concentrations, and function as the transport sites at high concentrations. Furthermore, it is found that the mathematical density of transport sites used in the numerical model corresponds to the physical number of transport sites in the numerical model.

In Chapter 5 the device operation of a blue-emitting PLED is discussed. The hole transport in this polymer has been treated in Chapter 4. The electron transport in this material is difficult to describe. For that reason the electron transport is investigated both by steady-state current-voltage measurements, as by transient electroluminescence measurements. It is found that the electron transport is limited by traps, although the intrinsic trap-free electron mobility is higher than the hole mobility. The combination of the electron current and hole current result in a shift of the recombination zone in the blue PLED.

In Chapters 6 and 7 a small detour is taken to the electron transport in a wider range of materials. The trap-limited electron transport in organic semiconductors is commonly described by assuming an exponential distribution of traps. In Chap-

ter 6 it is shown that the electron transport in three poly(*p*-phenylene vinylene) derivatives can alternatively be described using an Gaussian distribution of traps. In Chapter 7 the Gaussian trap model is used to evaluate the trap-limited current in a wider range of organic semiconductors. The trap parameters found in these materials point to a common trap distribution, centered at an energy of 3.6 eV below the vacuum level, and with a nearly identical concentration of 3×10^{23} traps/m^3.

Finally, in Chapter 8 the device operation of the white-emitting PLED will be discussed. With the charge transport in the blue backbone described in the previous chapters, all that remains is the influence of the green and red dye. It is found that the dyes act as emissive electron traps. From single-carrier devices the trap parameters describing the dyes can be determined. Combining all the relevant transport and trapping parameters, the device operation of the white PLED can be described. Moreover, the experimentally observed color shift can be qualitatively reproduced.

References

1. D. M. de Leeuw, *Physics World* **12**, 31 (1999).
2. H. Shirakawa, E. J. Louis, A. G. MacDiarmid, C. K. Chiang, and A. J. Heeger, *J. Chem. Soc., Chem. Commun.* **16**, 578 (1977).
3. C. K. Chiang, C. R. Fincher, Y. W. Park, A. J. Heeger, H. Shirakawa, E. J. Louis, S. C. Gau, and A. G. MacDiarmid, *Phys. Rev. Lett.* **39**, 1098 (1977).
4. C. K. Chiang, M. A. Druy, S. C. Gau, A. J. Heeger, E. J. Louis, A. G. MacDiarmid, Y. W. Park, and H. Shirakawa, *J. Am. Chem. Soc.* **100**, 1013 (1978).
5. F. G. Brunetti, R. Kumar, and F. Wudl, *J. Mater. Chem.* **20**, 2934 (2010).
6. G. Inzelt, *J. Solid State Electrochem.* **15**, 1711 (2011).
7. H. Akamatu, H. Inokuchi, and Y. Matsunaga, *Nature* **173**, 168 (1954).
8. B. Bolto, R. McNeill, and D. Weiss, *Aust. J. Chem.* **16**, 1090 (1963).
9. H. Mette and H. Pick, *Z. Phys.* **134**, 566 (1953).
10. R. G. Kepler, *Phys. Rev.* **119**, 1226 (1960).
11. O. H. LeBlanc, *J. Chem. Phys.* **33**, 626 (1960).
12. M. Pope, H. P. Kallmann, and P. Magnante, *J. Chem. Phys.* **38**, 2042 (1963).
13. W. Helfrich and W. G. Schneider, *Phys. Rev. Lett.* **14**, 229 (1965).
14. H. Hoegl, *J. Phys. Chem.* **69**, 755 (1965).
15. D. M. Pai, *J. Chem. Phys.* **52**, 2285 (1970).
16. W. D. Gill, *J. Appl. Phys.* **43**, 5033 (1972).
17. A. C. Grimsdale, K. Leok Chan, R. E. Martin, P. G. Jokisz, and A. B. Holmes, *Chem. Rev.* **109**, 897 (2009).
18. R. O. Loutfy, A. M. Hor, C. K. Hsiao, G. Baranyi, and P. Kazmaier, *Pure Appl. Chem.* **60**, 1047 (1988).
19. D. M. Pai and B. E. Springett, *Rev. Mod. Phys.* **65**, 163 (1993).
20. P. M. Borsenberger and D. S. Weiss, *Organic Photoreceptors for Xerography* (Marcel Dekker, Inc., New York, 1998).
21. J. H. Burroughes, D. D. C. Bradley, A. R. Brown, R. N. Marks, K. Mackay, R. H. Friend, P. L. Burns, and A. B. Holmes, *Nature* **347**, 539 (1990).
22. Q. Pei and Y. Yang, *J. Am. Chem. Soc.* **118**, 7416 (1996).

23. A. W. Grice, D. D. C. Bradley, M. T. Bernius, M. Inbasekaran, W. W. Wu, and E. P. Woo, *Appl. Phys. Lett.* **73**, 629 (1998).

24. D. Neher, *Macromol. Rapid Commun.* **22**, 1365 (2001).

25. S. A. Chen, H. H. Lu, and C. W. Huang, *Adv. Polym. Sci.* **212**, 49 (2008).

26. R. Abbel, A. P. H. J. Schenning, and E. W. Meijer, *J. Polym. Sci., Part A: Polym. Chem.* **47**, 4215 (2009).

27. M. Fukuda, K. Sawada, and K. Yoshino, *Jpn. J. Appl. Phys.* **28**, L1433 (1989).

28. Y. Ohmori, M. Uchida, K. Muro, and K. Yoshino, *Jpn. J. Appl. Phys.* **30**, L1941 (1991).

29. M. Inbasekaran, E. Woo, W. Wu, M. Bernius, and L. Wujkowski, *Synth. Met.* **111**, 397 (2000).

30. B. Liu, W.-L. Yu, Y.-H. Lai, and W. Huang, *Chem. Mater.* **13**, 1984 (2001).

31. P. Herguth, X. Jiang, M. S. Liu, and A. K.-Y. Jen, *Macromolecules* **35**, 6094 (2002).

32. E. Lim, B.-J. Jung, and H.-K. Shim, *Macromolecules* **36**, 4288 (2003).

33. W. Wu, M. Inbasekaran, M. Hudack, D. Welsh, W. Yu, Y. Cheng, C. Wang, S. Kram, M. Tacey, M. Bernius, R. Fletcher, K. Kiszka, S. Munger, and J. O'Brien, *Microelectron. J.* **35**, 343 (2004).

34. J. Salbeck, N. Yu, J. Bauer, F. Weissörtel, and H. Bestgen, *Synth. Met.* **91**, 209 (1997).

35. F. Steuber, J. Staudigel, M. Stössel, J. Simmerer, A. Winnacker, H. Spreitzer, F. Weissörtel, and J. Salbeck, *Adv. Mater.* **12**, 130 (2000).

36. T. P. I. Saragi, T. Spehr, A. Siebert, T. Fuhrmann-Lieker, and J. Salbeck, *Chem. Rev.* **107**, 1011 (2007).

37. W. Kreuder, D. Lupo, J. Salbeck, H. Schenk, and T. Stehlin, U.S. Patent 5621131 (1997).

38. W.-L. Yu, J. Pei, W. Huang, and A. J. Heeger, *Adv. Mater.* **12**, 828 (2000).

39. J. Speight, *Lange's Handbook of Chemistry, 70th Anniversary Edition*, 16th edition (McGraw-Hill Professional, New York, 2004).

40. V. D. Mihailetchi, P. W. M. Blom, J. C. Hummelen, and M. T. Rispens, *J. Appl. Phys.* **94**, 6849 (2003).

41. G. G. Malliaras, J. R. Salem, P. J. Brock, and J. C. Scott, *J. Appl. Phys.* **84**, 1583 (1998).

42. M. Kemerink, J. M. Kramer, H. H. P. Gommans, and R. A. J. Janssen, *Appl. Phys. Lett.* **88**, 192108 (2006).

43. N. I. Craciun, Y. Zhang, A. Palmaerts, H. T. Nicolai, M. Kuik, R. J. .P. Kist, G. A. H. Wetzelaer, J. Wildeman, J. Vandenbergh, J. Lutsen, D. Vanderzande, and P. W. M. Blom, *J. Appl. Phys.* **107**, 124504 (2010).

44. H. Bässler, *Polym. Adv. Technol.* **9**, 402 (1998).

45. P. W. M. Blom and M. C. J. M. Vissenberg, *Mater. Sci. Eng., R* **27**, 53 (2000).

46. Y. Shen, A. R. Hosseini, M. H. Wong, and G. G. Malliaras, *ChemPhysChem* **5**, 16 (2004).

47. I. H. Campbell, P. S. Davids, D. L. Smith, N. N. Barashkov, and J. P. Ferraris, *Appl. Phys. Lett.* **72**, 1863 (1998).

48. B. K. Crone, P. S. Davids, I. H. Campbell, and D. L. Smith, *J. Appl. Phys.* **84**, 833 (1998).

49. G. G. Malliaras and J. C. Scott, *J. Appl. Phys.* **85**, 7426 (1999).

50. N. F. Mott and R. W. Gurney, *Electronic Processes in Ionic Crystals*, 2nd edition (Dover, New York, 1964).

51. F. Laquai, G. Wegner, and H. Bässler, *Phil. Trans. R. Soc. A* **365**, 1473 (2007).

52. E. M. Conwell, *Phys. Rev.* **103**, 51 (1956).

53. N. F. Mott, *Can. J. Phys.* **34**, 1356 (1956).

54. A. Miller and E. Abrahams, *Phys. Rev.* **120**, 745 (1960).

55. M. Van der Auweraer, F. C. De Schryver, P. M. Borsenberger, and H. Bässler, *Adv. Mater.* **6**, 199 (1994).

56. P. W. M. Blom, M. J. M. de Jong, and M. G. van Munster, *Phys. Rev. B* **55**, R656 (1997).

57. J. Frenkel, *Phys. Rev.* **54**, 647 (1938).

58. H. Bässler, *Phys. Status Solidi B* **175**, 15 (1993).

59. Y. N. Gartstein and E. M. Conwell, *Chem. Phys. Lett.* **245**, 351 (1995).

60. D. H. Dunlap, P. E. Parris, and V. M. Kenkre, *Phys. Rev. Lett.* **77**, 542 (1996).

61. S. V. Novikov, D. H. Dunlap, V. M. Kenkre, P. E. Parris, and A. V. Vannikov, *Phys. Rev. Lett.* **81**, 4472 (1998).

62. C. Tanase, E. J. Meijer, P. W. M. Blom, and D. M. de Leeuw, *Phys. Rev. Lett.* **91**, 216601 (2003).

63. C. Tanase, E. J. Meijer, P. W. M. Blom, and D. M. de Leeuw, *Org. Electron.* **4**, 33 (2003).

64. G. Horowitz, M. E. Hajlaoui, and R. Hajlaoui, *J. Appl. Phys.* **87**, 4456 (2000).

65. A. R. Brown, C. P. Jarrett, D. M. de Leeuw, and M. Matters, *Synth. Met.* **88**, 37 (1997).

66. G. Horowitz, R. Hajlaoui, D. Fichou, and A. El Kassmi, *J. Appl. Phys.* **85**, 3202 (1999).

67. C. D. Dimitrakopoulos, S. Purushothaman, J. Kymissis, A. Callegari, and J. M. Shaw, *Science* **283**, 822 (1999).

68. M. C. J. M. Vissenberg and M. Matters, *Phys. Rev. B* **57**, 12964 (1998).

69. C. Tanase, P. W. M. Blom, and D. M. de Leeuw, *Phys. Rev. B* **70**, 193202 (2004).

70. W. F. Pasveer, J. Cottaar, C. Tanase, R. Coehoorn, P. A. Bobbert, P. W. M. Blom, D. M. de Leeuw, and M. A. J. Michels, *Phys. Rev. Lett.* **94**, 206601 (2005).

71. I. N. Hulea, H. B. Brom, A. J. Houtepen, D. Vanmaekelbergh, J. J. Kelly, and E. A. Meulenkamp, *Phys. Rev. Lett.* **93**, 166601 (2004).

72. O. Tal, Y. Rosenwaks, Y. Preezant, N. Tessler, C. K. Chan, and A. Kahn, *Phys. Rev. Lett.* **95**, 256405 (2005).

73. N. Vukmirović and L.-W. Wang, *J. Phys. Chem. B* **115**, 1792 (2011).

74. M. Cass, M. Roberts, S. King, C. Foden, M. Pintarni, C. Coward, and A. Lee, *Role of electrical modelling in the design of high performance OLED materials*, Presentation International Simulation Workshop (Winterthur, 2010).

75. P. W. M. Blom, C. Tanase, D. M. de Leeuw, and R. Coehoorn, *Appl. Phys. Lett.* **86**, 092105 (2005).

76. N. I. Craciun, J. J. Brondijk, and P. W. M. Blom, *Phys. Rev. B* **77**, 035206 (2008).

77. N. I. Craciun, J. Wildeman, and P. W. M. Blom, *Phys. Rev. Lett.* **100**, 056601 (2008).

78. R. Coehoorn, W. F. Pasveer, P. A. Bobbert, and M. A. J. Michels, *Phys. Rev. B* **72**, 155206 (2008).

79. S. L. M. van Mensfoort, S. I. E. Vulto, R. A. J. Janssen, and R. Coehoorn, *Phys. Rev. B* **78**, 085208 (2008).

80. P. W. M. Blom, M. J. M. de Jong, and J. J. M. Vleggaar, *Appl. Phys. Lett.* **68**, 3308 (1996).

81. M. A. Lampert, *Phys. Rev.* **103**, 1648 (1956).

82. P. Mark and W. Helfrich, *J. Appl. Phys.* **33**, 205 (1962).

83. L. J. A. Koster, E. C. P. Smits, V. D. Mihailetchi, and P. W. M. Blom, *Phys. Rev. B* **72**, 085205 (2005).

84. L.-L. Chua, J. Zaumseil, J.-F. Chang, E. C.-W. Ou, P. K.-H. Ho, H. Sirringhaus, and R. H. Friend, *Nature* **434**, 194 (2005).

85. Y. Zhang, B. de Boer, and P. W. M. Blom, *Phys. Rev. B* **81**, 085201 (2010).

86. M. M. Mandoc, B. de Boer, and P. W. M. Blom, *Phys. Rev. B* **73**, 155205 (2006).

87. M. M. Mandoc, B. de Boer, G. Paasch, and P. W. M. Blom, *Phys. Rev. B* **75**, 193202 (2007).

88. C. W. Tang and S. A. VanSlyke, *Appl. Phys. Lett.* **51**, 913 (1987).

89. A. Misra, P. Kumar, M. N. Kamalasanan, and S. Chandra, *Semicond. Sci. Technol.* **21**, R53 (2006).

90. J. Kido, M. Kimura, and K. Nagai, *Science* **267**, 1332 (1995).

91. P. E. Burrows, S. R. Forrest, S. P. Sibley, and M. E. Thompson, *Appl. Phys. Lett.* **69**, 2959 (1996).

92. R. S. Deshpande, V. Bulovic, and S. R. Forrest, *Appl. Phys. Lett.* **75**, 888 (1999).

93. M. Berggren, O. Inganäs, G. Gustafsson, J. Rasmusson, M. R. Andersson, T. Hjertberg, and O. Wennerström, *Nature* **372**, 444 (1994).

94. J. Kido, H. Shionoya, and K. Nagai, *Appl. Phys. Lett.* **67**, 2281 (1995).

95. H. Suzuki and S. Hoshino, *J. Appl. Phys.* **79**, 8816 (1996).

96. M. Granström and O. Inganäs, *Appl. Phys. Lett.* **68**, 147 (1996).

97. S. Tasch, E. J. W. List, O. Ekström, W. Graupner, G. Leising, P. Schlichting, U. Rohr, Y. Geerts, U. Scherf, and K. Müllen, *Appl. Phys. Lett.* **71**, 2883 (1997).

98. C. Ego, D. Marsitzky, S. Becker, J. Zhang, A. C. Grimsdale, K. Müllen, J. D. MacKenzie, C. Silva, and R. H. Friend, *J. Am. Chem. Soc.* **125**, 437 (2011).

99. G. Tu, Q. Zhou, Y. Cheng, L. Wang, D. Ma, X. Jing, and F. Wang, *Appl. Phys. Lett.* **85**, 2172 (2004).

100. J. Liu, Z. Y. Xie, Y. X. Cheng, Y. H. Geng, L. X. Wang, X. B. Jing, and F. S. Wang, *Adv. Mater.* **19**, 531 (2007).

3 Space-charge-limited hole current in poly(9,9-dioctylfluorene) diodes

Characterization of the hole transport in blue-emitting polymers as poly(9,9-dioctylfluorene) (PFO) is strongly hindered by their large ionization potential of $\sim$ 6 eV. Using common anodes as poly(3,4-ethylenedioxythiophene)/poly(styrenesulphonic acid) leads to a strongly injection limited current. In this chapter it is demonstrated that molybdenum trioxide forms an Ohmic hole contact on PFO, enabling the observation of a space-charge-limited hole current. This allows a direct determination of the hole mobility PFO of $1.3 \times 10^{-9}\,\mathrm{m}^2/\mathrm{Vs}$ at room temperature, in good agreement with previously reported mobility values determined by time-of-flight measurements.

3.1 Introduction

A prerequisite for full-color applications and white-emitting PLEDs is an efficient blue emitter. Polyfluorenes are a promising class of blue emitters due to their wide band gap and high photoluminescence efficiency. They are commonly used as blue emissive material in PLEDs or as host component for white emitting copolymers. The wide band gap, however, also complicates the charge injection; it is difficult to achieve efficient injection for both electrons and holes. Especially hole injection can be problematic in polyfluorenes due to the typical deep HOMO level.[1] As an example, poly(9,9-dioctylfluorene) (PFO) is an attractive material to function as the blue host material in white light-emitting PLEDs due to its efficient blue emission and high mobility.[2,3] The HOMO level of PFO is located at 5.8 eV below vacuum,[4] leading to a significant hole injection barrier of 0.6 eV when combined with PEDOT:PSS which has a work function of approximately 5.2 eV.[5] Such an injection barrier will strongly hamper the hole current and limit the device performance.

3.2 Electron-Enhanced Hole Injection in PFO PLEDs

It has been shown that an Ohmic hole contact can nevertheless be formed on PFO using PEDOT:PSS by electrical conditioning the PLED.[6,7] It is usually observed that the current density-voltage (J–V) curve of PFO PLEDs with a PEDOT:PSS anode shows a switching effect in the first scan due to trapping of electrons near the anode. These trapped electrons induce an interfacial dipole and reduce the injection barrier for hole injection. After electrical conditioning the hole contact could

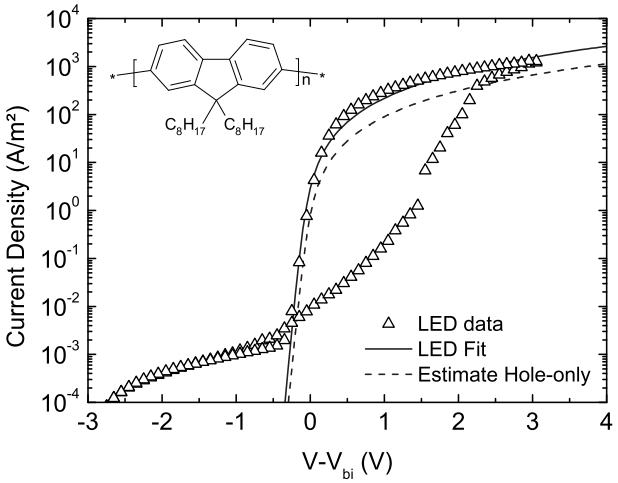

Figure 3.1. J–V characteristics of a 100 nm PFO LED using a PEDOT:PSS HIL, corrected for a built-in voltage of $V_{\mathrm{bi}} = 3.0$ V. The solid line represents the numerical fit taking into account Langevin recombination. The dotted line is the estimate of the hole-only device. The inset shows the chemical structure of PFO.

be even considered as Ohmic.[6] However, due to slow detrapping of the electrons the efficiency of the hole injection slowly decreases in time. Furthermore, since the formation of the Ohmic contact is driven by trapped electrons, this effect relies on the presence of an electron current. Accordingly a switching effect is not observed in hole-only devices of PFO and the hole current in such a device is severely injection limited.[1] Since the current is not space-charge limited (SCL) the hole mobility cannot directly be determined from hole-only devices using PEDOT:PSS as hole injection layer (HIL). In best case, an estimate of the hole mobility can be extracted from the double carrier current. In Figure 3.1 the first scan of a J–V curve of a PEDOT:PSS/PFO PLED is shown: using a numerical drift-diffusion model[8] the current-density is calculated assuming Langevin recombination. For this we assume the electron mobility to be equal to the hole mobility, an assumption which is supported by measurements of Chua *et al.* who reported similar mobilities for holes and electrons in field-effect transistors[9] and by measurements from Zhang *et al.* who reported identical mobilities for electrons and holes in MEH-PPV by disabling electron traps trough n-type doping,[10] as described in the previous chapter. Under these assumptions the PLED current can be modeled using a low-field mobility for both electrons and holes of $2 \times 10^{-9}\,\mathrm{m^2/Vs}$. This value of the mobility is comparable to values obtained by time-of-flight (TOF) measurements which range from $2 \times 10^{-9}\,\mathrm{m^2/Vs}$ to $3 \times 10^{-8}\,\mathrm{m^2/Vs}$.[3,11,12] The rather large spread of reported hole mobility values can be explained by the complex morphology of PFO.[13] It has been shown that PFO can exhibit different phases[14] and that therefore the morphology and transport properties can depend strongly on the processing conditions.

To find out if the hole transport in the PEDOT:PSS PLED after electrical conditioning is bulk limited (implying Ohmic contacts), or still limited by the hole injection, the hole mobility is measured with transient electroluminescence (TEL).[15] In this technique a voltage pulse of varying duration τ_{pulse} is applied, maintaining a constant repetition frequency. The delay time τ_{d} between this pulse and the resulting electroluminescence is derived from the relation between photocurrent and pulse length τ_{pulse}. This delay time τ_{d} is a direct measure of the transit time of the fastest carrier (holes) towards the recombination zone at the other electrode, from which the charge carrier mobility can directly be calculated. In $\mathrm{OC_1C_{10}}$-PPV the observed mobility exhibited a dependence on sample thickness, which is an indication of dispersive transport.[15] From TOF experiments on PFO[1] it has been shown that the hole transport in PFO is non-dispersive. As a result the TEL technique will provide direct information on the charge carrier mobility. The results for two PEDOT:PSS/PFO PLEDs with different thicknesses are shown in Figure 3.2. It is observed that the mobility is indeed independent of the thickness, indicating non-dispersive hole transport. From the measurements in Figure 3.2 an effective hole mobility of $\mu_{\mathrm{h}} = 2 \times 10^{-9}\,\mathrm{m^2/Vs}$ is found, in excellent agreement with the mobility as obtained from modeling of the PLED current.

3.3 Transition Metal Oxides

Recently transition metal oxides gained interest as hole injection layers in organic devices.[16,17] Specifically molybdenum trioxide ($\mathrm{MoO_3}$) has proven to be an attrac-

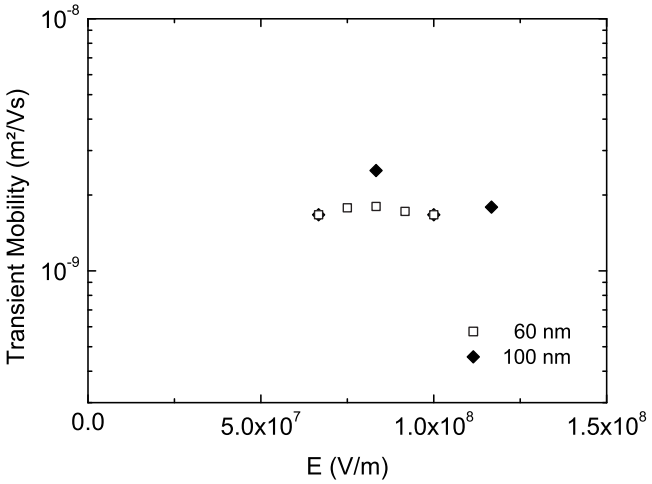

Figure 3.2. The hole mobility as a function of electric field for two devices with thicknesses of 60 nm and 100 nm, determined with transient electroluminescence (TEL).

tive material and has been used as a hole injection layer (HIL) in organic LEDs based on small molecules,[18–21] as buffer layer in organic solar cells[22,23] and as connecting layer in tandem organic LEDs.[24] The working mechanism of MoO_3 as HIL is generally ascribed to the formation of an interfacial dipole and consequently a reduction of the injection barrier.[25,26] More specifically, Kröger *et al.* reported MoO_3 to be a *n*-type material with a high electron affinity (EA) of 6.7 eV. The hole injection of MoO_3 into the semiconductor was described to proceed by electron extraction from the HOMO of the semiconductor trough the conduction band of MoO_3.[27,28] MoO_3 has also proven to be an efficient *p*-type dopant,[29,30] which can be understood from the high EA.

Single-carrier hole-only devices of PFO were fabricated, using MoO_3 as HIL. It should be noted that in this case the MoO_3 layer was evaporated as top contact and that the PEDOT:PSS bottom contact functions as an electron-blocking cathode. The top contact was evaporated trough a shadow mask at a base pressure of ca. 10^{-6} mbar and consisted of a 15 nm MoO_3 layer followed by a 100 nm aluminum capping layer. The MoO_3 layer thickness of 15 nm was found to be the optimal layer thickness with regards to device current and stability.

Figure 3.3 shows the *J*–*V* curves of three PFO hole-only devices of different thicknesses, corrected for a built-in potential of $V_{bi} = 0.25$ V. A clear quadratic dependence of the device current on the voltage is observed indicating a space-charge-limited (SCL) current. The mobility can then be directly obtained from the *J*–*V* curve using Mott-Gurney's square law (Equation 2.1). To the best of our knowledge this is first observation of a SCL current for a polymer with such a deep HOMO level.

At higher voltages a deviation from Equation 2.1 is observed for the thin devices due to the field and charge carrier density dependence of the mobility.[31,32] At

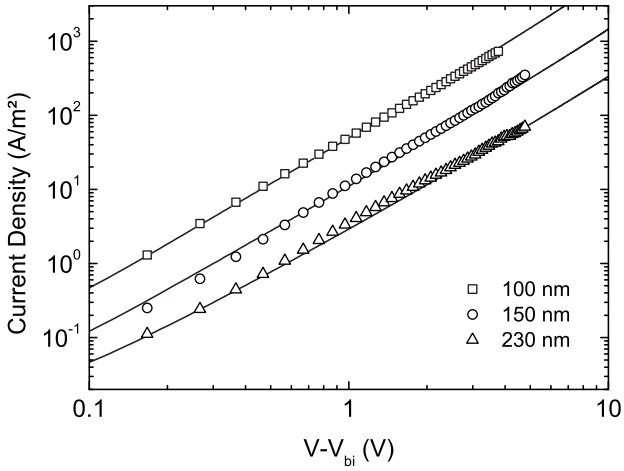

Figure 3.3. *J–V* characteristics of PFO hole-only devices with a MoO_3 HIL and fits at 295 K.

low voltages using Equation 2.1 a mobility of $1.3 \times 10^{-9}\,\mathrm{m^2/Vs}$ is obtained, which agrees very well with the mobility obtained from TEL and the double carrier current. This confirms that MoO_3 is indeed a truly Ohmic contact on PFO.

3.4 Device Modeling

Equation 2.1 is an approximation and only valid for a constant mobility, and neglecting diffusion. For a complete description, diffusion effects from the contacts,[33] the charge carrier density dependence- and field dependence of the mobility need to be taken into account. The occurrence of a SCL current enables us now to also further investigate the density- and field dependence of the hole mobility of PFO. The experimental data were therefore fitted with a numerical drift-diffusion model[8] in which the density and field dependence of the mobility are described by the EGDM (Equation 2.6).[34]

The thickness dependence (Figure 3.3) and temperature dependence (Figure 3.4) could be consistently described with a single set of parameters, $\sigma = 0.13$ eV and $N_\mathrm{s} = 1 \times 10^{28}\,\mathrm{m^{-3}}$. The same value for σ was recently found for a polyfluorene derivative by Van Mensfoort *et al.*[35] However, the value of N_s is larger than the expected physical site density. This discrepancy may result from the complicated morphology of PFO or from the use of an unsuitable mobility model. It has been suggested by Yu *et al.* that PFO exhibits a spatial correlation in the energies of the localized states[36] so that a mobility model incorporating correlation may be more appropriate for this material.[37]

The fact that the model gives a good description of the thickness dependence suggests that the MoO_3 does not diffuse into the active layer. In Figure 3.5 the resulting dependence of the hole mobility of PFO on hole density is shown for

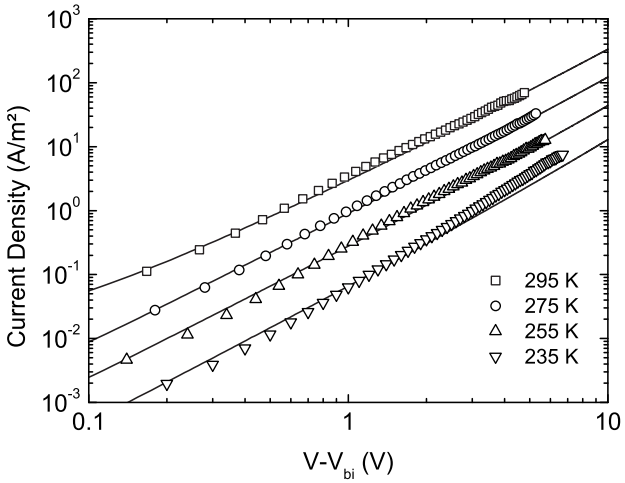

Figure 3.4. Temperature dependence of a 230 nm PFO hole-only device and fits.

various temperatures. As compared to PPV derivatives the mobility starts to rise at slightly higher carrier densities of $\sim 5 \times 10^{22}\,\mathrm{m}^{-3}$.[34] However, due to the smaller σ in PFO, which is also reflected in a higher low-field mobility, the increase of the mobility with density is weaker. This also explains why in Figure 3.3 the quadratic regime of the current density versus voltage plot is clearly discernible in the low voltage regime.

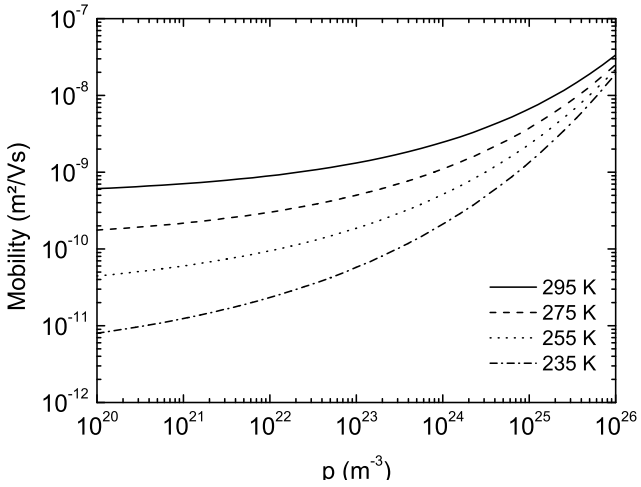

Figure 3.5. The dependence of the mobility on the charge carrier density according to the EGDM.

3.5 Conclusions

In conclusion, Ohmic hole injection was realized in a PFO hole-only device using a MoO_3 HIL. This enables us to measure a SCL current and to directly determine the hole mobility of PFO from J–V measurements, which is not possible using the common HIL PEDOT:PSS. The zero-field hole mobility was determined to be $1.3 \times 10^{-9}\,\mathrm{m}^2/\mathrm{Vs}$, agreeing well with previously reported mobilities measured by TEL and TOF. The fact that MoO_3 can form an Ohmic contact on PFO proves its potential as HIL and opens the door to the use of polymers with deeper HOMO and LUMO levels.

References

1. A. J. Campbell, D. D. C. Bradley, and H. Antoniadis, *J. Appl. Phys.* **89**, 3343 (2001).
2. A. W. Grice, D. D. C. Bradley, M. T. Bernius, M. Inbasekaran, W. W. Wu, and E. P. Woo, *Appl. Phys. Lett.* **73**, 629 (1998).
3. M. Redecker, D. D. C. Bradley, M. Inbasekaran, and E. P. Woo, *Appl. Phys. Lett.* **73**, 1565 (1998).
4. S. Janietz, D. D. C. Bradley, M. Grell, C. Giebeler, M. Inbasekaran, and E. P. Woo, *Appl. Phys. Lett.* **73**, 2453 (1998).
5. N. Koch, A. Vollmer, and A. Elschner, *Appl. Phys. Lett.* **90**, 043512 (2007).
6. D. Poplavskyy, J. Nelson, and D. D. C. Bradley, *Appl. Phys. Lett.* **83**, 707 (2003).
7. T. van Woudenbergh, J. Wildeman, P. W. M. Blom, J. J. A. M. Bastiaansen, and B. M. W. Langeveld-Voss, *Adv. Funct. Mater.* **14**, 677 (2004).
8. L. J. A. Koster, E. C. P. Smits, V. D. Mihailetchi, and P. W. M. Blom, *Phys. Rev. B* **72**, 85205 (2005).
9. L.-L. Chua, J. Zaumseil, J.-F. Chang, E. C.-W. Ou, P. K.-H. Ho, H. Sirringhaus, and R. H. Friend, *Nature* **434**, 194 (2005).
10. Y. Zhang, B. de Boer, and P. W. M. Blom, *Phys. Rev. B* **81**, 085201 (2010).
11. T. Kreouzis, D. Poplavskyy, S. M. Tuladhar, M. Campoy-Quiles, J. Nelson, A. J. Campbell, and D. D. C. Bradley, *Phys. Rev. B* **73**, 235201 (2006).
12. H.-E. Tseng, T.-H. Jen, K.-Y. Peng, and S.-A. Chen, *Appl. Phys. Lett.* **84**, 1456 (2004).
13. A. J. Cadby, P. A. Lane, H. Mellor, S. J. Martin, M. Grell, C. Giebeler, D. D. C. Bradley, M. Wohlgenannt, C. An, and Z. V. Vardeny, *Phys. Rev. B* **62**, 15604 (2000).
14. M. Grell and D. D. C. Bradley, *Adv. Mater.* **11**, 895 (1999).
15. P. W. M. Blom and M. C. J. M. Vissenberg, *Phys. Rev. Lett.* **80**, 3819 (1998).
16. S. Tokito, K. Noda, and Y. Taga, *J. Phys. D* **29**, 2750 (1996).
17. G. L. Frey, K. J. Reynolds, and R. H. Friend, *Adv. Mater.* **14**, 265 (2002).
18. H. You, Y. Dai, Z. Zhang, and D. Ma, *J. Appl. Phys.* **101**, 026105 (2007).
19. T. Matsushima, Y. Kinoshita, and H. Murata, *Appl. Phys. Lett.* **91**, 253504 (2007).

20. T. Matsushima and H. Murata, *J. Appl. Phys.* **104**, 34507 (2008).

21. H. J. Bolink, E. Coronado, D. Repetto, M. Sessolo, E. M. Barea, J. Bisquert, G. Garcia-Belmonte, J. Prochazka, and L. Kavan, *Adv. Funct. Mater.* **18**, 145 (2008).

22. V. Shrotriya, G. Li, Y. Yao, C.-W. Chu, and Y. Yang, *Appl. Phys. Lett.* **88**, 073508 (2006).

23. Y. Kinoshita, R. Takenaka, and H. Murata, *Appl. Phys. Lett.* **92**, 243309 (2008).

24. C.-W. Chen, Y.-J. Lu, C.-C. Wu, E. H.-E. Wu, C.-W. Chu, and Y. Yang, *Appl. Phys. Lett.* **87**, 241121 (2005).

25. H. Lee, S. W. Cho, K. Han, P. E. Jeon, C.-N. Whang, K. Jeong, K. Cho, and Y. Yi, *Appl. Phys. Lett.* **93**, 043308 (2008).

26. Y. Yi, P. E. Jeon, H. Lee, K. Han, H. S. Kim, K. Jeong, and S. W. Cho, *J. Chem. Phys.* **130**, 094704 (2009).

27. M. Kröger, S. Hamwi, J. Meyer, T. Riedl, W. Kowalsky, and A. Kahn, *Org. Electron.* **10**, 932 (2009).

28. M. Kröger, S. Hamwi, J. Meyer, T. Riedl, W. Kowalsky, and A. Kahn, *Appl. Phys. Lett.* **95**, 123301 (2009).

29. T. Matsushima and C. Adachi, *J. Appl. Phys.* **103**, 034501 (2008).

30. W. J. Shin, J. Y. Lee, J. C. Kim, T. H. Yoon, T. S. Kim, and O. K. Song, *Org. Electron.* **9**, 333 (2008).

31. C. Tanase, E. J. Meijer, P. W. M. Blom, and D. M. de Leeuw, *Phys. Rev. Lett.* **91**, 216601 (2003).

32. Y. Roichman, Y. Preezant, and N. Tessler, *Phys. Status Solidi A* **201**, 1246 (2004).

33. N. I. Craciun, J. J. Brondijk, and P. W. M. Blom, *Phys. Rev. B* **77**, 035206 (2008).

34. W. F. Pasveer, J. Cottaar, C. Tanase, R. Coehoorn, P. A. Bobbert, P. W. M. Blom, D. M. de Leeuw, and M. A. J. Michels, *Phys. Rev. Lett.* **94**, 206601 (2005).

35. S. L. M. van Mensfoort, S. I. E. Vulto, R. A. J. Janssen, and R. Coehoorn, *Phys. Rev. B* **78**, 085208 (2008).

36. Z. G. Yu, D. L. Smith, A. Saxena, R. L. Martin, and A. R. Bishop, *Phys. Rev. Lett.* **84**, 721 (2000).

37. M. Bouhassoune, S. L. M. van Mensfoort, P. A. Bobbert, and R. Coehoorn, *Org. Electron.* **10**, 437 (2009).

4 Guest-concentration dependence of the mobility in a fluorene-arylamine host-guest system

In this chapter the charge transport in a polyspirobifluorene derivative with copolymerized N,N,N',N'-tetraaryldiamino biphenyl (TAD) hole transport units is investigated as a function of the TAD content. For TAD concentrations larger than 5% guest-to-guest transport is observed. It is demonstrated that in this regime the charge carrier density dependent mobility can be described consistently with the Extended Gaussian Disorder Model, with a density of hopping sites which is proportional to the TAD concentration and comparable to the molecular density.

4.1 Introduction

In the previous chapter it was shown that the transition metal oxide MoO_3 can be used to fabricate an Ohmic hole contact on PFO. For the PFO hole-only devices the MoO_3 layer was used as a hole injecting top contact, while generally in PLEDs the cathode is evaporated as top contact. For PLEDs, the MoO_3 layer should therefore be used as bottom contact, or as top contact of an inverted structure with a bottom cathode. However, spincoating on low work function cathode materials is difficult due to the inherent reactivity of low work function materials. Additionally, it was found that spincoating on MoO_3 also was problematic. Another approach to improve the hole injection and transport in polyfluorene derivatives is the incorporation of arylamines. In this chapter the hole transport in such a copolymer is investigated.

4.2 Fluorene - Amine Copolymers

As shown in the previous chapter, the hole transport in PFO can be described by a mobility that depends on the electric field and the charge carrier density. A numerically exact description of the mobility in a Gaussian DOS, extended to include the dependence on the charge carrier density (EGDM), has been obtained from a master equation (ME) approach.[1] In this model, the mobility is characterized by three parameters, *viz.* the width (standard deviation) of the Gaussian DOS σ, the density of hopping sites N_s and the mobility in the limit of zero field, zero carrier density and infinite temperature, μ_0^*. Within the ME approach employed to derive the EGDM mobility functions, the hopping is assumed to take place between point-like sites on a cubic lattice. The question arises what the relationship is between the site density parameter N_s and the physical density of localized molecular states between which the hopping takes place. In this chapter, this question is addressed by studying the hole transport in a series of polyalkoxyspirobifluorene-N,N,N',N'-tetraaryldiamino biphenyl (PSF-TAD) copolymers. These materials belong to a larger class of polyfluorene derivatives within which the injection and transport of holes is modified by the incorporation of arylamines, either blended in the active layer or incorporated into the polymer chain.[2] Triarylamines are known to be good hole conductors[3] and are commonly used as hole transport layers.[4,5] Hole mobilities up to $3 \times 10^{-7}\,\mathrm{m^2/Vs}$ have been measured in fluorene-triarylamine copolymers.[6]

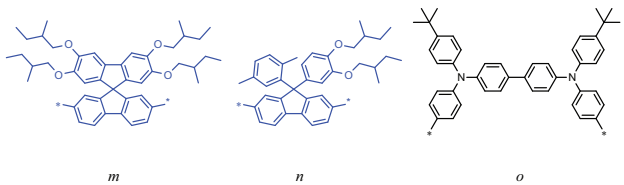

Figure 4.1. Structure of the blue-emitting PSF-TAD polymer. The concentration of the TAD unit is varied from $o = 0$ to 12.5 mol.%. The composition of the host material is $m = 50$ mol.% and $n = (50 - o)$ mol.%.

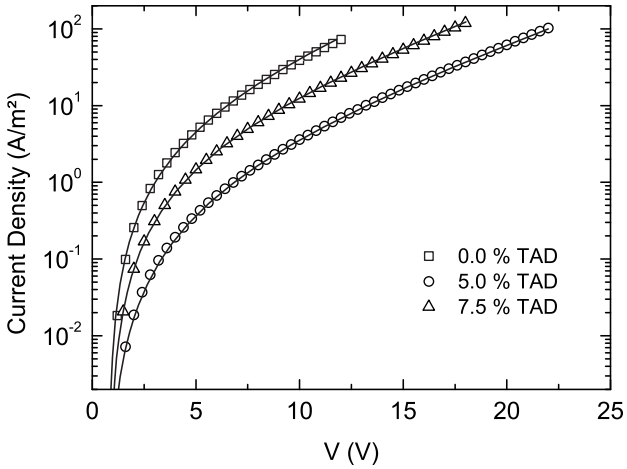

Figure 4.2. Current-density - voltage (J–V) characteristics at TAD concentrations of 0%, 5% and 7.5% and with a layer thickness of 207 nm, 215 nm and 198 nm, respectively. The curves are best fits from the device model.

Furthermore, the hole transport can be tuned by varying the arylamine content, under the condition that their HOMO energy is higher than that of the host polymer.[7] At low concentrations the amine units act then as hole traps and reduce the hole current, whereas above a critical concentration, typically $\sim 3\%$,[8] percolation can take place between the amine units and the hole transport will become governed by guest-to-guest hopping, leading to an increase of the mobility with increasing amine concentration.[9] The EGDM transport parameters are then expected to be related to the guest DOS. For sufficiently dilute systems, one might envisage that σ is independent of the amine concentration and that N_s is equal to, or at least proportional to the guest density. However, such relationships have so far not been established experimentally.

4.3 Guest-to-Guest Transport

The TAD hole transport unit studied here is functionalized with two tert-butyl groups and it is copolymerized in a polyalkoxyspirobifluorene (PSF) polymer. The structure of the copolymer is depicted in Figure 4.1. The HOMO levels of PSF and the TAD unit have been estimated at -5.6 eV and -5.4 eV, respectively.[10,11] The TAD concentration was varied from 5 to 12.5 mol%, enabling a systematic study of the influence of the TAD concentration on the guest-to-guest hole transport. Hole-only devices with a PSF-TAD layer thickness equal to (approximately) 80, 120, 200 and 280 nm were studied.

Figure 4.2 shows the room temperature current-density - voltage (J–V) characteristics of devices with an active layer thickness of $\sim$ 200 nm and a TAD concentration of 5% and 7.5%, and Figure 4.3 shows the current density as a function of the TAD concentration measured at 10 V. As a reference, also the results for

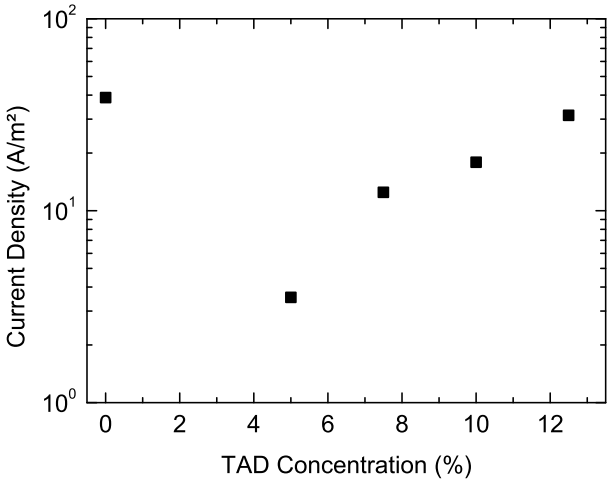

Figure 4.3. Current density at 10V as a function of the TAD concentration for the ~ 200 nm systems studied.

the PSF host polymer are given (0% TAD concentration). As in an earlier study for a similar type of copolymer, the inclusion of 5% TAD lowers the hole current by approximately one order of magnitude compared to the hole current in the pure PSF polymer.[8] No data are available for TAD concentrations below 5%. It can therefore not firmly be established whether at 5% the TAD units act still as traps for the hole transport through the polyspirobifluorene host. However, for TAD concentrations of 7.5% and above the hole transport increases with increasing TAD concentration, demonstrating the occurrence of guest-to-guest hopping for these concentrations. A simplified analysis of the J–V curves, using the Mott-Gurney equation[12] (Equation 2.1) which neglects diffusion and which assumes a constant mobility, gives rise to an effective mobility of approximately 8×10^{-11} m^2/Vs for the pure (0%) reference polymer, in reasonable agreement with the result of earlier time-of-flight measurements on a similar copolymer.[13] In that study the mobility could be increased beyond the host mobility by the inclusion of 50% TAD.

4.4 Device Modeling

To take the effects of disorder on the carrier density dependence and field dependence of the mobility as described within the EGDM into account, the numerical drift-diffusion model developed in Ref. 14 has been used. The voltage, temperature and layer thickness dependence of the current density are analyzed to obtain the parameters describing the mobility function in the guest-to-guest hopping regime (TAD concentration $> 5\%$). The polymer with 5% TAD is included, although it is not a priori clear whether the transport is then already well within this regime. The PEDOT:PSS contact is assumed to be Ohmic. For each polymer, a least-squares method was used to fit the dependence on voltage, thickness and temperature to

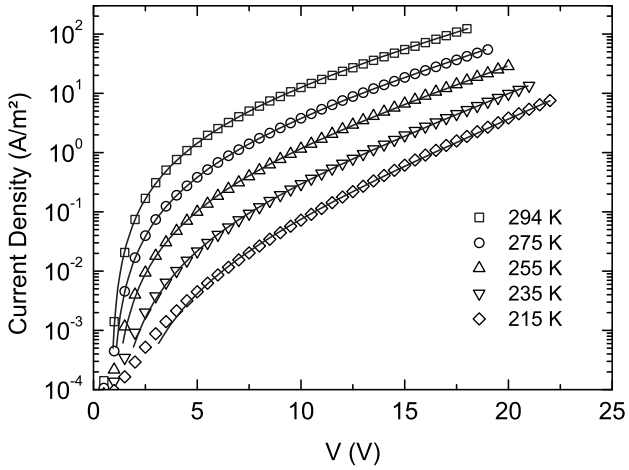

Figure 4.4. Temperature dependent hole transport at 7.5% TAD and fits to the EGDM, for a 198 nm device.

the EGDM equations using a common set of parameters σ, N_s and $\mu_0(T)$.

Figure 4.4 shows the measured and calculated temperature dependence of the J–V curves for a 198 nm device with a TAD concentration of 7.5%, with $V_{bi} = 1.6$ V. Figure 4.5 shows the measured and calculated $1/T^2$ dependence of $\mu_0(T)$. The mobility is found to scale excellently with $1/T^2$ according to $\mu_0(T) = \mu_0^* \exp\left[-C\hat{\sigma}^2\right]$ with $\hat{\sigma} \equiv \sigma/k_B T$ (Equation 2.6). For the systems studied, C ranged from ~ 0.42 to ~ 0.47, with an error margin of approximately ± 0.04.

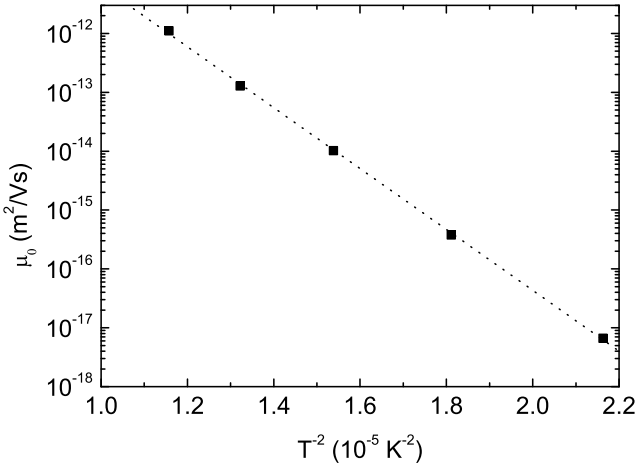

Figure 4.5. The $1/T^2$ dependence of the determined values of $\mu_0(T)$ for the polymer with 7.5% TAD.

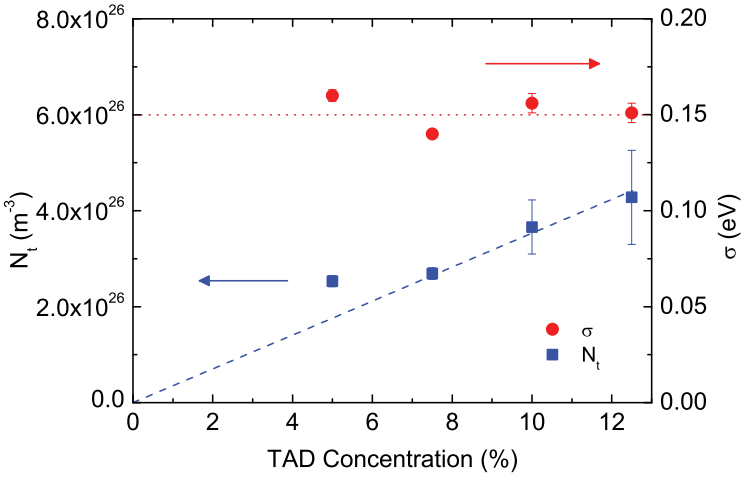

Figure 4.6. Optimal values of N_s and σ for each polymer. The experimental uncertainties are similar to the symbol sizes, or as indicated. The dashed and dotted lines are a guide to the eye.

The values found are close to the value 0.42 given in Ref. 1 or 4/9 in Ref. 15. The values of V_{bi} ranged from 1.45 to 1.75 V for the various samples, perhaps because of variations of the dipole layer formed at the cathode interface. Well above V_{bi}, the shape of the J–V curves is almost independent of V_{bi}, greatly facilitating the accurate determination of the EGDM parameters.

4.5 Conclusions

Figure 4.6 shows the optimal values of N_s and σ for each polymer. The error margins indicate the range of values of N_s and σ for which the fit error (defined as the sum of the squares of the logarithmic deviation) is within 3% of the minimum fit error. The width of the Gaussian DOS needed to fit the data is close to $\sigma = 0.15$ eV, essentially independent of the TAD concentration. For a TAD concentration of 7.5% and above, the TAD concentration dependence of N_s is, taking the error margins into account, well described by the proportionality relation given by the dashed line in Figure 4.6. For the concentration of 5%, N_s is slightly higher than expected, which might be due to the possibility that at this concentration the charge transport is in an intermediate regime where both the TAD units and the fluorene units contribute to the transport. In this regime, a more complicated model is required.[16] It should be noted that for higher concentrations the quality of the fit was less sensitive to the value of N_s, leading to a large error margin in N_s.

The hopping site density, as roughly estimated by assuming a density of 1 g/cm^{-3} for the polyspirobifluorene copolymer and assuming two transport sites per TAD unit, is equal to $\sim 2 \times 10^{26}$ m^{-3} for the 10% copolymer. The value of

N_s obtained from the present transport study ($\sim 3.5 \times 10^{26}\,\mathrm{m}^{-3}$) is in reasonable agreement with this estimate. This supports the point of view that the parameters as obtained when describing the transport properties within the EGDM are physically meaningful.

In conclusion, it is found that the hole transport in the polyspirobifluorene copolymers as studied in the guest-to-guest regime is well-described using the EGDM. The analysis supports the point of view that the parameters obtained, describing the Gaussian DOS, are physically meaningful. Firstly, the site density N_s is found to be proportional to the TAD concentration and reasonably close to the actual molecular site density. Secondly, the disorder parameter σ (~ 0.15 eV), is found to be essentially independent of the TAD concentration, as expected for sufficiently dilute systems. The results open the prospect that the EGDM can also provide the appropriate framework for describing the guest concentration dependence of the charge carrier transport in other host-guest systems operating in the guest-to-guest regime, including dye-doped fluorescent and phosphorescent emissive layers in small-molecule based OLEDs at high dye-concentrations.

References

1. W. F. Pasveer, J. Cottaar, C. Tanase, R. Coehoorn, P. A. Bobbert, P. W. M. Blom, D. M. de Leeuw, and M. A. J. Michels, *Phys. Rev. Lett.* **94**, 206601 (2005).
2. E. Bellmann, S. E. Shaheen, S. Thayumanavan, S. Barlow, R. H. Grubbs, S. R. Marder, B. Kippelen, and N. Peyghambarian, *Chem. Mater.* **10**, 1668 (1998).
3. M. Stolka, J. F. Yanus, and D. M. Pai, *J. Phys. Chem.* **88**, 4707 (1984).
4. A. W. Grice, D. D. C. Bradley, M. T. Bernius, M. Inbasekaran, W. W. Wu, and E. P. Woo, *Appl. Phys. Lett.* **73**, 629 (1998).
5. C. W. Tang and S. A. VanSlyke, *Appl. Phys. Lett.* **51**, 913 (1987).
6. M. Redecker, D. D. C. Bradley, M. Inbasekaran, W. W. Wu, and E. P. Woo, *Adv. Mater.* **11**, 241 (1999).
7. S. Harkema, R. A. H. J. Kicken, B. M. W. Langeveld-Voss, S. L. M. van Mensfoort, M. M. de Kok, and R. Coehoorn, *Org. Electron.* **11**, 755 (2010).
8. R. J. de Vries, S. L. M. van Mensfoort, V. Shabro, S. I. E. Vulto, R. A. J. Janssen, and R. Coehoorn, *Appl. Phys. Lett.* **94**, 163307 (2009).
9. D. M. Pai, J. F. Yanus, and M. Stolka, *J. Phys. Chem.* **88**, 4714 (1984).
10. L.-B. Lin, R. H. Young, M. G. Mason, S. A. Jenekhe, and P. M. Borsenberger, *Appl. Phys. Lett.* **72**, 864 (1998).
11. F. Laquai and D. Hertel, *Appl. Phys. Lett.* **90**, 142109 (2007).
12. N. F. Mott and R. W. Gurney, *Electronic Processes in Ionic Crystals*, 2nd edition (Dover, New York, 1964).
13. F. Laquai, G. Wegner, C. Im, H. Bässler, and S. Heun, *J. Appl. Phys.* **99**, 023712 (2006).
14. S. L. M. van Mensfoort and R. Coehoorn, *Phys. Rev. B* **78**, 085207 (2008).
15. H. Bässler, *Phys. Status Solidi B* **175**, 15 (1993).
16. Y. Y. Yimer, P. A. Bobbert, and R. Coehoorn, *J. Phys.: Condens. Matter* **20**, 335204 (2008).

5 Charge transport and recombination in polyspirobifluorene blue light-emitting diodes

The charge transport in blue light-emitting polyspirobifluorene PLEDs is investigated by both steady-state current-voltage measurements and transient electroluminescence. Both measurement techniques yield consistent results and show that the hole transport is space-charge limited. The electron current is found to be governed by a high intrinsic mobility in combination with electron traps. Numerical simulations on light-emitting diodes reveal a shift of the recombination zone from the cathode to the anode with increasing bias.

5.1 Introduction

A critical issue for the efficiency of PLEDs is the charge balance. Polyfluorene PLEDs have been reported to exhibit an unbalanced charge transport and to be dominated by electrons.[1,2] However, polyfluorene derivatives often have a high ionization potential resulting in an injection barrier for holes,[3] as described in Chapter 3. It is therefore not always clear whether the unbalanced transport is the result of an intrinsic unbalanced charge transport or the result of an unbalanced charge injection. As described in the previous chapter, triarylamines are commonly used to improve the hole transport. The device operation of such a copolymer based PLED is more complicated as compared to conventional PLEDs based on for example PPV derivatives. In PPV the mobility of electrons and holes is identical,[4] facilitating the understanding of the trap-limited electron transport that is typically described by an exponential distribution of states in the band gap.[5] In a copolymer, however, the hole transport is modified by the presence of the triarylamine units, such that the hole and electron mobility are not necessarily equal. In order to disentangle the various processes the charge transport of a blue-emitting polyspirobifluorene copolymer is studied by both steady-state current-voltage (J–V) and time-resolved electroluminescence measurements.

The polyalkoxyspirobifluorene (PSF) polymer studied in this chapter is a copolymer containing 3 monomers including a N,N,N',N'-tetraaryldiamino biphenyl (TAD) hole transport unit. The hole transport in this material has been investigated in the previous chapter. The PSF-TAD copolymer with a concentration of 10 mol.% functions as the blue backbone material for a white emitting copolymer described in Chapter 8.[6,7] A detailed understanding of the charge transport in the blue backbone polymer is a prerequisite for the understanding of the device operation of the white light emitting diode.

5.2 Steady-State Current-Voltage Measurements

PLEDs and single-carrier devices of the polyspirobifluorene copolymer PSF-TAD were fabricated and characterized by steady-state and transient measurements. The hole transport as characterized in Chapter 4 showed a voltage and thickness dependence indicative of a space-charge limited hole current. The effective zero-field mobility can then be directly obtained from the J–V characteristics using the Mott-Gurney law[8] (Equation 2.1) The room temperature hole mobility at low electric fields was determined to be $\mu_0(T) = 1 \times 10^{-11}\,\mathrm{m^2/Vs}$.

In contrast to the hole current, the electron-only devices exhibit steep J–V curves with a strong dependence on the polymer layer thickness (Figure 5.6), indicative of trap-limited conduction with an exponential energy distribution of traps as also has been observed for PPV derivatives.[9] In that case, the electron current can be expressed analytically by the Mark and Helfrich expression[10] (Equation 2.9). As described in Chapter 2, the magnitude of a trap-limited current depends on the mobility of the free charge carriers as well as the amount and energy distribution of the traps. From J–V measurements only it is therefore not possible to independently determine the mobility of the free carriers and the amount of

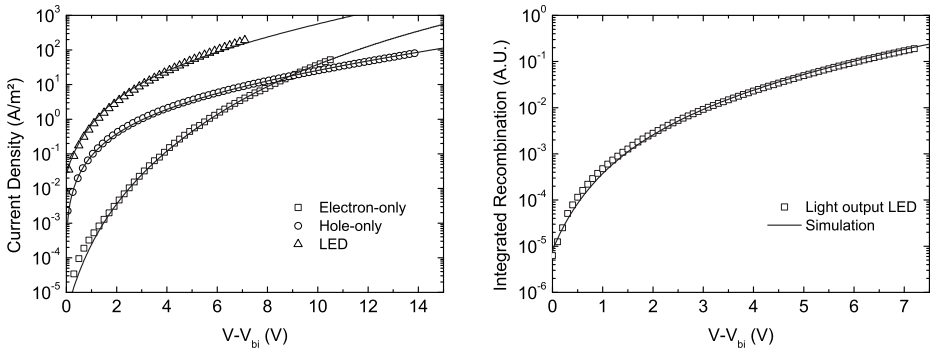

(a) (b)

Figure 5.1. (a) J–V characteristics of hole-only, electron-only and double carrier devices with an active layer thickness of ~ 180 nm. There is a cross-over point between the J–V curves of the hole-only device and the electron-only device at $V - V_{\mathrm{bi}} = 9$ V. Solid lines represent the modeling results. (b) The light output of the PLED and calculated integral of the recombination in arbitrary units.

traps. For PPV derivatives it has been demonstrated that the electron mobility is equal to the hole mobility by passivating the electron traps with the n-type dopant dimethylcobaltocene.[4] A similar result was obtained by Chua *et al.* who reported similar intrinsic mobilities of electrons and holes in transistors.[11] However, as described in the previous chapter, for the polyspirobifluorene polymer studied here the hole transport is governed by the presence of TAD hole transporting units,[12,13] which makes such an assumption questionable. As a result, Equation 2.9 can only be used to obtain an estimate for T_{t} from the thickness dependence of the PSF-TAD electron current, which yielded $T_{\mathrm{t}} = 1750$ K.

Figure 5.1(a) shows the electron-, hole- and double carrier current at room temperature for a polymer thickness of $L \approx 180$ nm. A cross-over point in the J–V curves of the hole current and electron current is observed, suggesting that the double carrier device is dominated by holes below a voltage of $V - V_{\mathrm{bi}} = 9$ V, and dominated by electrons above this voltage where the electrons traps become filled. This cross-over already indicates that the intrinsic trap-free electron-mobility must be higher than the hole mobility. Figure 5.2 shows the normalized current efficiency (light output/current) of the PLED. The current efficiency increases up to a maximum value at a bias of $V - V_{\mathrm{bi}} = 5$ V above the built-in voltage, after which it slowly decreases with increasing bias.

5.3 Transient electroluminescence Measurements

To obtain an independent measure for the electron mobility transient electroluminescence (TEL) measurements were performed.[14,15] This measurement technique is based on the delay time between the application of a voltage pulse and the onset of light emission. When a voltage is applied to the PLED charges are injected from

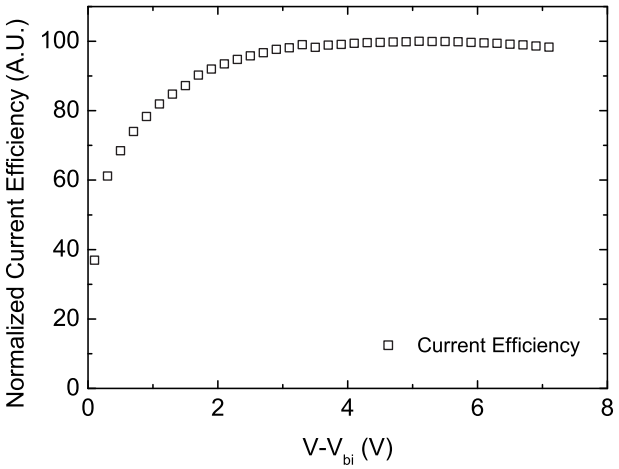

Figure 5.2. Normalized current efficiency of a PLED with an active layer thickness of 180 nm. The current efficiency increases with increasing bias up to a maximum at $V - V_{\mathrm{bi}} = 5$ V.

both electrodes and travel towards each other driven by the electric field. When the two types of charges meet, an exciton can be formed which can decay radiatively. Due to the time required for the charge carriers to travel towards each other, there is a delay between the application of a voltage pulse and the onset of light emission. Assuming that one of the two charge carrier types is dominant, this time delay represents the transit time through the polymer layer for the fastest charge carrier type. Neglecting diffusion and on the assumption of a constant mobility, the transient mobility can then be estimated using

$$\mu = \frac{L^2}{\tau(V_{\mathrm{pulse}} - V_{\mathrm{bi}})}, \tag{5.1}$$

with L the active layer thickness, V_{pulse} the voltage pulse height, and V_{bi} the built-in voltage. A sensitive method to measure the delay time also at low light intensities is to apply a voltage pulse train with an increasing pulse width to the PLED and then measure the integrated light emission.[16] If the pulse width is too short, the charges do not have enough time to reach each other and no light emission will be detected. When the pulse width is long enough, light emission will occur, and the integrated light-output scales linearly with the pulse width. By extrapolating this linear regime to small pulse width a measure for the delay time τ can be obtained. Since light output is required for a TEL measurement, this technique can only be employed on double carrier devices and it is therefore not known a priori which type of charge carrier determines the transit time and the measured mobility. To distinguish whether the measured transit times originate from electrons or holes double layer devices have been fabricated, consisting of the polymer layer and a

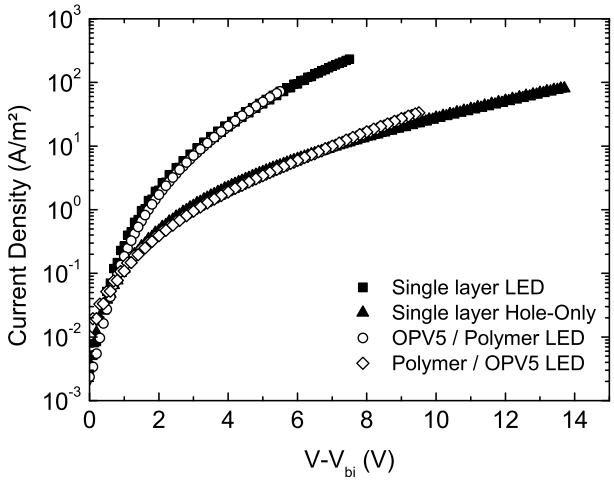

Figure 5.3. J–V characteristics of single- and double-layer devices. The single-layer devices have an active polymer layer thickness of 200 nm, the double-layer devices have a polymer layer thickness of 200 nm with an additional 40 nm OPV5 layer either between the polymer layer and the cathode, or between the polymer layer and the anode. The inclusion of the OPV5 layer between the anode and the polymer layer does not significantly affect the device current. The inclusion of the OPV5 layer between the polymer and the cathode lowers the device current to the level of the polymer hole-only device.

thin ($L \sim 40$ nm) layer of the oligomer *p*-Bis(*p*-styrylstyryl)benzene (OPV5). This oligomer can be evaporated and is insoluble in toluene, allowing it to be deposited either before or after spincoating of the polymer layer. The HOMO levels of OPV5 and the TAD unit have both been estimated at ~ -5.4 eV.[17,18] The HOMO levels of both materials are therefore expected to align relatively well. As a result there is no significant injection barrier for holes expected when a thin OPV5 layer is deposited between the anode and the PSF-TAD layer. Indeed, we observe that such an additional OPV5 layer of 40 nm gives rise to an approximately equal device current as compared to the 200 nm single-layer PLED (Figure 5.3), in spite of the increased total layer thickness. This confirms the absence of an injection barrier of holes. The OPV5 oligomer has a smaller band gap (~ 2.6 eV) than the blue-emitting PSF-TAD (~ 3.1 eV), emitting yellow light. An injection barrier for electrons is therefore expected when the OPV5 layer is placed on top of the polymer layer. In Figure 5.3 it is demonstrated that for this case the double carrier current is reduced to the level of the single-layer hole-only device. This clearly shows that the electron injection into the polymer layer is now suppressed to such an extent that the device current is completely dominated by holes.

Figure 5.4 shows the transient mobilities obtained from TEL measurements on single- and double-layer LEDs with the OPV5 layer in between the polymer layer and the cathode. In the double layer PLED the electrons face an injection barrier at the OPV5/polymer interface and accumulate in the OPV5 layer. Holes have to travel through the polymer layer and recombine with electrons in the OPV5 layer.

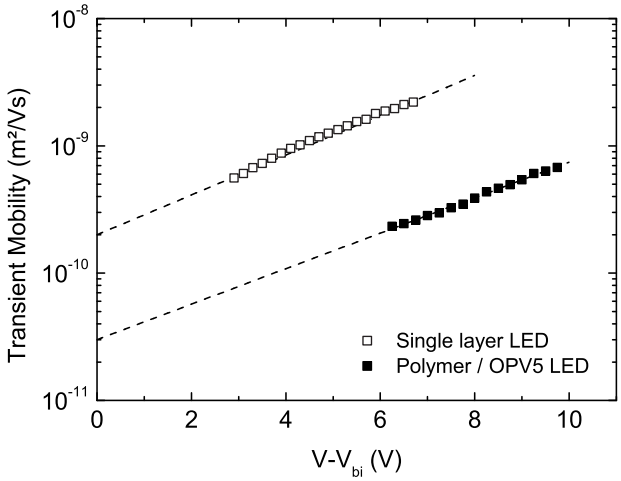

Figure 5.4. Transient mobility of single- and double-layer devices with a polymer layer thickness of 200 nm. The transient mobility of the double layer device (dominated by the holes transport) is one order of magnitude lower than the transient mobility of the single-layer device (dominated by electron transport).

The yellow emission from this double layer device confirms that the recombination in these double layer devices indeed takes place in the OPV5 layer. As a result the TEL measurements in a double layer device reflect the transport properties of holes in the polyspirobifluorene. We observe that the transient mobility of the double layer device is approximately one order of magnitude lower than the transient mobility of the single-layer PSF-TAD PLED. This clearly demonstrates that the faster transit times of the single-layer devices must originate from the electron transport. The hole mobilities measured in the double layer devices extrapolate to a zero-field mobility of $\sim \mu_0(T) = 10^{-11}\,\mathrm{m}^2/\mathrm{Vs}$ which is in agreement with the zero-field mobility obtained from the steady-state J–V measurements. The electron mobility as measured in the single-layer device is one order of magnitude larger than the hole mobility and extrapolates to a zero-field mobility of $\sim \mu_0(T) = 10^{-10}\,\mathrm{m}^2/\mathrm{Vs}$. The higher electron mobility as observed in these TEL measurements is also in agreement with the cross-over of the hole- and electron current (Figure 5.1(a)), showing a better electron transport once sufficient traps are filled.

5.4 Device Modeling

The mobilities obtained by the TEL measurements on the single-carrier devices serve as input to model the electrical characteristics of the light-emitting diode. We apply a numerical device model which solves the continuity and Poisson equations using an iterative scheme.[19] The model takes into account both drift and diffusion of charge carriers, a density dependent mobility[20] and recombination of the Langevin-type.[21] The electric field and density dependence of the hole mobility

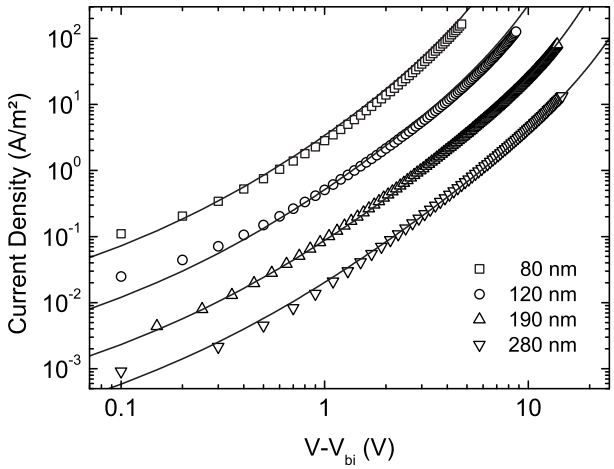

Figure 5.5. J–V characteristics and simulation of hole-only devices with different thicknesses. The hole transport can be modeled with one set of parameters, $\mu_0^* = 1.3 \times 10^{-6}\,\mathrm{m^2/Vs}$, $N_\mathrm{s} = 3.6 \times 10^{26}\,\mathrm{m^{-3}}$, and $\sigma = 0.15$ eV.

are defined by the EGDM[22] and governed by 3 parameters: the site density N_s, the width of the Gaussian distribution of density of states σ and the mobility in the limit of zero field, zero carrier density, and infinite temperature μ_0^*. The temperature and thickness dependence (Figure 5.5) of the hole current could be consistently modeled using the fit parameters: $\mu_0^* = 1.3 \times 10^{-6}\,\mathrm{m^2/Vs}$, $N_\mathrm{s} = 3.6 \times 10^{26}\,\mathrm{m^{-3}}$ and $\sigma = 0.15$ eV, as established in Chapter 4. A relative dielectric constant of $\varepsilon_\mathrm{r} = 3.1$ was obtained from impedance spectroscopy measurements, and a built-in voltage of $V_\mathrm{bi} \approx 1.3$ V was used. At low electric field and low charge carrier densities, these parameters yield a mobility in the order of $\mu_0(T) = 10^{-11}\,\mathrm{m^2/Vs}$ which agrees well with the zero-field mobility found using Equation 2.1. The found value of σ is higher than reported for other arylamine containing polyfluorenes[23,24] which suggests that the polymer studied here has a larger energetic disorder.

As shown above the transient electron mobility was found to be approximately one order higher than the transient hole mobility. However, the question still arises whether the measured transient electron mobility is an effective mobility, which is influenced by the presence of electron traps. The temperature, thickness and voltage dependence of the electron current can be consistently described by the parameters: $\mu_0^* = 1.8 \times 10^{-6}\,\mathrm{m^2/Vs}$, $N_\mathrm{s} = 1.3 \times 10^{26}\,\mathrm{m^{-3}}$ and $\sigma = 0.12$ eV for the free electron mobility, in combination with an exponential electron trap distribution with a trap density $N_\mathrm{t} = 6.5 \times 10^{23}\,\mathrm{m^{-3}}$ and $T_\mathrm{t} = 1750$ K (Figure 5.6). A built-in voltage of $V_\mathrm{bi} \approx 0.5$ V was used. The resulting free electron mobility at room temperature and low fields is one order of magnitude larger than the measured transient mobility. This is likely due to the fact that the parameters used to model the J–V characteristics describe the intrinsic trap-free electron mobility, in contrast to the trapping-dependent transient mobility.

By combining the parameters for the hole and electron transport the double

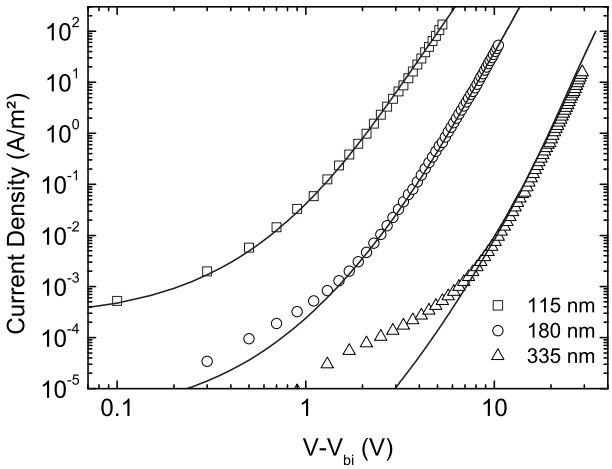

Figure 5.6. J–V characteristics and simulation of electron-only devices with different thicknesses. The electron transport can be modeled with the mobility parameters $\mu_0^* = 1.8 \times 10^{-6}\,\mathrm{m^2/Vs}$, $N_\mathrm{s} = 1.3 \times 10^{26}\,\mathrm{m^{-3}}$, and $\sigma = 0.12$ eV, with the inclusion of electron traps distributed exponentially in energy characterized by $N_\mathrm{t} = 6.5 \times 10^{23}\,\mathrm{m^{-3}}$ and $T_\mathrm{t} = 1750$ K.

carrier device can be modeled (Figure 5.1(a)). The numerical calculations carried out on the PSF-TAD based PLED provide insight into internal quantities that are otherwise inaccessible, such as the distribution of the electric field and the concentration profiles of the electrons and holes. Of direct relevance for the quantum efficiency as well as the outcoupling efficiency of the generated excitons is the position of the recombination zone inside the PLED. In PPV-based PLEDs it has been demonstrated that the recombination zone is located close to the cathode due to the poor electron transport, leading to quenching of the excitons at the metallic cathode.[25] With increasing bias the distribution moves on average slightly away from the cathode, giving rise to an increase of the efficiency. In the PSF-TAD PLEDs, as shown in Figure 5.7, the recombination zone shifts completely from the cathode towards the anode with increasing bias. This is due to the combination of a relative low hole mobility, a relative high electron mobility and the presence of electron traps. A similar shift of the recombination zone was observed in a different fluorene-amine copolymer.[26]

As shown in Figure 5.1(a) at low bias the PLED is hole dominated and the recombination zone is located at the cathode. For a sufficiently high bias the electron traps are filled and the electron currents surpasses the hole current due to the higher mobility of the free electrons. In that case the recombination is shifted towards the anode. At an intermediate bias of $V - V_\mathrm{bi} = 5$ V the recombination zone is relatively spread out in the center of the active layer. This point corresponds exactly to the maximum in the current efficiency as shown in Figure 5.2. This shows that the dependence of the current efficiency on voltage is the result of the shift of the recombination zone. The maximum efficiency is obtained at the voltage

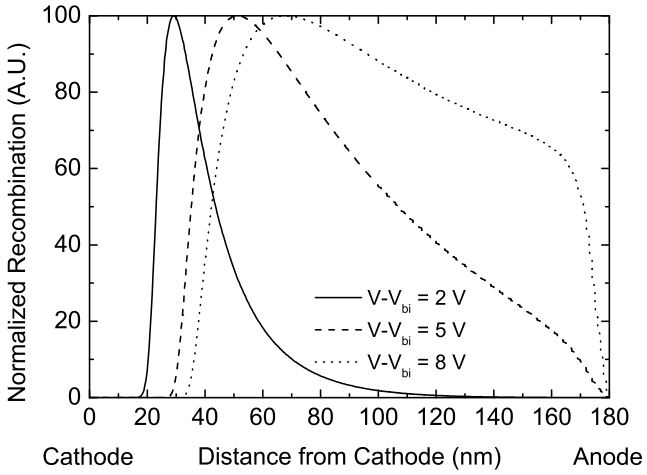

Figure 5.7. Distribution of the recombination zone in the PLED. A shift in the location of the recombination zone is observed with increasing bias. At higher bias the recombination shifts away from the cathode.

where the best combination is obtained between reduced quenching losses at the electrodes and an enhanced outcoupling. The average distance of the recombination profile from the cathode amounts to 50 nm for the blue-emitting polyspirobifluorene PLED.

5.5 Conclusions

The charge transport in PLEDs based on a blue-emitting polyspirobifluorene derivative has been investigated. Steady-state current voltage measurements and TEL measurements both show that the intrinsic electron mobility is significantly larger than the hole mobility, but the electron current is reduced by the presence of electron traps. The combination of a high intrinsic electron mobility with the presence of electron traps results in a cross-over point in the J–V curves of the electron current and the hole current. For the PLED this leads to a large shift of the recombination zone depending on the applied voltage. Ideally, the recombination zone is located in the middle of the emissive layer where the quenching at the electrodes is minimized and the optical outcoupling is maximized. To optimize the performance of the PLED it is therefore necessary to tune the mobilities of the electrons and holes such that the recombination is located at typically 50 nm away from the cathode.

References

1. M. Inbasekaran, E. Woo, W. Wu, M. Bernius, and L. Wujkowski, *Synt. Met.* **111**, 397 (2000).
2. T. Miteva, A. Meisel, W. Knoll, H. G. Nothofer, U. Scherf, D. C. Müller, K. Meerholz, A. Yasuda, and D. Neher, *Adv. Mater.* **13**, 565 (2001).
3. A. J. Campbell, D. D. C. Bradley, and H. Antoniadis, *J. Appl. Phys.* **89**, 3343 (2001).
4. Y. Zhang, B. de Boer, and P. W. M. Blom, *Phys. Rev. B* **81**, 085201 (2010).
5. M. M. Mandoc, B. de Boer, and P. W. M. Blom, *Phys. Rev. B* **73**, 155205 (2006).
6. D. Buchhauser, M. Scheffel, W. Rogler, C. Tschamber, K. Heuser, A. Hunze, G. Gieres, D. Henseler, W. Jakowetz, K. Diekmann, A. Winnacker, H. Becker, A. Büssing, A. Falcou, L. Rau, S. Vögele, and S. Göttling, *Proc. SPIE-Int. Soc. Opt. Eng.* **5519**, 70 (2004).
7. M. A. Parshin, J. Ollevier, M. Van der Auweraer, M. M. de Kok, H. T. Nicolai, A. J. Hof, and P. W. M. Blom, *J. Appl. Phys.* **103**, 113711 (2008).
8. N. F. Mott and R. W. Gurney, *Electronic Processes in Ionic Crystals*, 2nd edition (Dover, New York, 1964).
9. M. M. Mandoc, B. de Boer, G. Paasch, and P. W. M. Blom, *Phys. Rev. B* **75**, 193202 (2007).
10. P. Mark and W. Helfrich, *J. Appl. Phys.* **33**, 205 (1962).
11. L.-L. Chua, J. Zaumseil, J.-F. Chang, E. C.-W. Ou, P. K.-H. Ho, H. Sirringhaus, and R. H. Friend, *Nature* **434**, 194 (2005).
12. F. Laquai, G. Wegner, C. Im, H. Bässler, and S. Heun, *J. Appl. Phys.* **99**, 023712 (2006).
13. F. Laquai and D. Hertel, *Appl. Phys. Lett.* **90**, 142109 (2007).
14. S. Karg, V. Dyakonov, M. Meier, W. Riess, and G. Paasch, *Synth. Met.* **67**, 165 (1994).
15. P. Ranke, I. Bleyl, J. Simmerer, D. Haarer, A. Bacher, and H. W. Schmidt, *Appl. Phys. Lett.* **71**, 1332 (1997).
16. P. W. M. Blom and M. C. J. M. Vissenberg, *Phys. Rev. Lett.* **80**, 3819 (1998).
17. P. F. van Hutten, J. Wildeman, A. Meetsma, and G. Hadziioannou, *J. Am. Chem. Soc.* **121**, 5910 (1999).
18. L. B. Lin, R. H. Young, M. G. Mason, S. A. Jenekhe, and P. M. Borsenberger, *Appl. Phys. Lett.* **72**, 864 (1998).

19. L. J. A. Koster, E. C. P. Smits, V. D. Mihailetchi, and P. W. M. Blom, *Phys. Rev. B* **72**, 085205 (2005).

20. C. Tanase, E. J. Meijer, P. W. M. Blom, and D. M. de Leeuw, *Phys. Rev. Lett.* **91**, 216601 (2003).

21. M. P. Langevin, *Ann. Chim. Phys.* **28**, 433 (1903).

22. W. F. Pasveer, J. Cottaar, C. Tanase, R. Coehoorn, P. A. Bobbert, P. W. M. Blom, D. M. de Leeuw, and M. A. J. Michels, *Phys. Rev. Lett.* **94**, 206601 (2005).

23. R. U. A. Khan, D. Poplavskyy, T. Kreouzis, and D. D. C. Bradley, *Phys. Rev. B* **75**, 035215 (2007).

24. S. L. M. van Mensfoort, S. I. E. Vulto, R. A. J. Janssen, and R. Coehoorn, *Phys. Rev. B* **78**, 085208 (2008).

25. P. W. M. Blom and M. C. J. M. Vissenberg, *Mater. Sci. Eng., R* **27**, 53 (2000).

26. S. L. M. van Mensfoort, J. Billen, M. Carvelli, S. I. E. Vulto, R. A. J. Janssen, and R. Coehoorn, *J. Appl. Phys.* **109**, 064502 (2011).

6 Electron traps in semiconducting polymers: Exponential versus Gaussian trap distribution

The low electron currents in PPV derivatives and their steep voltage dependence are generally explained by trap-limited conduction in the presence of an exponential trap distribution. In this chapter it is demonstrated that the electron transport of several PPV derivatives can also be well described with a trap distribution that is Gaussianly distributed within the band gap. In contrast to the exponential distribution the trap-limited electron currents can now be modeled using the same Gaussian trap distribution for the various PPV derivatives.

6.1 Introduction

As described in Chapter 2, the charge carrier density dependence of the mobility has initially been described using the Vissenberg and Matters expression, originating from hopping in an exponential density of states (DOS).[1] This description has been used to unify the charge transport in FETs and LEDs.[2] Later, a description for the mobility incorporating both the density and field dependence was obtained, based on charge carrier hopping within a Gaussian DOS.[3] The fact that both models provide a consistent description of the diode current-voltage (J–V) curves can be understood from the fact that the section of the Gaussian DOS that is being filled during a J–V scan may also be approximated by an exponential, or vice versa.[2]

The electron current in most conjugated polymer diodes is observed to be strongly reduced as compared to the hole current.[4] Moreover, a steeper voltage dependence and a stronger layer thickness dependence are observed. This characteristic is generally explained by a trap-limited electron current (TLC), with an exponential distribution of trap states in the band gap according to

$$D_{\mathrm{t}}(E) = \frac{N_{\mathrm{t}}}{k_{\mathrm{B}}T_{\mathrm{t}}} \exp\!\left[-\frac{(E_{\mathrm{c}} - E)}{k_{\mathrm{B}}T_{\mathrm{t}}}\right], \tag{6.1}$$

with N_{t} the total concentration of electron traps, T_{t} a characteristic temperature specifying the decay of the exponential distribution and $E_{\mathrm{c}} - E$ the energy below the LUMO of the polymer.[5,6] Neglecting diffusion, the current can then be expressed analytically as[7]

$$J_{\mathrm{TLC}} = N_{\mathrm{c}} q \mu \left(\frac{\varepsilon_0 \varepsilon_r}{q N_{\mathrm{t}}}\right)^{r+1} \left(\frac{2r+1}{r+1}\right)^{r+1} \left(\frac{r}{r+1}\right)^{r} \frac{V^{r+1}}{L^{2r+1}}, \tag{6.2}$$

with q the elementary charge, $\varepsilon_0\varepsilon_{\mathrm{r}}$ the dielectric constant, μ the trap-free mobility, V the applied voltage, L the sample thickness and $r = T_{\mathrm{t}}/T$. From Equation 6.2, the trap temperature T_{t} can directly be estimated from the thickness and voltage scaling of the electron transport.

6.2 The Gaussian Trap Distribution

Since the charge transport in conjugated polymers is generally described by hopping in a Gaussian DOS that is broadened due to disorder,[8] it would perhaps be more obvious that the broadening of the trap states is also described by a Gaussian distribution, centered at a depth E_{t} below the LUMO, according to

$$D_{\mathrm{t}}(E) = \frac{N_{\mathrm{t}}}{\sqrt{2\pi}\sigma_{\mathrm{t}}} \exp\!\left[-\frac{(E - (E_{\mathrm{c}} - E_{\mathrm{t}}))^2}{2\sigma_{\mathrm{t}}^2}\right], \tag{6.3}$$

with σ_{t} the width of the distribution and $E_{\mathrm{c}} - E_{\mathrm{t}}$ the trap energy. However, the applicability of a model based on a TLC in the presence of a Gaussian distribution

of trap states has not been investigated so far. In literature, a number of approximations have been reported for a TLC with Gaussian trap states, but these are only valid in a limited voltage regime.[9] Hwang and Kao obtained a description for the case of a shallow Gaussian trap, given by[10]

$$J_{\mathrm{TLC}} = \frac{9}{8}\theta\varepsilon_0\varepsilon_r\mu\frac{V^2}{L^3}. \tag{6.4}$$

Equation 6.4 is essentially the expression for trap-free SCLC given by the Mott-Gurney square law[11] (Equation 2.1) scaled with a factor θ given by

$$\theta = \frac{N_{\mathrm{c}}}{N_{\mathrm{t}}}\exp\left[-\frac{E_{\mathrm{t}}}{k_{\mathrm{B}}T} - \frac{1}{2}\left(\frac{\sigma_{\mathrm{t}}}{k_{\mathrm{B}}T}\right)^2\right], \tag{6.5}$$

with N_{c} the effective density of states in the LUMO. For a narrow trap distribution Equation 6.5 reduces to the expression for a single discrete trap level (Equation 2.7b).[12] In the derivation of Equation 6.5 it is assumed that only the tail of the Gaussian is filled and it is therefore only valid when the Fermi energy lies below the center of the trap DOS (shallow trap). For the case that the Fermi energy is above the center of the trap DOS, defined as a deep Gaussian trap, another approximation was obtained by Nešpůrek and Smejtek[13] and later by Hwang and Kao.[10] Remarkably, in this case the obtained approximation for the current-voltage characteristic is equal to Equation 6.2, but now with the exponent r given by

$$r' = \sqrt{1 + 2\pi\left(\frac{\sigma_{\mathrm{t}}}{4k_{\mathrm{B}}T}\right)^2}, \tag{6.6}$$

and involving an effective trap density N'_{t} according to:

$$N'_{\mathrm{t}} = \frac{N_{\mathrm{t}}}{2}\exp\left[\frac{E_{\mathrm{t}}}{r'k_{\mathrm{B}}T}\right]. \tag{6.7}$$

Both approximations for the case of a Gaussian trap distribution are essentially the equations for an exponential trap DOS and a single discrete trap level. This would mean that the current-voltage characteristics of the trap limited transport in the presence of a Gaussian trap distribution can be approximated by a single discrete trap level at low trap occupancies, meaning low voltages, and an exponential trap distribution level at high occupancies and thus high voltages.

However, in the approximations leading to Equations 6.2 (deep traps) and 6.4 (shallow traps) several assumptions and simplifications are made. For instance, in all cases diffusion is neglected and a constant mobility is assumed. More importantly, these approximations are only valid in the range where the free carrier density is much smaller than the density of trapped charges ($n \ll n_{\mathrm{t}}$). For a more accurate description of the trap-limited current a numerical device model has to

be used, which includes diffusion and allows for the use of a density- and field-dependent mobility. In such a device model only the free charges contribute to the current, while both free and trapped carriers influence the electric field via the Poisson equation. To numerically calculate the trap-limited current it is therefore required to separate the total carrier density into free and trapped carriers. This relation can be calculated by assuming local thermal equilibrium.[14] The occupancy of the trap distribution is then calculated using Fermi-Dirac statistics. While the occupancy of an exponential trap distribution or a single level trap can be relatively easily calculated analytically, the occupancy of a Gaussian trap distribution, given by the product of the trap DOS and the Fermi-Dirac function is not straightforward. Only very recently an accurate approximation of the Gauss-Fermi integral was reported by Paasch and Scheinert.[15] In this chapter their approximation is used to evaluate the effect of Gaussianly distributed traps on the transport and compare it with the approximations of exponentially distributed traps and a discrete level trap. It is demonstrated that the numerical device model including Gaussian traps well describes the temperature dependent electron transport in three PPV derivatives. As a result the trap-limited currents in PPV, previously described with an exponential trap distribution, can also be explained with the Gaussian trap model.

6.3 Analysis

As stated above, the calculation of trap-limited currents requires a separation of the total carrier density into free (n) and trapped (n_t) carriers. For a single trap level the relation is simply linear: $n_\mathrm{t} \propto n$, whereas for an exponentially distribution of traps n and n_t are related via a power-law given by $n_\mathrm{t} \propto n^{1/r}$, with $r = T_\mathrm{t}/T$. In general, a dependence of the form $n_\mathrm{t} \propto n^{1/r}$ leads to $J \propto V^{r+1}/L^{2r+1}$ (giving $J \propto V^2/L^3$ for a single trap level ($r = 1$)). Figure 6.1 shows the relation between n_t and n as obtained by Paasch and Scheinert for a Gaussian distribution, as well as the relations for the exponential and single trap level distribution. The trap parameters for the latter two are calculated using Equations 6.5-6.7, such that Equations 6.2 and 6.4 should be valid approximations of the trap-limited current for the case of a Gaussian trap DOS. It can be observed from Figure 6.1 that the $n_\mathrm{t}(n)$ relation of the Gaussian trap DOS asymptotically reaches a slope equal to 1 in the log-log plot for small densities, which corresponds to the behavior of a discrete trap level. Accordingly, the current in this low density regime will have a slope of 2 and the current density can then be well approximated with Equation 6.4. The exponential trap distribution gives a constant and smaller slope of the $n_\mathrm{t}(n)$ dependence (higher r), leading to a stronger voltage and thickness dependence. However, the $n_\mathrm{t}(n)$ relation for the Gaussian trap DOS does not have a constant slope. In the low trap density limit, the slope equals 1, and when the Gaussian is filled up further, the slope of $n_\mathrm{t}(n)$ changes. It can therefore be expected that the slope of the J–V characteristics in a log-log plot is not constant but depends on the part of the Gaussian trap DOS being filled during a voltage sweep.

As a next step, the Gaussian distribution of trap states is implemented in a numerical drift-diffusion model.[16] To evaluate the charge transport in the presence of a Gaussian trap distribution a number of metal-semiconductor-metal sandwich

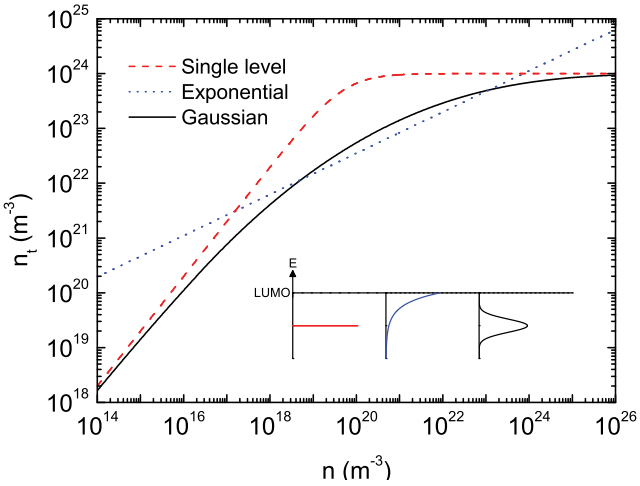

Figure 6.1. Dependence of n_t on n for a Gaussian, exponential and single level trap distribution at room temperature. The total trap density is $N_t = 1 \times 10^{24}\,m^{-3}$, $E_t = 0.2$ eV, $\sigma_t = 0.10$ eV. The effective density in the LUMO N_c is set at $3 \times 10^{26}\,m^{-3}$. The parameters for the single level and the exponential are chosen such that Equation 6.2 and Equation 6.4 should give a correct description. For the exponential trap DOS N_t' and T_t are given by Equation 6.6 and Equation 6.7 as $N_t' = 9.6 \times 10^{24}\,m^{-3}$, $T_t = 785$ K. The effective trap depth for the single level trap is $E_t = 0.40$ eV. The inset shows a schematic representation of a discrete single level trap, an exponential distribution and a Gaussian distribution.

devices are simulated, using a mobility of $1 \times 10^{-11}\,m^2/Vs$, and symmetric Ohmic contacts ($V_{bi} = 0$). To keep the calculations as transparent as possible these simulations are performed with a constant mobility, so that the effects of the trap parameters can be independently distinguished from the influence of a field- or density-dependent mobility. Since the single level trap can be regarded as a limiting case of the Gaussian distribution with $\sigma_t = 0$, it is interesting to compare the calculated currents for varying values of σ_t (Figure 6.2). The trap-limited current in the case of a single discrete trap level can be described by a quadratic behavior up to the trap filled limit given by $V_{TFL} = qN_tL^2/2\varepsilon_0\varepsilon_r$.[17] At this point the traps are completely filled and all additional injected carriers contribute to the transport, causing a rapid increase of the current towards the trap-free SCLC. For the Gaussian trap distribution, this change is more gradual due to the broadness of the trap distribution and for a broad distribution (large σ_t), this transition region becomes indiscernible from the rest of the J–V characteristic.

An interesting feature can be seen in Figure 6.2. All the calculated J–V curves cross at $V \approx 24$ V. At this bias, the Fermi level passes through the middle of the Gaussian trap distribution and exactly half of the traps are occupied, independently of the width of the Gaussian distribution. Analogous to the calculation of the trap-

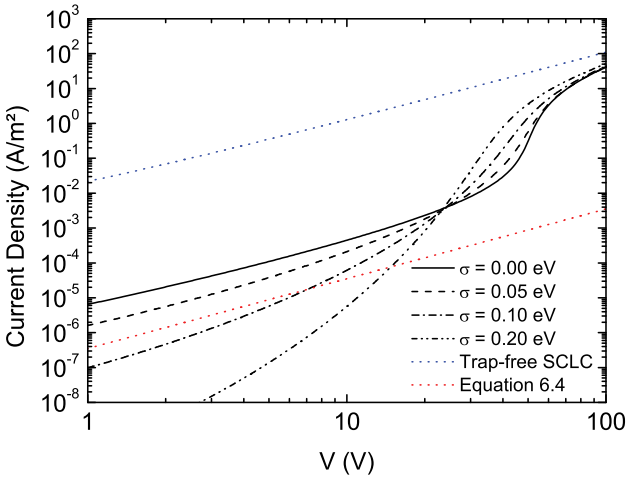

Figure 6.2. Simulated J–V plots for $L = 300$ nm, $N_\mathrm{t} = 2 \times 10^{23}\,\mathrm{m}^{-3}$, $E_\mathrm{t} = 0.40$ eV, and varying values of σ_t. The prediction from Equation 6.4 is shown for $\sigma_\mathrm{t} = 0.05$ eV.

filled limit, this voltage can be calculated as

$$V_\mathrm{half} = \frac{qL^2}{4\varepsilon_0\varepsilon_\mathrm{r}}(N_\mathrm{t} - n_\mathrm{t0}), \tag{6.8}$$

with n_t0 the density of trapped electrons in the absence of applied voltage. Furthermore, for the broader trap distributions also the quadratic part cannot be discerned anymore at low voltages. For the approximation of a shallow trap (Equation 6.4) it is assumed that only the tail of the Gaussian trap DOS is filled, which is a valid assumption if the Fermi level E_F lies at least a distance $\sigma_\mathrm{t}^2/(k_\mathrm{B}T)$ below the center of the Gauss. The voltage at which the Fermi level passes this energy can be approximated by [18]

$$V_\mathrm{q} = \frac{qL^2}{4\varepsilon_0\varepsilon_\mathrm{r}}(N_\mathrm{t} - n_\mathrm{t0}) \exp\left[-\frac{1}{2}\left(\frac{\sigma_\mathrm{t}}{k_\mathrm{B}T}\right)^2\right]. \tag{6.9}$$

Equation 6.9 thus defines the voltage range where approximation of a shallow Gaussian trap (Equation 6.4) is applicable and where the current-density follows a quadratic relation with voltage. From Equation 6.9 it can be therefore concluded that the approximation of a shallow Gaussian trap is only applicable to thick devices with a high trap density and a narrow trap distribution.

In Figure 6.3 the dependence of the J–V curve on the trap depth is depicted. It follows that a deeper trap results in a steeper J–V. As the voltage passes $V_\mathrm{half} = 50$ V, the Gaussian trap distribution gradually fills up, and the density of free electrons increases rapidly so that it surpasses the density of trapped electrons. The current then eventually becomes limited by the trap-free SCLC. For deeper

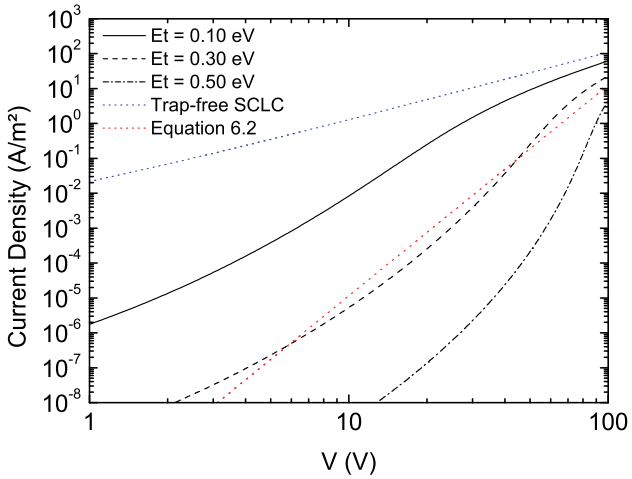

Figure 6.3. Simulated J–V curves for $L = 300$ nm, $N_t = 4 \times 10^{23}\,m^{-3}$, $\sigma_t = 0.20$ eV, and varying trap depths. Also shown is approximation Equation 6.2 for the case of $E_t = 0.30$ eV, with r' and N_t' given by Equations 6.6 and 6.7.

trap levels, the trap-limited current is lower, so the transition towards the trap-free SCLC is steeper. It should be noted that this behavior is fundamentally different as compared to an exponential distribution of traps. In the latter case the slope of the J–V curve is only determined by $r = T_t/T$, and is independent on the trap depth. As is clear from Figures 6.2 and 6.3 the slope of the J–V curve for Gaussian traps is both dependent on the shape of the distribution (σ_t) as well on the trap depth (E_t). The approximation according to Equation 6.2 is also shown in Figure 6.3 for $E_t = 0.30$ eV. It is clear that Equation 6.2 gives a poor description of the numerically calculated J–V's as expected from the different dependence of n_t in Figure 6.1 and as was previously shown by Paasch and Scheinert.[19] The slope of the J–V differs significantly while the currents start to deviate beyond V_{half}. This is due to a critical simplification made in the derivation of Equation 6.2. The concentration of free carriers is assumed to be small compared to the concentration of trapped carriers. This actually implies that it is assumed that the Gaussian is never filled up beyond the center. Accordingly, in Equation 6.2 the trap distribution is never filled up completely, and n_t eventually exceeds the total trap density N_t, while in the numerical simulation the concentration of trapped electrons asymptotically approaches N_t.

Equations 6.2 and 6.4, as well as the simulations shown in Figure 6.2 and Figure 6.3, are derived and carried out using the band transport formalism, based on Boltzmann statistics for the density of free charges. However, as mentioned before, the charge transport in organic semiconductors is generally described by hopping in a Gaussian DOS, in which case Boltzmann statistics are not valid. Assuming that only the tail of the Gaussian LUMO is filled, the density of free electrons is given by the nondegenerate limit.[20] This equation has the same functional form as the Boltzmann approximation only shifted by a temperature-dependent

factor $\sigma^2_{\mathrm{LUMO}}/(k_{\mathrm{B}}T)$. This makes it possible to take into account the Gaussian distribution of the LUMO by introducing an effective trap depth, analogous to the correction for the case of an exponential trap distribution.[21] Incorporating the effect of energetic disorder for the mobile carriers into the model leads to an effective trap depth,[22]

$$E_{\mathrm{t,eff}} = E_{\mathrm{t,abs}} - \frac{\sigma^2_{\mathrm{LUMO}}}{2k_{\mathrm{B}}T}. \tag{6.10}$$

By plotting $E_{\mathrm{t,eff}}$ versus $1/(k_{\mathrm{B}}T)$, the absolute trap depth $E_{\mathrm{t,abs}}$ and the width of the Gaussian DOS of the LUMO σ_{LUMO} can be obtained.

6.4 Experimental Results

Having evaluated the transport in the presence of a Gaussian trap distribution the model is now applied to electron transport measurements of three PPV derivatives: OC_1C_{10}-PPV, MEH-PPV and NRS-PPV. As mentioned previously, it has been demonstrated for the case of MEH-PPV that the electron traps are located energetically at least 0.4 eV below the LUMO level, and that the electron mobility is equal to the mobility of free holes.[23] As a result the dependencies of the mobility on electric field and density are known.[24] For OC_1C_{10}-PPV and NRS-PPV the hole mobility was described by the Vissenberg-Matters formalism with parameters derived from FET measurements[25], while for MEH-PPV a Poole-Frenkel type mobility was assumed, with parameters determined from hole-onle diodes. Ohmic electron injection was assumed and the built-in voltage V_{bi} ranged from 0.3 to 0.7 V.

As shown in Figure 6.4 the electron transport of the three polymers can be well described with a broad Gaussian trap with parameters $\sigma_{\mathrm{t}} = 0.10$ eV and $N_{\mathrm{t}} = 1.1 \times 10^{23}\,\mathrm{m}^{-3}$ (MEH-PPV and NRS-PPV) and $N_{\mathrm{t}} = 1.3 \times 10^{23}\,\mathrm{m}^{-3}$ for OC_1C_{10}-PPV. Figure 6.5 shows the dependence of $E_{\mathrm{t,eff}}$ on temperature. For all three polymers the dependence can be well described by Equation 6.10 with $\sigma_{\mathrm{LUMO}} = 0.13$ eV for OC_1C_{10}-PPV, $\sigma_{\mathrm{LUMO}} = 0.12$ eV for MEH-PPV and $\sigma_{\mathrm{LUMO}} = 0.14$ eV for NRS-PPV. These values of the width of the Gaussian DOS are in good agreement with previous reported values for these polymers.[3,25,26] The absolute trap depth amounts to approximately 0.70 eV for OC_1C_{10}-PPV and MEH-PPV, respectively, and to 0.82 eV for NRS-PPV. Remarkably, the trap-limited electron transport for the three PPV derivatives can be described with one and the same trap distribution: a total amount of traps of $\sim N_{\mathrm{t}} = 1 \times 10^{23}\,\mathrm{m}^{-3}$, Gaussianly distributed with a width of $\sigma_{\mathrm{t}} = 0.10$ eV and with its center located $0.7 - 0.8$ eV below the LUMO. The electron transport of these materials has been previously described with the exponential trap model.[21] The fact that this is also possible with the Gaussian trap can be understood from Figure 6.6 which shows the resulting Gaussian trap distribution for the case of MEH-PPV together with the exponential trap distribution that was used previously to fit the same data. During a J–V scan, only a part of the trap DOS is filled, that can alternatively be approximated by an exponential trap DOS. However, for each PPV-derivative the trap parameters N_{t} and T_{t} had to be adjusted individually to get agreement with experiment. When

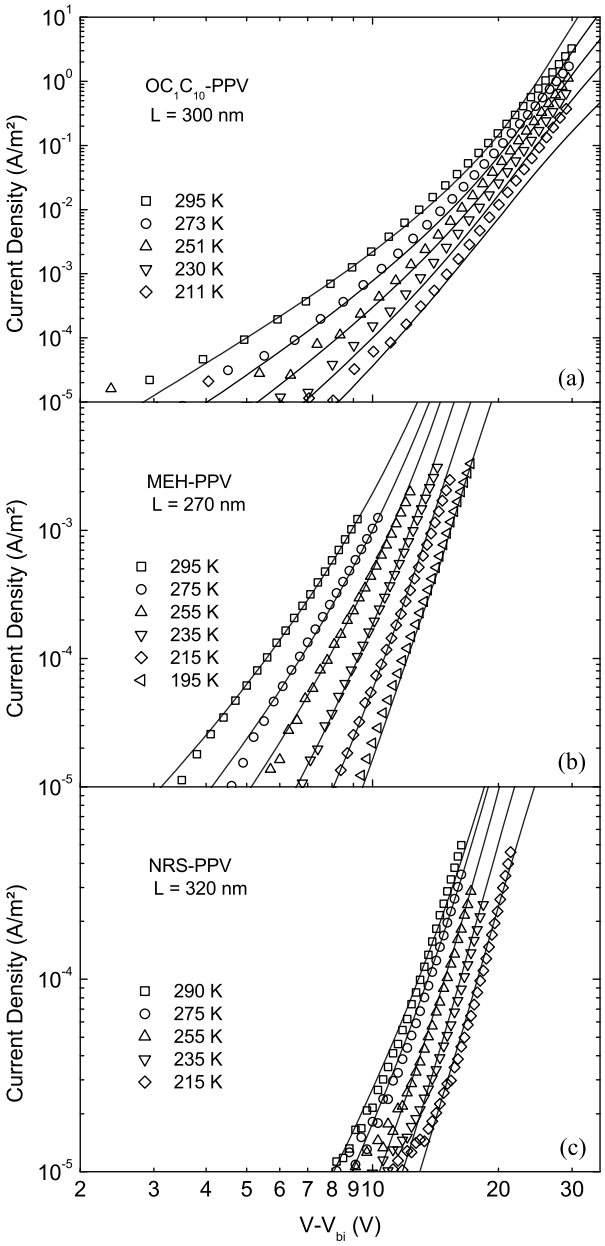

Figure 6.4. Temperature dependence of the electron current for three PPV derivatives. The lines are numerical fits incorporating a Gaussian trap with trap parameters for (a) OC_1C_{10}-PPV: $N_t = 1.3 \times 10^{23}\,m^{-3}$, $\sigma_t = 0.10$ eV, (b) MEH-PPV: $N_t = 1.1 \times 10^{23}\,m^{-3}$, $\sigma_t = 0.10$ eV and (c) NRS-PPV: $N_t = 1.1 \times 10^{23}\,m^{-3}$, $\sigma_t = 0.10$ eV.

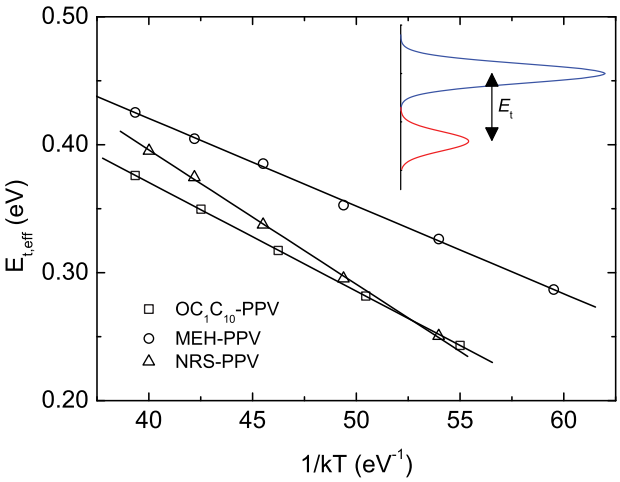

Figure 6.5. Dependence of the effective trap depth $E_{\mathrm{t,eff}}$ on temperature. The lines are fits of Equation 6.10 with $E_{\mathrm{t,abs}} = 0.71$ eV and $\sigma_{\mathrm{LUMO}} = 0.13$ eV for OC_1C_{10}-PPV, $E_{\mathrm{t,abs}} = 0.69$ eV and $\sigma_{\mathrm{LUMO}} = 0.12$ eV for MEH-PPV, and $E_{\mathrm{t,abs}} = 0.82$ eV and $\sigma_{\mathrm{LUMO}} = 0.14$ eV for NRS-PPV. The inset shows a schematic representation of the Gaussian LUMO and trap DOS. The trap density is exaggerated for clarity.

the traps in PPV have a common physical origin, i.e., an oxygen related defect, it is far more realistic that the trap-limited currents in the various PPV derivatives can be described with a single (Gaussian) trap distribution.

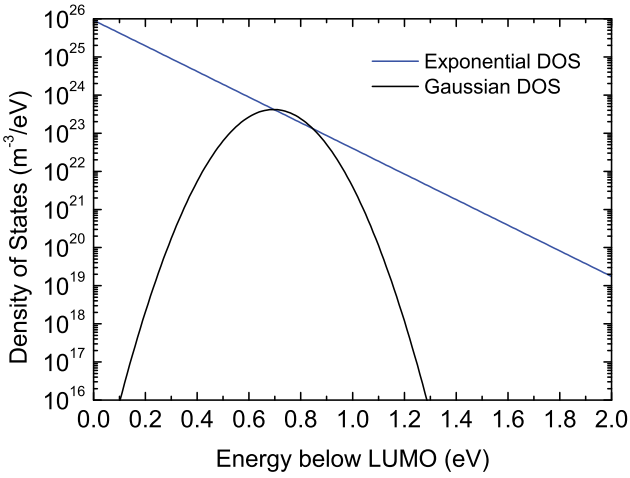

Figure 6.6. The Gaussian trap DOS as determined for the electron transport in MEH-PPV together with the exponential trap DOS determined previously. The overlap of both distributions corresponds to the part of the trap DOS that is filled during a J–V scan.

6.5 Conclusions

In conclusion, the trap-limited current in disordered semiconductor diodes is investigated for the case of a Gaussian trap distribution. The Gaussian trap distribution was implemented in a numerical drift-diffusion model for device simulation and the numerical results were compared to previously reported analytical approximations for shallow and deep traps. It is shown that the Gaussian trap model can be used to describe the temperature dependent electron transport in three PPV derivatives. These experimental data, which had previously been described using an exponential trap distribution, can also be explained with the Gaussian trap model using the same trap distribution for the three derivatives.

References

1. M. C. J. M. Vissenberg and M. Matters, *Phys. Rev. B* **57**, 12964 (1998).
2. C. Tanase, E. J. Meijer, P. W. M. Blom, and D. M. de Leeuw, *Phys. Rev. Lett.* **91**, 216601 (2003).
3. W. F. Pasveer, J. Cottaar, C. Tanase, R. Coehoorn, P. A. Bobbert, P. W. M. Blom, D. M. de Leeuw, and M. A. J. Michels, *Phys. Rev. Lett.* **94**, 206601 (2005).
4. P. W. M. Blom, M. J. M. de Jong, and J. J. M. Vleggaar, *Appl. Phys. Lett.* **68**, 3308 (1996).
5. M. M. Mandoc, B. de Boer, and P. W. M. Blom, *Phys. Rev. B* **73**, 155205 (2006).
6. S. L. M. van Mensfoort, J. Billen, S. I. E. Vulto, R. A. J. Janssen, and R. Coehoorn, *Phys. Rev. B* **80**, 033202 (2009).
7. P. Mark and W. Helfrich, *J. Appl. Phys.* **33**, 205 (1962).
8. H. Bässler, *Phys. Status Solidi B* **175**, 15 (1993).
9. J. Bonham, *Aust. J. Chem.* **26**, 927 (1973).
10. W. Hwang and K. C. Kao, *Solid-State Electron.* **19**, 1045 (1976).
11. N. F. Mott and R. W. Gurney, *Electronic Processes in Ionic Crystals*, 2nd edition (Dover, New York, 1964).
12. M. A. Lampert, *Phys. Rev.* **103**, 1648 (1956).
13. S. Nešpůrek and P. Smejtek, *Czech. J. Phys., Sect. B* **22**, 160 (1972).
14. J. Cottaar, R. Coehoorn, and P. A. Bobbert, *Phys. Rev. B* **82**, 205203 (2010).
15. G. Paasch and S. Scheinert, *J. Appl. Phys.* **107**, 104501 (2010).
16. L. J. A. Koster, E. C. P. Smits, V. D. Mihailetchi, and P. W. M. Blom, *Phys. Rev. B* **72**, 085205 (2005).
17. K. C. Kao and W. Hwang, *Electrical Transport in Solids, With Particular Reference to Organic Semiconductors*, 1st edition (Pergamon, Oxford, 1981).
18. R. Coehoorn, W. F. Pasveer, P. A. Bobbert, and M. A. J. Michels, *Phys. Rev. B* **72**, 155206 (2005).
19. G. Paasch and S. Scheinert, *J. Appl. Phys.* **106**, 084502 (2009).
20. G. Paasch and S. Scheinert, *J. Appl. Phys.* **101**, 024514 (2007).
21. M. M. Mandoc, B. de Boer, G. Paasch, and P. W. M. Blom, *Phys. Rev. B* **75**, 193202 (2007).

22. T. van Woudenbergh, P. W. M. Blom, and J. N. Huiberts, *Appl. Phys. Lett.* **82**, 985 (2003).

23. Y. Zhang, B. de Boer, and P. W. M. Blom, *Phys. Rev. B* **81**, 085201 (2010).

24. C. Tanase, P. W. M. Blom, and D. M. de Leeuw, *Phys. Rev. B* **70**, 193202 (2004).

25. C. Tanase, P. W. M. Blom, D. M. de Leeuw, and E. J. Meijer, *Phys. Status Solidi A* **201**, 1236 (2004).

26. D. E. Markov, C. Tanase, P. W. M. Blom, and J. Wildeman, *Phys. Rev. B* **72**, 045217 (2005).

7 Unification of the trap-limited electron transport in semiconducting polymers

The electron transport in a wide range of semiconducting polymers is investigated by current-voltage measurements of single-carrier devices. It is observed that in this class of materials the electron transport can be described using a common Gaussian trap distribution, centered at an energy 3.6 eV below the vacuum level and with a nearly identical concentration of 3×10^{23} traps/m^3. This indicates that the traps have a common origin and allows us to predict the trap-limited electron current in any conjugated polymer.

7.1 Introduction

As described in the previous chapters, the electron current of several semiconducting polymers exhibits a very distinct behavior: the magnitude of the electron current is often found to be much lower than the hole current. Additionally, it is characterized by a steeper voltage dependence accompanied with a strong thickness dependence.[1] This behavior is generally attributed to trap-limited conduction (TLC) with electron traps distributed exponentially in the band gap.[2,3] These traps have been related to intrinsic defects such as kinks in the polymer backbone,[4] to impurities remaining from the synthesis, or to contamination from the environment.[5] Techniques such as thermally stimulated currents (TSC) and deep level transient spectroscopy (DLTS) have been commonly used to obtain information on the properties of traps.[6,7] These measurements revealed for PPV the existence of a shallow and a deep electron trap, with trap depths of typically ~ 0.5 eV and 1.0 eV, respectively.[2,5,8,9] Furthermore, by elimination of the trapping by n-type doping is was shown that the electron traps that govern the TLC in MEH-PPV are located at least ~ 0.4 eV below the LUMO and are thus well separated from the Gaussian DOS.[10]

7.2 Trap-Limited Transport in Disordered Semiconductors

In this chapter we investigate the electron transport of nine different polymers which are used as the active layers in PLEDs or organic photovoltaics (OPV). The LUMO levels (Table 7.1) of these polymers cover a range of more than 1 eV. In Figure 7.1 the J–V characteristics of electron-only diodes of four of these polymers are shown on a double logarithmic scale. It appears that the

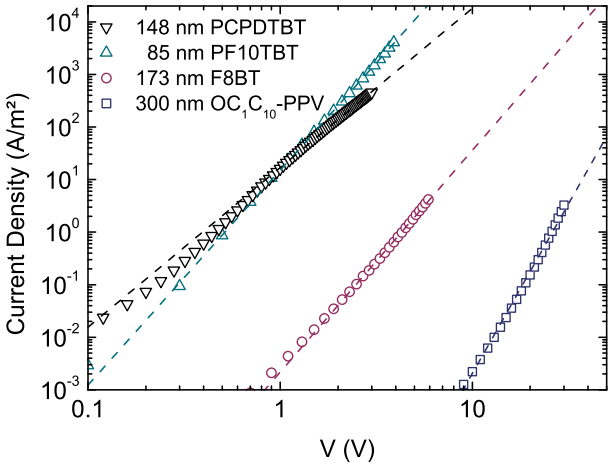

Figure 7.1. The electron transport of four different polymers with LUMO values ranging from -2.8 eV to -3.6 eV. The dotted lines are fits to a power law.

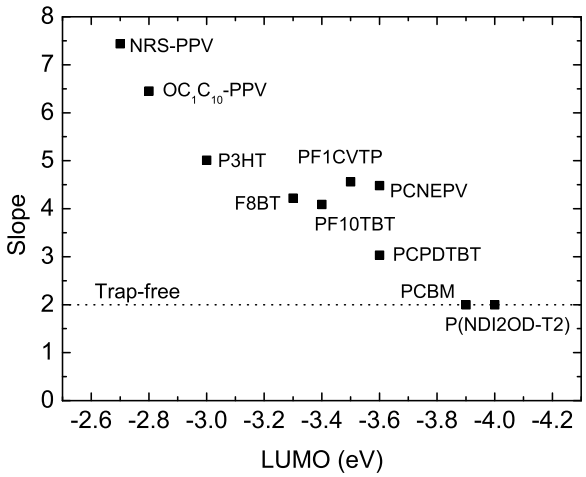

Figure 7.2. The slope of the electron-only J–V curves on a double-logarithmic scale. The value of the slope was determined by fitting the experimental J–V curve with a power law. The dotted line indicates a slope of 2 as observed for trap-free space-charge-limited currents.

J–V curve of OC_1C_{10}-PPV has a slope of approximately 6, whereas the J–V curve of poly[2,6-(4,4-bis-(2-ethylhexyl)-4H-cyclopenta(2,1-b;3,4-b′)-dithiophene)-*alt*-4,7-(2,1,3-benzothiadiazole)] (PCPDTBT) has a slope close to 3. Figure 7.2 shows the double logarithmic slope of a larger range of polymers versus their LUMO level. A clear trend can be observed, suggesting that polymers with a deeper LUMO level exhibit a less steep voltage dependence of the electron current.

In case of an exponential trap distribution the TLC can be approximated by a power law $J \propto V^{r+1}$ where $r = T_t/T$ and T_t is the characteristic trap temperature describing the decay of the exponential distribution.[11] The value of T_t directly determines the slope of the J–V curve and therefore for each polymer a different trap distribution would be required to describe its TLC. If the electron traps in these

Polymer	LUMO (eV)	σ (eV)	N_t (m^{-3})	E_t (eV)	Reference
NRS-PPV	-2.7	0.125	1.3×10^{23}	0.76	12,13
OC_1C_{10}-PPV	-2.8	0.110	1.3×10^{23}	0.70	12,14
P3HT	-3.0	0.098	4.0×10^{23}	0.59	15
F8BT	-3.3	0.130	3.0×10^{23}	0.55	14
PF10TBT	-3.4	0.100	1.8×10^{23}	0.34	16
PCPDTBT	-3.6	0.090	4.0×10^{23}	0.21	17

Table 7.1. Trap parameters determined by numerical fitting the electron transport with the Gaussian trap model. The width of the Gaussian trap distribution was assumed to be equal to the width of the LUMO, which was estimated from the temperature dependence of the zero-field hole mobility. The built-in voltage used was $V_{bi} = 0.5 \pm 0.1$ V.

polymers would have a common origin a large variation in the trap distribution would be highly unlikely. In the previous chapter, it was shown that the electron transport in three PPV derivatives can alternatively be described with a Gaussian distribution of trap states. The electron transport of these PPV derivatives were modeled by incorporating a single Gaussian distribution of trap states, located ~ 0.7 eV below the LUMO of PPV.

A conceptual difference with the exponential distribution is that for Gaussianly distributed traps the slope of the J–V also depends on the trap depth, with a deeper trap yielding a steeper J–V characteristic. In this chapter, the Gaussian trap model is applied to the electron transport measurements of the nine polymers, as partly shown in Figure 7.1. In order to model the TLC also the mobility of the free electrons needs to be known. As described in the previous chapters, it is demonstrated for the case of MEH-PPV that the electron mobility is equal to the hole mobility.[10] This allows us to independently determine the mobility parameters from hole-only diodes or from FET measurements. The measurement of hole transport in polymers with a deep lying HOMO level, such as poly(9,9-dioctylfluorene-*alt*-benzothiadiazole) (F8BT), was enabled by using MoO_3 as hole injection layer, as described in Chapter 3. The width of the Gaussian DOS of the HOMO and LUMO is then determined from temperature dependent measurements.[12,13] To further limit the number of free parameters, the width of the trap distribution σ_t is assumed to be equal to σ, with the rationale that the width of the trap distribution is related to the width of the LUMO since both will be governed by the same disorder. As a result, the assumed trap widths for the case of PPV derivatives differ slightly from those in the previous chapter where a width of $\sigma_t = 0.10$ eV was assumed.

7.3 Results

The temperature dependent electron transport was modeled for all polymers listed in Table 7.1, only adjusting the trap parameters N_t and E_t. The hole mobility parameters were described by the Vissenberg-Matters equation for the case of NRS-PPV, OC_1C_{10}-PPV and P3HT. For F8BT, poly[9,9-didecanefluorene-*alt*-(bisthienylene) benzothiadiazole] (PF10TBT) and PCPDTBT a Poole-Frenkel type mobility was used, with parameters determined from hole-only diodes. A relative dielectric constant of $\varepsilon_r = 3$ was assumed for all materials. The blue-emitting polyspirobifluorene (PSF) discussed in Chapter 5 is left out of this analysis, since its LUMO level is not well established. Furthermore, in the PSF polymer, the hole and electron mobility are not equal, which hampers the accurate determination of the intrinsic trap-free electron mobility, and the width of the LUMO σ. It should be noted however, that the trap temperature used for the fits in Figure 5.6 ($T_t = 1750$ K) is higher than the value typically found for PPV derivatives ($T_t \approx 1500$ K) consistent with a steeper J–V. An even higher trap temperature of $T_t \approx 2100$ K was found for the case of another polyfluorene derivative.[18]

As an example, the temperature dependent electron transport of F8BT and PF10TBT are shown in Figure 7.3. Remarkably, for all the polymers with a TLC the amount of traps is nearly equal, with a typical value of 3×10^{23} traps/m^3.

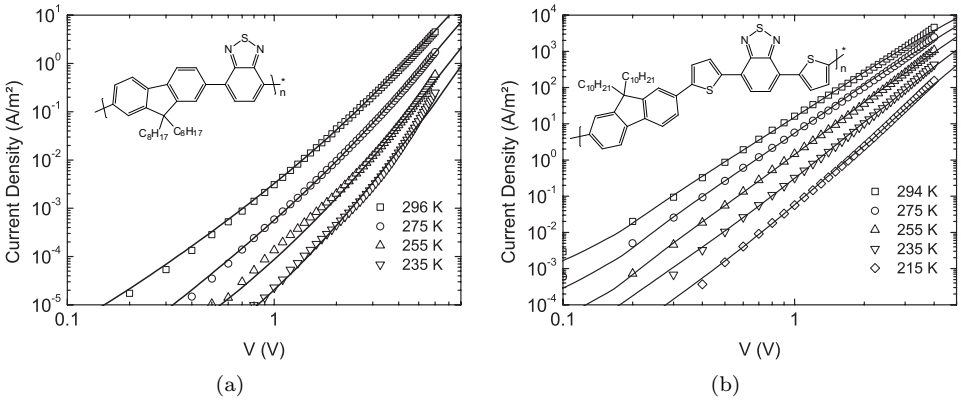

Figure 7.3. Temperature dependent electron transport of (a) 173 nm F8BT and (b) 85 nm PF10TBT electron-only devices and fits with the Gaussian trap model and parameters listed in Table 7.1. The insets show the chemical structures of F8BT and PF10TBT.

The only parameter that changes to explain the TLC of the various polymers with different slopes is the trap-depth E_t. In Figure 7.4 the resulting energy level diagram containing the LUMOs of the polymers with the corresponding trap energy is plotted. Figure 7.4 shows that the polymers investigated here exhibit a common trap distribution, located at an energy of $\sim$ 3.6 eV below the vacuum level. This is a remarkable result: firstly, it allows us to predict the trap-limited electron current in any conjugated polymer, which was not

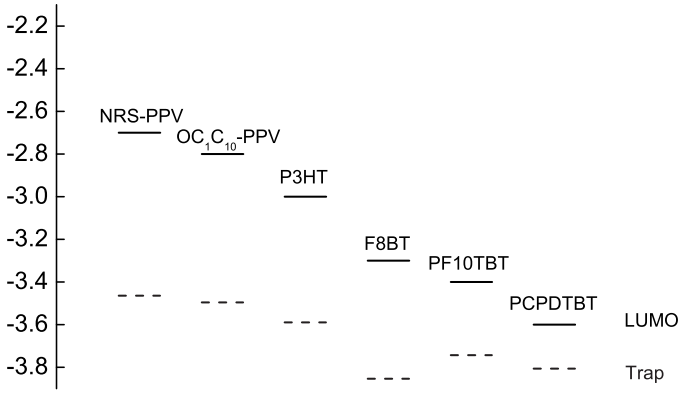

Figure 7.4. Schematic representation of the energies of the LUMO and the center of the trap distribution. The solid lines indicate the LUMO level and the dashed lines indicate the trap level.

possible until now. For this, only the hole mobility of the polymer should be known together with the position of its LUMO level. With the total amount of traps being constant at 3×10^{23} traps/m^3 and the trap-distribution fixed at 3.6 eV all electron trap-related parameters are known. It should be noted that for polymers with the LUMO approaching the trap distribution at 3.6 eV, the trap distribution starts to overlap with the LUMO. In this regime the trap states may start to participate in the transport and the TLC model will become less accurate. Secondly, our findings indicate that the electron trapping in conjugated polymers has a common origin. The electron traps cannot result from structural defects like kinks, since different polymers have different stiffness, and some are crystalline or amorphous. A more likely origin is a chemical defect related to water or oxygen.[9,19] In earlier work by de Leeuw *et al.* the redox potential of water was calculated to be -0.658 V versus SCE.[20] From this it was reasoned that *n*-type materials are stable against ambient atmosphere when their LUMO is deeper than 4 eV. This was in agreement by measurements on FETs where ambient stability was observed in materials with such a deep lying LUMO level.[21] Here, by systematically varying the LUMO level of the materials we demonstrate the presence of a universal electron trap level around 3.6 eV, in diodes that are fabricated and characterized in inert atmosphere. Thus these traps are already present in the material after synthesis, and are not necessarily related to ambient stability. As shown in Figure 7.2 for organic semiconductors with LUMOs deeper than 3.8 eV, such as [6,6]-phenyl C_{61}-butyric acid methyl ester (PCBM) and poly[*N*,*N*′-bis(2-octyldodecyl)-naphthalene-1,4,5,8-bis(dicarboximide)-2,6-diyl-*alt*-5,5′-(2,2′-bithiophene)] (P(NDI2OD-T2)), the transport is trap-free and space-charge limited, characterized by a quadratic current-voltage dependence (slope 2). The fact that the trap levels are energetically not that far away from the redox potential of water could point in the direction that the universal electron traps in conjugated polymers are a water-related complex, which is a subject of further study.

7.4 Conclusions

In conclusion, it is shown that the electron transport of a wide range of polymers can be described by a Gaussian distribution of electron traps. The dependence of the trap depth on the LUMO energy demonstrates that the polymers exhibit a common electron trap distribution, centered at approximately $E_{\mathrm{trap}} \approx 3.6$ eV below the vacuum level. This Gaussian trap distribution consistently explains the relation between slope of the (log-log) J–V curve slope and the LUMO level of the polymer. Moreover, it demonstrates that balanced trap-free charge transport can only be obtained in polymers with a LUMO level deeper than 3.6 eV below vacuum.

References

1. P. W. M. Blom, M. J. M. de Jong, and J. J. M. Vleggaar, *Appl. Phys. Lett.* **68**, 3308 (1996).
2. A. J. Campbell, D. D. C. Bradley, and D. G. Lidzey, *J. Appl. Phys.* **82**, 6326 (1997).
3. M. M. Mandoc, B. de Boer, G. Paasch, and P. W. M. Blom, *Phys. Rev. B* **75**, 193202 (2007).
4. W. Graupner, G. Leditzky, G. Leising, and U. Scherf, *Phys. Rev. B* **54**, 7610 (1996).
5. M. Meier, S. Karg, K. Zuleeg, W. Brütting, and M. Schwoerer, *J. Appl. Phys.* **84**, 87 (1998).
6. J. G. Simmons and G. W. Taylor, *Phys. Rev. B* **5**, 1619 (1972).
7. D. V. Lang, *J. Appl. Phys.* **45**, 3023 (1974).
8. P. Stallinga, H. L. Gomes, H. Rost, A. B. Holmes, M. G. Harrison, and R. H. Friend, *J. Appl. Phys.* **89**, 1713 (2001).
9. V. Kažukauskas, *Semicond. Sci. Technol.* **19**, 1373 (2004).
10. Y. Zhang, B. de Boer, and P. W. M. Blom, *Phys. Rev. B* **81**, 085201 (2010).
11. P. Mark and W. Helfrich, *J. Appl. Phys.* **33**, 205 (1962).
12. C. Tanase, P. W. M. Blom, D. M. de Leeuw, and E. J. Meijer, *Phys. Status Solidi A* **201**, 1236 (2004).
13. D. E. Markov, C. Tanase, P. W. M. Blom, and J. Wildeman, *Phys. Rev. B* **72**, 045217 (2005).
14. L.-L. Chua, J. Zaumseil, J.-F. Chang, E. C.-W. Ou, P. K.-H. Ho, H. Sirringhaus, and R. H. Friend, *Nature* **434**, 194 (2005).
15. C. Tanase, E. J. Meijer, P. W. M. Blom, and D. M. de Leeuw, *Phys. Rev. Lett.* **91**, 216601 (2003).
16. D. J. D. Moet, P. de Bruyn, and P. W. M. Blom, *Appl. Phys. Lett.* **96**, 153504 (2010).
17. D. Mühlbacher, M. Scharber, M. Morana, Z. Zhu, D. Waller, R. Gaudiana, and C. Brabec, *Adv. Mater.* **18**, 2884 (2006).
18. S. L. M. van Mensfoort, J. Billen, S. I. E. Vulto, R. A. J. Janssen, and R. Coehoorn, *Phys. Rev. B* **80**, 033202 (2009).
19. H. E. Tseng, K. Y. Peng, and S. A. Chen, *Appl. Phys. Lett.* **82**, 4086 (2003).

20. D. M. de Leeuw, M. M. J. Simenon, A. R. Brown, and R. E. F. Einerhand, *Synth. Met.* **87**, 53 (1997).

21. T. D. Anthopoulos, G. C. Anyfantis, G. C. Papavassiliou, and D. M. de Leeuw, *Appl. Phys. Lett.* **90**, 122105 (2007).

8 Device Physics of White Polymer Light-Emitting Diodes

In the previous chapters, the device operation of a blue backbone polymer has been investigated. Furthermore, the Gaussian trap distribution was evaluated. In this chapter, we will apply the gained insights to develop a device model for the operation of a PLED based on a single layer of a white-emitting copolymer. From single-carrier devices the effect of the green- and red-emitting dyes on the hole and electron transport are determined. The red dye acts as a deep electron trap thereby strongly reducing the electron transport. By incorporating trap-assisted recombination for the red emission and bimolecular Langevin recombination for the blue emission the current and light-output of the white PLED can be consistently described. The color shift of single-layer white-emitting PLEDs can be explained by the different voltage dependence of trap-assisted and bimolecular recombination.

8.1 Introduction

As mentioned in Chapter 2, an attractive way to generate white light with only one emissive layer is the use of a copolymer in which red and green dyes are incorporated in the backbone of the polymer. Due to energy transfer to, and a preferred recombination on the dyes, in practice only a small concentration ($\ll 1\%$) of dyes is required to obtain white light emission. The color coordinates of the emission may be tuned by adjusting the dye concentrations.[1,2] An apparently inherent issue of single-layer white PLEDs is the color shift: it is usually observed that the emission spectrum exhibits a voltage dependence, ranging from red-white towards a blue-white with increasing bias.[3–7] Such a color shift is undesired since it makes PLEDs less suitable for dimmable lighting. The color shift of white PLEDs has been explained both by a saturation of the dyes[8,9] as well as by a shift of the recombination zone.[10] Gather *et al.* showed that the color shift in a single-layer white-emitting OLED can be explained by charge trapping and recombination on the dye.[11] In that work the relative contributions from blue and red could be described by a simple model taking into account the trapping rate on the red dye.

The bimolecular recombination in PLEDs is shown to be limited by the diffusion of free electrons and holes toward each other in their mutual Coulomb field which is described by the Langevin relation,[12–14]

$$R_{\mathrm{Lan}} = \frac{q}{\varepsilon_0 \varepsilon_r}(\mu_{\mathrm{e}} + \mu_{\mathrm{h}})\big(np - n_{\mathrm{i}}^2\big), \tag{8.1}$$

with q the elementary charge, $\varepsilon_0\varepsilon_{\mathrm{r}}$ the dielectric constant, μ_{e} and μ_{h} the electron and hole mobility, n and p the free electron and hole density, and n_{i} the intrinsic carrier concentration. However, as shown in the previous chapters, in semiconducting polymers it is generally observed that the electron transport is reduced by the presence of traps. As a result, a substantial part of the electron concentration is therefore localized in traps and does not contribute to the electron transport.[15–17] It has recently been demonstrated that an additional recombination process involving these trapped electrons constitutes a significant loss mechanism in PLEDs.[18] Recombination involving trapped carriers is described by the Shockley-Read-Hall (SRH) formalism.[19,20]

$$R_{\mathrm{SRH}} = \frac{C_{\mathrm{n}} C_{\mathrm{p}} N_{\mathrm{t}}}{C_{\mathrm{n}}(n + n_1) + C_{\mathrm{p}}(p + p_1)}\big(np - n_{\mathrm{i}}^2\big), \tag{8.2}$$

with C_{n} and C_{p} the capture coefficients for electrons and holes, respectively, N_{t} the density of electron traps, and n_1 and p_1 the electron and hole density in the case that the Fermi level coincides with the trap level. The most prominent difference between the Langevin and SRH mechanism is the different dependence on the charge carrier densities, and consequently they exhibit a different voltage dependence in PLEDs.[18]

In a conventional PLED based on PPV, the trap-assisted recombination is non-radiative and therefore constitutes a loss mechanism. It was shown that SRH re-

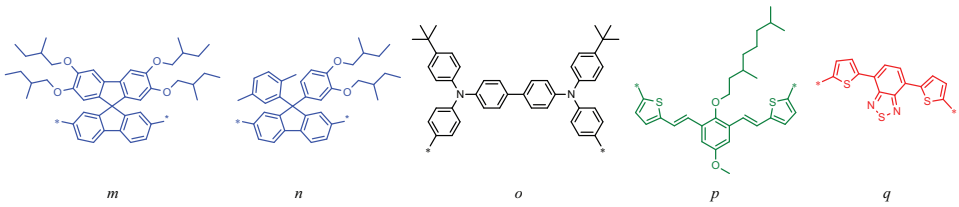

Figure 8.1. The structure of the polymers investigated. The components p and q are the green and red dye, respectively. The composition of the three investigated polymers is given in Table 8.1.

combination competes with Langevin recombination and that SRH recombination is dominant over Langevin recombination at low bias. However, due to the different voltage dependence Langevin recombination eventually surpasses SRH recombination. Furthermore, it has been demonstrated that the current ideality factor of the diffusion regime is a measure for the strength of trap-assisted recombination, with an ideality factor of 2 indicating that trap-assisted recombination is dominant and an ideality factor of unity that Langevin recombination is dominant.[21,22] The measurement of the luminance ideality factor in conventional PLEDs revealed that the light emission originates from Langevin recombination, as expected. However, the luminance ideality factor of white PLEDs revealed different ideality factors for blue and red light. While the blue emission exhibits an ideality factor of unity (indicating Langevin recombination), the luminance ideality factor of the red emission amounts to 2, demonstrating that the red emission originates from trap-assisted recombination.[22] In this Chapter we apply a numerical device model[23] that includes the results of charge transport studies as well as Langevin and SRH recombination to model the device operation of a single-layer white-emitting PLED.

8.2 Experimental Results

In addition to the mobility parameters, the parameters describing the trap states are essential constituents of the device simulation, since they determine the strength of the trap-assisted recombination. The large number of relevant parameters renders it a great challenge to achieve a quantitative description of the device operation. In order to disentangle the various processes we investigate a set of three polymers (Merck KGaA) which contain an incremental number of dyes incorporated in the blue backbone; the blue backbone polymer (B), the backbone polymer

Polymer	m	n	o	p	q
B	50	40	10	0	0
BG	50	39.9	10	0.1	0
BGR	50	39.88	10	0.1	0.02

Table 8.1. The composition in percentages of the three polymers investigated in this chapter.

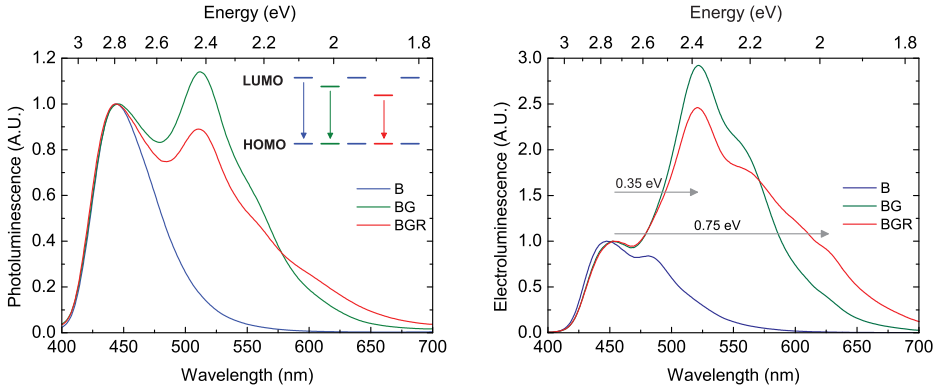

Figure 8.2. (a) The photoluminescence spectra of B, BG, and BGR polymers. The excitation was at the maximum of the absorption at 370 nm. The inset shows a schematic representation of the band diagram of the white-emitting copolymer. (b) The electroluminescence spectra of 90 nm PLEDs, driven at a bias of 5 V, normalized to the blue emission peak at 450 nm.

with a green dye (BG) and the white-emitting polymer with both a green and red dye (BGR).[24,25] The structure of the white-emitting copolymer BGR is shown in Figure 8.1, the composition of the three copolymers investigated is shown in Table 8.1. The charge transport in the polyspirobifluorene backbone has already been investigated in Chapter 5. The fact that the dyes are incorporated in a systematic way enables us to stepwise unravel the device operation of the white-emitting PLED.

As a start, Figure 8.2 shows the photoluminescence (PL) and electroluminescence (EL) spectra of the three polymers investigated. Despite the low concentration of the green and red dye, a clear emission from the green dye can be observed upon the excitation of the blue backbone, demonstrating the energy transfer from the backbone to the dyes. Anni *et al.* have shown that the energy transfer is intermolecular and that energy transfer occurs from blue to green to red and from blue to red directly.[26] In the EL spectrum, the contribution from the green peak is much stronger and the red emission is better discernible. The concentrations of the dyes are too low for guest-to-guest transport to occur. Consequently, the device current in the copolymer is carried by the blue backbone. Emission from the dyes can then originate from either recombination on the blue backbone and consecutive energy transfer to the dyes, or from charge trapping and recombination on the dyes. Since the latter mechanism is not present in PL, the stronger contribution of the dyes in the EL spectrum can be attributed to charge trapping and recombination on the dyes. As a result, it can be expected that the electronic processes are dominant in determining the spectrum of the white emitting diode. For white-emitting OLEDs containing a blend of dyes it has been concluded previously that emission due to trapping and recombination on dyes is dominant over energy

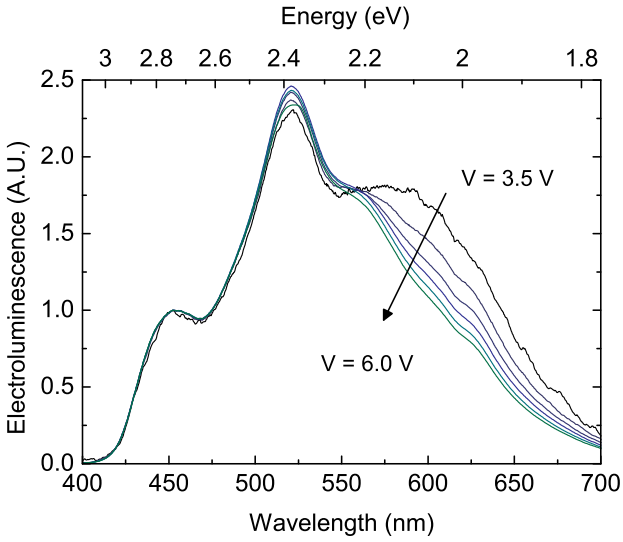

Figure 8.3. The voltage dependence of the electroluminescence spectrum of an 90 nm BGR PLED. The bias is ranged from $V = 3.5$ V to $V = 6.0$ V and the intensity is normalized to the blue emission peak at 450 nm.

transfer.[5,7,27–31] Figure 8.3 shows the voltage dependence of the EL spectrum of a 90 nm white-emitting BGR PLED, normalized to the blue emission peak. A clear color shift is observed; with increasing bias the relative contribution of red decreases and the emission shifts towards blue. Our device model enables us to quantify the voltage dependencies of the Langevin (blue emission) and SRH (red emission) recombination mechanisms and their role in the observed color shift.

8.3 Charge Transport

As a first step towards a quantitative description of a white-emitting PLED we analyse the electron- and hole transport in the host and host-guest systems. The charge transport in the blue backbone has already been investigated in Chapter 5. The hole transport could be described as trap-free with mobility parameters $\mu_0^* = 1.3 \times 10^{-6}\,\mathrm{m^2/Vs}$, $N_\mathrm{s} = 3.6 \times 10^{26}\,\mathrm{m^{-3}}$ and $\sigma = 0.15$ eV. The relative dielectric constant of the white-emitting polymer was assumed to be equal to that of the blue polymer at $\varepsilon_\mathrm{r} = 3.1$. The intrinsic mobility of the free electrons was found to be at least one order of magnitude larger than the hole mobility although the electron current was hampered by electron traps, assumed to be distributed exponentially in the band gap. As described in Chapter 6, it was found that the electron transport in PPV derivatives can alternatively be described with a Gaussian distribution of electron traps, which justifies a re-examination of the electron transport in the blue polymer. Figure 8.4 shows the J–V characteristics of electron-only devices of the blue-emitting polymer with three different thicknesses. A fit procedure was used to determine the optimal set of mobility parameters and trap parameters

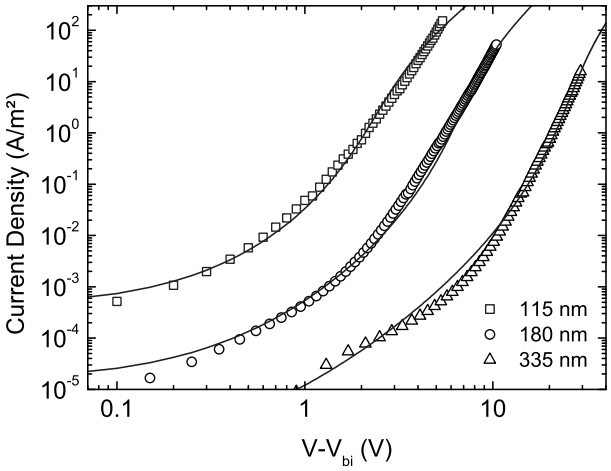

Figure 8.4. The room temperature electron transport of the blue backbone polymers, corrected for a built-in voltage of $V_{\mathrm{bi}} \approx 0.5$ V. The lines are fits of the numerical device model, including a density-dependent mobility with parameters $\sigma = 0.09$ eV, $N_{\mathrm{s}} = 1.3 \times 10^{27}\,\mathrm{m}^{-3}$, $\mu_0^* = 4.2 \times 10^{-8}\,\mathrm{m}^2/\mathrm{Vs}$ and a Gaussian trap distribution with parameters $E_{\mathrm{t}} = 0.81$ eV, $\sigma_{\mathrm{t}} = 0.09$ eV and $N_{\mathrm{t}} = 1 \times 10^{23}\,\mathrm{m}^{-3}$.

describing the electron transport in the blue backbone polymer. The thickness and temperature dependence of the electron transport could be described with a density-dependent mobility according to $\sigma = 0.09$ eV, $N_{\mathrm{s}} = 1.3 \times 10^{27}\,\mathrm{m}^{-3}$ and $\mu_0^* = 4.2 \times 10^{-8}\,\mathrm{m}^2/\mathrm{Vs}$, and a Gaussian trap located at 0.81 eV below the LUMO of the blue-emitting polymer with a trap density of $N_{\mathrm{t}} = 1 \times 10^{23}\,\mathrm{m}^{-3}$. To limit the number of unknown parameters, the width of the Gaussian trap distribution was assumed to be equal to the width of the density of states (DOS) of the LUMO at $\sigma_{\mathrm{t}} = 0.09$ eV. We note that especially at low bias, the quality of the fit is improved significantly by assuming a Gaussian trap density compared to an exponential trap density (Figure 5.6).

Since the green and red dyes by definition have a smaller band gap than the blue backbone, they are expected to introduce charge traps for the transport through the blue backbone. Figure 8.5(a) shows the J–V characteristics of ~ 130 nm double carrier devices (PLEDs) of the three polymers. A clear decrease in device current is observed upon the inclusion of the dyes. The question now arises whether the dyes act as hole traps, electron traps, or perhaps as both. Figure 8.5(b) shows the J–V characteristics of hole-only diodes of the three polymers with a thickness of 130 nm. It is apparent that the hole transport is essentially unaffected by the inclusion of the dyes, which was also confirmed by time-of-flight measurements.[32] This demonstrates that the dyes do not act as hole traps and that the HOMO levels of the dyes are thus located energetically at, or below the HOMO level of the blue backbone. For recombination on the dyes to occur the hole can either originate directly from the blue backbone HOMO, or via the dye HOMO level. The latter case would be improbable if the dye HOMO level would lie well below the host

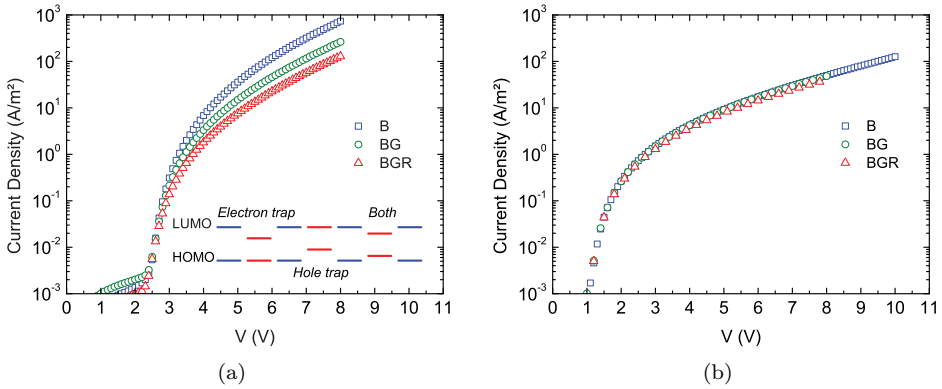

Figure 8.5. Device current of (a) 130 nm PLEDs of B, BG, and BGR and (b) hole-only devices of 130 nm B, BG, BGR devices. The inset of (a) shows a schematic representation of the possible alignments of the energy levels of the dyes with respect to the backbone material.

HOMO level. It can therefore be concluded that both the green and red dye are relatively well aligned with the HOMO level of the blue backbone material. From this result it can already be anticipated that the dyes should function as electron traps.

Figure 8.6 shows the J–V curves of 135 nm electron-only devices. Indeed, the incorporation of the green dye causes a dramatic decrease of the electron current. The inclusion of the red dye reduces the electron current even further. This clearly

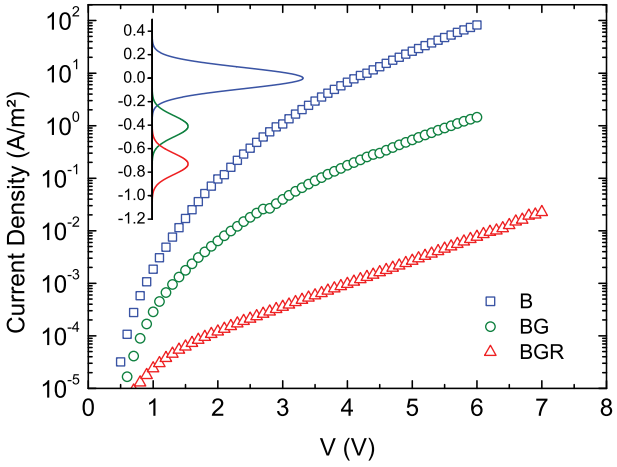

Figure 8.6. Electron transport of the three polymers investigated. The active layer thickness is 135 nm. The inset shows a schematically density of states of the LUMO and the green and red dye. The concentrations of the dyes are exaggerated by a factor 1000.

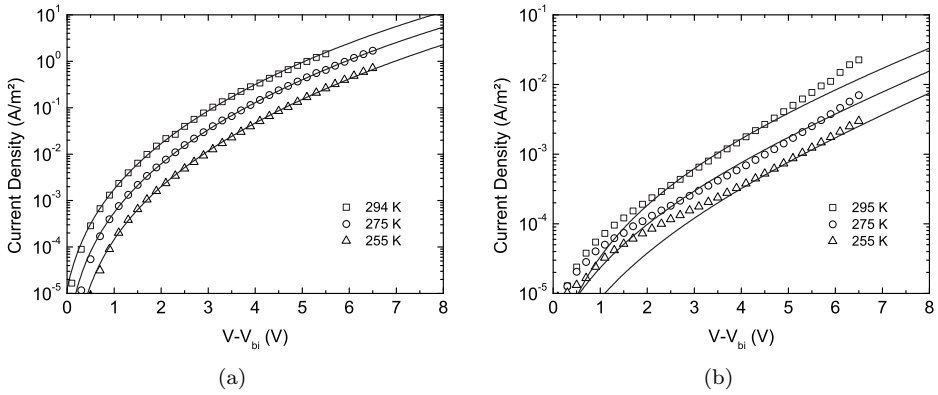

Figure 8.7. Temperature dependent electron transport of the polymers (a) BG and (b) BGR, measured in a 135 nm electron-only device. The lines are fits of the device model, including a Gaussian electron trap to represent the green and red dye. The built-in voltage used was $V_{\mathrm{bi}} = 0.5$ V.

demonstrates that the dyes behave as electron traps for the electron transport through the blue backbone. Since the HOMO levels of the dyes and the blue backbone are well aligned, the energy offset between the LUMO levels from the blue backbone LUMO can be directly estimated from the emission spectrum (Figure 8.2(b)). From this, we estimate the trap depths at approximately 0.35 eV and 0.75 eV for the green and red dye, respectively. Furthermore, the density of the dyes may be roughly estimated from the feed ratio of the monomers during syntheses of the polymers. On the assumption of a density of $1\,\mathrm{g\,cm^{-3}}$ the densities of the green and red dye amounts to $1 \times 10^{24}\,\mathrm{m^{-3}}$ and $2 \times 10^{23}\,\mathrm{m^{-3}}$, respectively.

Since the dye concentration is considerably below the percolation limit, the electron current is carried solely through the blue host polymer LUMO. It is therefore reasonable to assume the same mobility parameters as determined for the blue backbone polymer. To describe the temperature-dependent electron transport in the BG and BGR polymers (Figure 8.7) we incorporate Gaussianly distributed electron traps representing the green and red dye. Again, the width of the trap distributions is assumed to be equal to the width of the LUMO DOS at $\sigma_{\mathrm{t}} = 0.09$ eV. The only free parameters remaining are then the trap density N_{t} and the trap depth E_{t}. The temperature-dependent electron transport in the BG polymer (Figure 8.7(a)) can be accurately described using the parameter set $E_{\mathrm{t}} = 0.42$ eV and $N_{\mathrm{t}} = 3 \times 10^{23}\,\mathrm{m^{-3}}$. Whereas the fitted trap depth agrees very well with the estimated trap depth, the obtained trap density is lower than one might expect from the feed ratios. The reason for this discrepancy is yet unknown. One explanation would be that not all monomers involved in the synthesis are electrically active in the polymer. Finally, keeping all parameters fixed and including an additional trap distribution representing the red dye, the temperature-dependent electron current in the BGR polymer can be described (Figure 8.7(b)). For this case the quality of the fit that could be achieved is slightly less. We do not know the reason for this

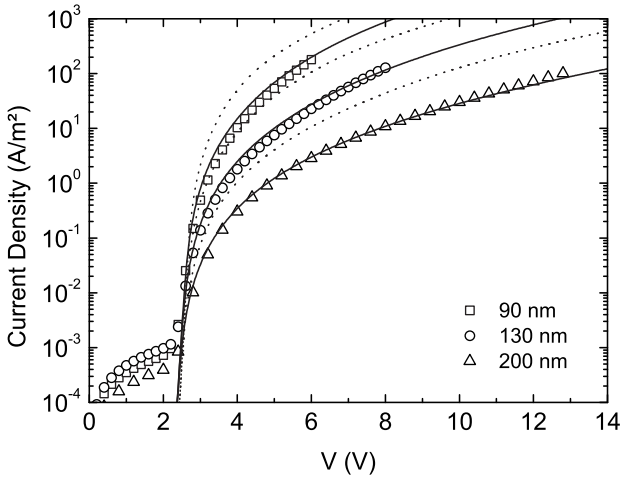

Figure 8.8. Device current of BGR PLED with three different thicknesses. The dotted lines are the prediction of the device model. The solid lines represent the fits with an enhancement of the trap-assisted recombination rate.

discrepancy. However, it should be noted that the electron currents as measured in the BGR electron-only devices are rather low, which makes it more sensitive for the influence of leakage currents or noise. The trap parameters found for the red dye are a trap depth of $E_\mathrm{t} = 0.73$ eV with a density of $N_\mathrm{t} = 3 \times 10^{23}\,\mathrm{m}^{-3}$. In this case both the trap depth and density are in good agreement to the expected values.

8.4 Device Modeling

At this point, all the ingredients for a complete device simulation of the white-emitting PLED have been determined. As mentioned above, the hole transport of the BGR polymer is equal to the hole transport of the blue backbone polymer. We can therefore adopt the hole transport parameters as obtained in Chapter 4. The electron transport can be described as the electron transport in the blue backbone material, with the inclusion of two additional electron trap distributions representing the green and red dye. The recombination rate of the blue light is then given by the Langevin equation, while the emission from the green and the red dye is calculated by the SRH relation. It should be noted that the trap-assisted recombination for the electron traps that are already present in the blue backbone polymer is taken as nonradiative, similar to PPV-based PLEDs.[18] For the SRH recombination only the capture coefficient C_n and C_p remain as a free parameter. It has however recently been establish that the capture coefficients are related to the mobility of the free carrier.[33] This essentially fixes the strength of the SRH recombination mechanism. As a result, there are no unknown parameters remaining that are necessary for the description of the double carrier device.

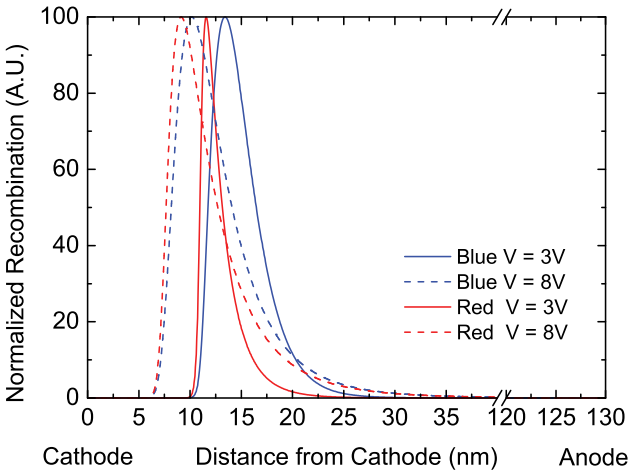

Figure 8.9. Distribution of the blue and red recombination in a 130 nm thick white-emitting PLED, for a voltage of $V = 3$ V and $V = 8$ V.

Figure 8.8 shows the room temperature J–V characteristics of BGR PLEDs with three different thicknesses of the active layer. With the capture coefficient described by the hole mobility, the device model overestimates the PLED data by approximately a factor 4 (dotted line). The reason for this discrepancy is yet unknown. One possibility is that the electron transport parameters as obtained from the blue electron-only devices overestimate the mobility of the free electrons. In the case of trap-limited transport the current is determined by both the trap parameters and the intrinsic trap-free mobility. As a result there is a limited interchangeability between the trap parameters and the electron mobility. Another explanation may be that the strength of the trap-assisted recombination is underestimated. As previously mentioned, in the device model the capture coefficient C_{n} is determined by the hole mobility. The strength of the trap-assisted recombination depends therefore strongly on the mobility of holes. However, in the blue backbone the hole transport is governed by the presence of tetraaryldiamino biphenyl (TAD) hole transport units, which complicates the description of the hole transport. In the polymer investigated here, the TAD concentration is 10% and the hole current is described as trap-free transport through the TAD, as was found in Chapter 4. However, it may be that the hole transport is in an intermediate regime, where the hole current is both carried through the host material and the TAD. In that case the hole current would be more appropriately described with a higher hole mobility in combination with shallow hole traps. Such a difference is difficult to discriminate experimentally, since the shape of a J–V curve of a trap-limited current with shallow traps is identical to that of a trap-free current.[34] If the hole transport of the blue polymer would be described as trap limited, a higher intrinsic trap-free hole mobility would have been found, which would increase the strength of the SRH mechanism. At this point we address this issue by enhancing the strength of the trap-assisted recombination by a factor of 10. With this enhancement, an

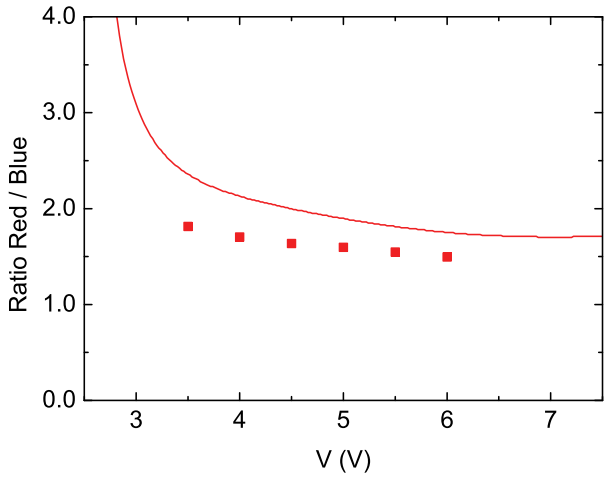

Figure 8.10. The ratio of red emission relative to the blue emission of a 90 nm PLED as obtained from the spectrum in Figure 3. The line is the calculated ratio of SRH recombination to Langevin recombination.

excellent fit is obtained for the device current of the BGR PLED.

Having established a numerical description of the white-emitting PLED, we can use our device model to evaluate the spatial distribution of internal quantities such as the electron and hole density. Of direct relevance for the photon outcoupling efficiency is the position of the recombination zone. The spatial resolved recombination rate is calculated by the Langevin relation (Equation 8.1) for the blue emission, while the red emission is attributed to SRH recombination on the red dye (Equation 8.2). Figure 8.9 shows the distribution of the recombination rate of blue and red in a 130 nm thick RGB PLED at a bias of $V = 3$ V and $V = 8$ V. It was found in Chapter 5 that the blue backbone PLED changed from hole dominated to electron dominated with increasing bias, leading to a shift of the recombination zone. In contrast, due to the electron trapping dyes, the white-emitting BGR PLED is hole dominated over the entire voltage range and the recombination zone is located at the cathode. A recombination zone close to the cathode is disadvantageous for the device efficiency, since a part of the formed exitons will be lost due to quenching by the metallic cathode.[35,36] As a result the performance of the materials system studied is strongly hindered by the unbalanced charge transport. For an optimized device, the recombination should lie in the middle of the emissive layer. It is therefore important to engineer the backbone and the dyes in such a way that, not only the output spectrum is observed as white, but also that the charge transport remains well balanced. This may be achieved by tuning the energy levels of the dyes and backbone polymer. For example, shifting the energy levels of the present host polymer down will reduce the electron trapping and will induce/enhance hole trapping.

As a final step, the proportion of red emission relative to the blue emission is examined. We extract the ratio red/blue from the EL spectra shown in Figure

8.3, defined as the intensity of the red emission at 575 nm divided by the intensity of the blue peak. The total blue and red emission is calculated as the integral of Langevin recombination (blue) and SRH recombination (red). Over the voltage range measured, the ratio red/blue decreases from ~ 1.8 to ~ 1.5. The numerically calculated ratio exhibits a similar decrease over that voltage range. Only an approximate fit is achieved, however it should be noted that there are several factors which inhibit a complete quantitative description of the output spectrum. Firstly, it cannot be assumed that the blue backbone and the dyes have an equal luminescence efficiency. As a result, the calculated recombination rate cannot be directly translated into the emission intensity. Secondly, the contribution of energy transfer from the blue backbone to the red dye is not taken into account in the model. However, assuming that the energy transfer is independent of the applied bias, the voltage dependence of the red/blue ratio is not influenced by energy transfer. Finally, for a similar copolymer it was found that the field dependence of exciton quenching also introduces a small voltage dependence of the spectrum. [2] Considering the many effects contributing to the emission spectrum of a PLED, the result as shown in Figure 8.10 can be considered as reasonably satisfactory. As can be observed in the EL spectra in Figure 8.3, the emission from the green dye (relative to the blue emission) exhibits a considerably weaker voltage dependence than the red emission. While the clearly different voltage dependencies of the red and blue emission point to different recombination mechanisms, the same cannot be claimed for the green emission. It would therefore be questionable to attribute the green emission solely to SRH recombination on the green dye. As a result, we cannot apply the same analysis to the green emission peak.

8.5 Conclusions

In this chapter a complete electrical device description of a single-layer white-emitting PLED is presented. All parameters involved in the description of the charge transport and recombination in the PLED, i.e., the mobility parameters and the trap parameters of the dyes, have been determined independently from single-carrier devices. Keeping all the determined parameters fixed, and without introducing any additional parameters, the device current of the PLED is overestimated by a factor of ~ 4. However, by enhancing the trap-assisted recombination the electrical characteristics can be consistently modeled and the recombination rates on the dyes and on the blue backbone can be calculated. The observed color shift of the white PLED can qualitatively be reproduced by the ratio of red to blue emission. The color shift of single-layer white-emitting PLEDs can therefore be explained by the different voltage dependence of trap-assisted recombination.

References

1. J. Liu, L. Chen, S. Y. Shao, Z. Y. Xie, Y. X. Cheng, Y. H. Geng, L. X. Wang, X. B. Jing, and F. S. Wang, *Adv. Mater.* **19**, 4224 (2007).
2. M. de Kok, W. Sarfert, and R. Paetzold, *Thin Solid Films* **518**, 5265 (2010).
3. M. Berggren, O. Inganäs, G. Gustafsson, J. Rasmusson, M. R. Andersson, T. Hjertberg, and O. Wennerström, *Nature* **372**, 444 (1994).
4. M. Granstrom and O. Inganäs, *Appl. Phys. Lett.* **68**, 147 (1996).
5. S. Tasch, E. J. W. List, O. Ekström, W. Graupner, G. Leising, P. Schlichting, U. Rohr, Y. Geerts, U. Scherf, and K. Müllen, *Appl. Phys. Lett.* **71**, 2883 (1997).
6. Y. W. Ko, C. H. Chung, J. H. Lee, Y. H. Kim, C. Y. Sohn, B. C. Kim, C. S. Hwang, Y. H. Song, J. Lim, Y. J. Ahn, G. W. Kang, N. Lee, and C. Lee, *Thin Solid Films* **426**, 246 (2003).
7. M. Suzuki, T. Hatakeyama, S. Tokito, and F. Sato, *IEEE J. Sel. Top. Quantum Electron.* **10**, 115 (2004).
8. B. Hu and F. E. Karasz, *J. Appl. Phys.* **93**, 1995 (2003).
9. J. Huang, G. Li, E. Wu, Q. Xu, and Y. Yang, *Adv. Mater.* **18**, 114 (2006).
10. Y. S. Wu, S. W. Hwang, H. H. Chen, M. T. Lee, W. J. Shen, and C. H. Chen, *Thin Solid Films* **488**, 265 (2005).
11. M. C. Gather, R. Alle, H. Becker, and K. Meerholz, *Adv. Mater.* **19**, 4460 (2007).
12. M. P. Langevin, *Ann. Chim. Phys.* **28**, 433 (1903).
13. U. Albrecht and H. Bässler, *Phys. Status Solidi B* **191**, 455 (1995).
14. P. W. M. Blom, M. J. M. de Jong, and S. Breedijk, *Appl. Phys. Lett.* **71**, 930 (1997).
15. P. W. M. Blom, M. J. M. de Jong, and J. J. M. Vleggaar, *Appl. Phys. Lett.* **68**, 3308 (1996).
16. M. M. Mandoc, B. de Boer, G. Paasch, and P. W. M. Blom, *Phys. Rev. B* **75**, 193202 (2007).
17. H. T. Nicolai, M. M. Mandoc, and P. W. M. Blom, *Phys. Rev. B* **83**, 195204 (2011).
18. M. Kuik, H. T. Nicolai, M. Lenes, G. J. A. H. Wetzelaer, M. Lu, and P. W. M. Blom, *Appl. Phys. Lett.* **98**, 093301 (2011).
19. W. Shockley and W. T. Read, *Phys. Rev.* **87**, 835 (1952).

20. R. N. Hall, *Phys. Rev.* **87**, 387 (1952).

21. C. T. Sah, R. N. Noyce, and W. Shockley, *Proc. IRE* **45**, 1228 (1957).

22. G. A. H. Wetzelaer, M. Kuik, H. T. Nicolai, and P. W. M. Blom, *Phys. Rev. B* **83**, 165204 (2011).

23. L. J. A. Koster, E. C. P. Smits, V. D. Mihailetchi, and P. W. M. Blom, *Phys. Rev. B* **72**, 085205 (2005).

24. D. Buchhauser, M. Scheffel, W. Rogler, C. Tschamber, K. Heuser, A. Hunze, G. Gieres, D. Henseler, W. Jakowetz, K. Diekmann, A. Winnacker, H. Becker, A. Büssing, A. Falcou, L. Rau, S. Vögele, and S. Göttling, *Proc. SPIE-Int. Soc. Opt. Eng.* **5519**, 70 (2004).

25. A. Falcou, A. Büsing, S. Heun, J. Steiger, A. Gerhard, N. Schulte, and H. Becker, WO Patent 2005/030827 (2005).

26. M. Anni, S. Lattante, M. M. De Kok, R. Cingolani, and G. Gigli, *Appl. Phys. Lett.* **89**, 221903 (2006).

27. H. Suzuki and S. Hoshino, *J. Appl. Phys.* **79**, 8816 (1996).

28. W. Wu, M. Inbasekaran, M. Hudack, D. Welsh, W. Yu, Y. Cheng, C. Wang, S. Kram, M. Tacey, M. Bernius, R. Fletcher, K. Kiszka, S. Munger, and J. O'Brien, *Microelectron. J.* **35**, 343 (2004).

29. S. E. Shaheen, B. Kippelen, N. Peyghambarian, J. F. Wang, J. D. Anderson, E. A. Mash, P. A. Lee, N. R. Armstrong, and Y. Kawabe, *J. Appl. Phys.* **85**, 7939 (1999).

30. P. A. Lane, L. C. Palilis, D. F. O'Brien, C. Giebeler, A. J. Cadby, D. G. Lidzey, A. J. Campbell, W. Blau, and D. D. C. Bradley, *Phys. Rev. B* **63**, 235206 (2001).

31. X. Gong, M. R. Robinson, J. C. Ostrowski, D. Moses, G. C. Bazan, and A. J. Heeger, *Adv. Mater.* **14**, 581 (2002).

32. M. A. Parshin, J. Ollevier, M. Van der Auweraer, M. M. de Kok, H. T. Nicolai, A. J. Hof, and P. W. M. Blom, *J. Appl. Phys.* **103**, 113711 (2008).

33. M. Kuik, L. J. A. Koster, G. A. H. Wetzelaer, and P. W. M. Blom, *Phys. Rev. Lett.* **107**, 256805 (2011).

34. W. Hwang and K. C. Kao, *Solid-State Electron.* **19**, 1045 (1976).

35. H. Becker, S. E. Burns, and R. H. Friend, *Phys. Rev. B* **56**, 1893 (1997).

36. D. E. Markov and P. W. M. Blom, *Appl. Phys. Lett.* **87**, 233511 (2005).

Summary

The invention of electrical lighting is something that we take for granted. At the same time, it is difficult to overestimate the influence of the availability of electrical lighting on civilization. The most ubiquitous form of electrical lighting today is still the incandescent light bulb, invented at the end of the 19th century. Considering that approximately 95% of the energy consumed by a light bulb is converted into heat rather than light, it is apparent that there is the potential for a considerable energy saving by switching to more energy efficient lighting solutions.

A promising emerging lighting technology is the organic light-emitting diode (OLED). An OLED consists of a thin layer of an organic semiconductor sandwiched between two electrodes. Upon the application of a voltage, electrons can be injected from the cathode into the semiconductor. The electrons leave the semiconducting layer at the counter electrode (anode) leaving behind a positive charge which is called a 'hole' in the terminology of semiconductor physics. The electrons and holes move towards each other through the semiconducting layer until they meet and recombine. The energy that is released by recombination is emitted as light, while the color of the light is determined by the band gap of the semiconductor.

Although OLEDs are nowadays already used for the pixels of displays in, for instance, mobile phones, they are not yet widely available as lighting products. One factor hampering the breakthrough of OLEDs for lighting is the fabrication cost. A special class of OLEDs is the polymer light-emitting diode (PLED) in which the active layer consists of polymer semiconductors. The advantage of PLEDs is the fact that they offer the potential of cheap fabrication using solution processing. Lighting requires the simultaneous emission of two or three colors so that the output is perceived as white.

Small molecule based OLEDs are generally fabricated using thermal evaporation which enables the fabrication of multilayer devices. White-emitting OLEDs consist therefore usually of separate layers for red, green and blue emission. However, multilayer devices are difficult to process from solution because an orthogonal solvent system is required to prevent that deposited layers are redissolved by the consecutive layer. A promising approach is the use of a copolymer in which red- and green- emitting dyes are incorporated in a blue-emitting copolymer. The benefit of such a polymer is that white light emission can be obtained using only one emissive layer. In this thesis, the device operation of such a single-layer white-emitting PLED is investigated.

The final objective of this work is to develop a description of the device operation of a white-emitting PLED based on a copolymer in which green and red dyes

are incorporated in a blue backbone. For this purpose a set of polymers is investigated with an incremental number of dyes which allows for the stepwise unraveling of the device operation of white PLEDs. Due to energy transfer to, and a preferred recombination on the dyes, only a very small concentration of dyes is required to obtain white light emission. Consequentially, the material consists almost completely of the blue backbone polymer. The charge transport in the blue material is therefore vital for the understanding of the operation of the white-emitting PLED.

Blue emitting materials have by definition a wide band gap and it is therefore often observed that the injection of holes is limited by an injection barrier. In Chapter 3 and 4, two approaches are described to counter this issue. First, the use of an alternative hole injection material, molybdenum trioxide (MoO_3) is investigated. It is shown in Chapter 3 that using MoO_3 as hole injecting material Ohmic hole injection can be achieved in poly(9,9-dioctylfluorene) (PFO), something that is not possible using the common hole injection material poly(3,4-ethylenedioxythiophene)/poly(styrenesulphonic acid) (PEDOT:PSS). For the case of PFO, MoO_3 was used as the top contact of hole-only devices. For double carrier PLED devices, the hole injecting contact is usually deposited as the bottom contact. To use MoO_3 in a PLED, it would therefore be necessary to use an inverted structure with the cathode as bottom contact, or use the MoO_3 as bottom contact. However, both approaches are difficult to realize due to the fact that both on MoO_3 and on low work function materials the film forming properties are poor.

Another approach to promote hole injection and transport in wide band gap materials is the incorporation of arylamine units. Arylamines are known to be good hole conductors and they are often used to tune the hole transport. In Chapter 4 the hole transport in the blue backbone material with incorporated N,N,N',N'-tetraaryldiamino biphenyl (TAD) units is investigated. It is observed that for small TAD concentrations the TAD units act as traps for the hole transport in the blue polymer. For TAD concentrations larger than 5% guest-to-guest transport is observed and the hole transport is carried by the TAD units. It is demonstrated that in this regime the hole mobility can be described by a density dependent mobility, in which the density of hopping sites is proportional to the TAD concentration and comparable to the molecular density.

Having established a description of the hole transport in the blue backbone polymer, we turn our attention to the device operation of a blue PLED in Chapter 5. From single-carrier devices it is found that the electron transport is trap-limited, but that the intrinsic electron mobility is higher than the hole mobility. To obtain a measure for the electron mobility transient electroluminescence (TEL) measurements are performed. From this it is found that the electron mobility in the blue-emitting polymer is at least one order of magnitude larger than the hole mobility. Combining the results of single-carrier measurements in a numerical device model, the operation of a blue-emitting PLED can be investigated. It is revealed that the combination of a large electron mobility with electron traps results in a shift of the recombination zone from the cathode to the anode with increasing bias.

As mentioned above, the electron transport in the blue backbone is limited by traps. This behavior is actually observed for most semiconducting polymers and generally explained by trap-limited conduction in the presence of an exponential

trap distribution. In Chapter 6 it is demonstrated that the electron transport of several PPV derivatives can also be well described with a trap distribution that is Gaussianly distributed within the band gap. Considering that the density of states (DOS) of the lowest unoccupied molecular orbital (LUMO) is generally assumed to be Gaussian shaped, a Gaussian trap DOS may be more obvious than an exponential trap DOS. In Chapter 7 the developed Gaussian trap model is applied to the electron transport in a wider range of semiconducting polymers. The LUMO levels of these polymers cover a range of more than 1 eV. It is found that in this class of materials the electron transport can be described using a common Gaussian trap distribution, centered at an energy of 3.6 eV below the vacuum level and with a nearly identical concentration of $3 \times 10^{23}\,\mathrm{traps/m^3}$. This result indicates that the traps have a common origin and allows us to predict the trap-limited electron current in any conjugated polymer.

Finally, in Chapter 8 the white-emitting PLED is treated. Building on the results described in previous chapters, a description for the device operation of the white-emitting PLED is developed. The red and green dyes that are incorporated in the blue backbone polymer have by definition a smaller band gap than the blue material. Consequentially, they are expected to introduce traps for the transport in the backbone material. Indeed, it is observed from single-carrier devices that the red and green dyes acts as a deep electron traps. The hole transport is unaffected by the dyes and the hole transport can thus be described as determined in Chapter 4. The electron transport is given by the electron transport as determined in Chapter 5, with the addition of 2 trap distributions representing the red and green dyes. By incorporating trap-assisted recombination for the red and green dyes and bimolecular Langevin recombination for the blue backbone the current and light-output of the white PLED can be consistently described. The color shift of single-layer white-emitting PLEDs can be explained by the different voltage dependence of trap-assisted and bimolecular recombination.

Samenvatting

De beschikbaarheid van elektrische verlichting is een luxe die we tegenwoordig als vanzelfsprekend beschouwen. Tegelijkertijd is het moeilijk om de invloed van elektrische verlichting op de beschaving te overschatten. De meest alomtegenwoordige vorm van elektrische verlichting is vandaag de dag nog steeds de gloeilamp, die al aan het einde van de 19e eeuw werd uitgevonden. De efficiëntie van de gloeilamp is erg laag; ongeveer 95% van de opgenomen energie wordt omgezet in warmte in plaats van in licht. Er is dus de mogelijkheid tot een aanzienlijke energiebesparing door over te stappen op efficiëntere verlichtings technieken.

Een veelbelovende verlichtingstechnologie is de organische licht-emitterende diode (OLED). Een OLED bestaat uit een dunne laag van een organische halfgeleider die tussen twee elektrodes zit. Wanneer een spanning over de elektrodes wordt aangelegd, kunnen vanuit de kathode elektronen de laag binnen komen. De elektronen verlaten de laag bij de tegenoverliggende elektrode (anode). De achterblijvende positieve ladingen worden in het jargon van de halfgeleider fysica aangeduid als 'gaten'. De elektronen en gaten bewegen in tegengestelde richting door de halfgeleider tot ze elkaar tegenkomen en met elkaar recombineren. Hier komt energie bij vrij in de vorm van licht, waarbij de kleur van het licht bepaald wordt door de energiekloof van de halfgeleider (het verschil in energie tussen gaten en elektronen).

Hoewel OLED's tegenwoordig al gebruikt worden, bijvoorbeeld als pixels in de displays van mobiele telefoons, worden ze nog niet op grote schaal gebruikt voor verlichting. Een van de obstakels die een doorbraak van OLED's voor verlichting in de weg staat is dat de fabricage van OLED's nog erg duur is. Een speciaal type OLED is de polymere licht-emitterende diode (PLED). In PLED's bestaat de actieve laag uit een polymere (*plastic*) halfgeleider. Het voordeel van PLED's boven OLED's is dat ze mogelijkheid bieden om goedkoop geproduceerd te worden vanuit oplosmiddelen, zoals door middel van printen of spincoaten. Voor verlichting is uiteraard wit licht nodig, wat betekend dat licht gegenereerd moet worden in twee of drie kleuren, zodat het gezamenlijke spectrum als wit gezien wordt.

OLED's zijn gebaseerd op kleine moleculen waarvan de actieve laag die door middel van opdampen aangebracht wordt. Hiermee is het relatief eenvoudig om diodes te fabriceren met meerdere actieve lagen. Witte OLED's bestaan daarom doorgaans uit afzonderlijke lagen voor de emissie van rood, groen en blauw licht. Zoals vermeld, worden PLED's doorgaans gefabriceerd vanuit oplosmiddelen. Hiermee is het moeilijk om diodes te maken met meerdere lagen, aangezien de achtereenvolgende laag de vorige laag zou kunnen oplossen. Een veelbelovende manier om witte PLED's te maken is het gebruik van een copolymeer, waarin rood en groen

emitterende kleurstoffen in een blauw emitterend copolymeer ingebouwd zijn. Het voordeel van een dergelijk copolymeer is dat wit licht gegenereerd kan worden met een enkele actieve laag. In dit proefschrift wordt de werking van een witte PLED op basis van een dergelijk wit copolymeer onderzocht.

Het uiteindelijke doel van dit onderzoek is om een beschrijving te ontwikkelen van de werking van een witte PLED, op basis van een enkel copolymeer met groene en rode kleurstoffen ingebouwd in een blauwe keten. Hiervoor is een set van drie polymeren onderzocht, waarin een toenemend aantal kleurstoffen is ingebouwd: een blauw emitterend polymeer, een polymeer met een groene kleurstof ingebouwd in de blauwe keten, en een wit emitterend polymeer waarin zowel een rode als een groene kleurstof in de blauwe keten zijn ingebouwd. Deze set polymeren stelt ons in staat om stapsgewijs de werking van de witte PLED te onderzoeken. Door energie overdracht van de blauwe keten op de rode en groene kleurstoffen, en een dominante recombinatie op de kleurstoffen is er in de praktijk maar een hele kleine concentratie van de kleurstoffen nodig om wit licht te genereren. Als gevolg hiervan bestaat het wit-emitterende copolymeer bijna geheel uit het blauwe materiaal. Het ladingstransport in dit blauwe materiaal is hierdoor erg belangrijk voor het beschrijven van de witte PLED.

Blauw emitterende materialen hebben daardoor per definitie een grote energiekloof, wat het lastig maakt om goede injectie te bereiken van zowel gaten als elektronen. In de Hoofdstukken 3 en 4 worden twee benaderingen onderzocht om het gaten transport in dit soort materialen te verbeteren. Allereerst wordt het gebruik van een nieuw type injectie materiaal onderzocht: molybdeen trioxide (MoO_3). In Hoofdstuk 3 wordt laten zien dat met MoO_3 een Ohms contact gevormd kan worden op poly(9,9-dioctylfluorene) (PFO). Dit is niet mogelijk met het veel gebruikte gaten injectie materiaal poly(3,4-ethylenedioxythiophene)/poly(styrenesulphonic acid) (PEDOT:PSS). In Hoofdstuk 3 is MoO_3 gebruikt als gaten injecterend topcontact. Voor PLED's wordt het gaten injecterend contact doorgaans als bodemcontact gebruikt. Om MoO_3 in een PLED te gebruiken, zou het daarom in een geïnverteerde structuur gebruikt moeten worden, of met MoO_3 als bodem contact. Beide methodes zijn moeilijk te bewerkstelligen, vanwege het feit dat het lastig is om nette lagen te spincoaten op MoO_3 of op typische kathode materialen.

Een andere benadering om de gaten injectie en het gaten transport te verbeteren is het inbouwen van arylamine eenheden in de blauwe keten. Arylamines zijn goede gaten geleiders en worden veel gebruikt om het gaten transport in blauwe polymeren te beïnvloeden. In Hoofdstuk 4 wordt het gaten transport in een blauw polymeer met ingebouwde N,N,N',N'-tetraaryldiamino biphenyl (TAD) eenheden onderzocht. Het blijkt dat met kleine concentratie de TAD eenheden als ladingvallen ('*traps*') werken voor het gaten transport in het blauwe polymeer. Voor TAD concentraties groter dan 5% blijkt dat de gaten stroom door de TAD eenheden loopt. In dit regime kan de gatenmobiliteit beschreven worden met een dichtheidsafhankelijke mobiliteit waarbij het aantal transportlocaties evenredig is aan de TAD concentratie en van dezelfde orde van grootte als moleculaire dichtheid. Dit toont aan dat het aantal transportlocaties in het gebruikte mathematische mobiliteits model een fysieke betekenis heeft.

Nu het gaten transport in het blauwe polymeer beschreven is, richten we in

Hoofdstuk 5 onze aandacht op de werking van de blauwe PLED. Uit metingen van het elektronen transport blijkt dat het elektronen transport beperkt is door elektronen traps, maar dat de intrinsieke mobiliteit van de elektronen groter is dan de gaten mobiliteit. Om een maat voor de elektronen mobiliteit te verkrijgen zijn metingen van de schakeltijd uitgevoerd. De schakeltijd van een PLED is het gevolg van het feit dat de ladingsdragers eerst de polymeerlaag over moeten steken, voordat recombinatie plaats kan vinden. De schakeltijd van een PLED bied daardoor informatie over de mobiliteit van de ladingsdragers. Uit deze metingen blijkt dat de elektronen mobiliteit in het blauwe polymeer minstens een orde van grootte hoger is dan de gaten mobiliteit. Door middel van een numeriek model is ten slotte de werking van de blauw-emitterende PLED onderzocht. Hieruit blijkt dat de combinatie van een hoge intrinsieke elektronen mobiliteit en de aanwezigheid van elektronen traps resulteert in een verschuiving van de recombinatie zone van de kathode naar de anode, met toenemende spanning.

Zoals hierboven vermeld, wordt het elektronentransport in het blauw emitterend polymeer beperkt door traps. Dit gedrag is waargenomen in de meeste halfgeleidende polymeren. Dit wordt meestal beschreven met een verdeling van traps in de energiekloof, waarvan over het algemeen wordt aangenomen dat de vorm van de verdeling exponentieel is. In Hoofdstuk 6 wordt aangetoond dat het elektronen transport van drie verschillende PPV afgeleiden ook goed beschreven kan worden met een Gaussische verdeling. Aangezien de energie banden in organische halfgeleiders doorgaans ook beschreven wordt met een Gauss, ligt het voor de hand dat de distributie van traps ook Gaussisch verdeeld is. In Hoofdstuk 7 wordt het Gaussische trap model toegepast op het elektronen transport in een bredere selectie van halfgeleidende polymeren. De energie niveau's van deze polymeren overspannen een bereik van meer dan 1 eV. Het blijkt dat in deze materialen het elektronen transport beschreven kan worden met een gemeenschappelijke Gaussische verdeling van elektronen traps, op een energie van ongeveer 3.6 eV onder het vacuüm niveau en met een density van $3 \times 10^{23}\,\mathrm{traps/m^3}$. Dit resultaat toont aan dat de elektronen traps een gemeenschappelijke oorsprong hebben, en stelt ons bovendien in staat om het elektronen transport in elk halfgeleidend polymeer te voorspellen.

In Hoofdstuk 8 wordt ten slotte de witte PLED behandeld. Voortbordurend op de resultaten van de voorgaande hoofdstukken wordt een beschrijving ontwikkeld van de werking van de witte PLED. Aangezien de energiekloof van een halfgeleidend materiaal de kleur van het licht bepaald, hebben de rode en groene kleurstoffen per definitie een kleinere energiekloof. Hierdoor kan verwacht worden dat ze als traps voor het elektronen of gaten transport door de blauwe keten werken. Inderdaad blijkt uit metingen van het elektronentransport van de drie polymeren dat de rode en groene kleurstoffen werken als diepe elektronen traps. Het gatentransport blijft echter onveranderd, waardoor het gaten transport in de witte PLED beschreven kan worden als het gaten transport in de blauwe PLED, zoals eerder bepaald in Hoofdstuk 4. Het elektronen transport kan beschreven worden als het elektronen transport zoals bepaald in Hoofdstuk 5, met de toevoeging van 2 elektronen trap verdelingen die de rode en groene kleurstoffen vertegenwoordigen. De recombinatie op de blauwe keten wordt dan beschreven als de recombinatie van vrije ladingen op de blauwe keten, terwijl de recombinatie op de rode en groene kleurstoffen beschre-

ven wordt als trap-gedreven recombinatie op de kleurstoffen. Met de combinatie van deze beide recombinatie mechanismen kan de stroom en de lichtopbrengst van de witte PLED goed beschreven worden. Bovendien kan de kleur verschuiving die in witte PLED's waargenomen wordt kwalitatief gereproduceerd worden.

List of Publications

1. *Charge transport in white light-emitting polymers*,
H. T. Nicolai, A. J. Hof, and P .W. M. Blom, *Proc. SPIE-Int. Soc. Opt. Eng.* **6192**, 61922H (2006).

2. *Hole transport in blue and white emitting polymers*,
M. A. Parshin, J. Ollevier, M. Van der Auweraer, M. M. de Kok, H. T. Nicolai, A. J. Hof, and P .W. M. Blom, *J. Appl. Phys.* **103**, 113711 (2008).

3. *Space-charge-limited hole current in poly(9,9-dioctylfluorene) diodes*,
H. T. Nicolai, G. A. H. Wetzelaer, M. Kuik, A. J. Kronemeijer, B. de Boer, and P. W. M. Blom, *Appl. Phys. Lett.* **96**, 172107 (2010).

4. *Hysteresis-free electron currents in poly(p-phenylene vinylene) derivatives*,
N. I. Craciun, Y. Zhang, A. Palmaerts, H. T. Nicolai, M. Kuik, R. J. .P. Kist, G. A. H. Wetzelaer, J. Wildeman, J. Vandenbergh, J. Lutsen, D. Vanderzande, and P. W. M. Blom, *J. Appl. Phys.* **107**, 124504 (2010).

5. *Determination of the trap-assisted recombination strength in polymer light emitting diodes*,
M. Kuik, H. T. Nicolai, M. Lenes, G. J. A. H. Wetzelaer, M. Lu, and P. W. M. Blom, *Appl. Phys. Lett.* **98**, 093301 (2011).

6. *Photoluminescence of conjugated polymer blends at the nanoscale*,
D. Jarzab, M. Lu, H. T. Nicolai, P. W. M. Blom, and M. A. Loi, *Soft Matter* **7**, 1702 (2011).

7. *Trap-assisted and Langevin-type recombination in organic light-emitting diodes*,
G. A. H. Wetzelaer, M. Kuik, H. T. Nicolai, and P. W. M. Blom, *Phys. Rev. B* **83**, 165204 (2011).

8. *Charge Transport and Recombination in Polyspirobifluorene Blue Light-Emitting Diodes*,
H. T. Nicolai, A. J. Hof, J. L. M. Oosthoek, and P. W. M. Blom, *Adv. Funct. Mater.* **21**, 1505 (2011).

9. *Electron traps in semiconducting polymers: Exponential versus Gaussian trap distribution*,
H. T. Nicolai, M. M. Mandoc, and P. W. M. Blom, *Phys. Rev. B* **83**, 195204 (2011).

10. *Polymer light-emitting diodes with doped hole-transport layers*,
M. Lu, H. T. Nicolai, M. Kuik, G. A. H. Wetzelaer, J. Wildeman, A. Palmaerts, and P. W. M. Blom, *Phys. Status Solidi A* **208**, 2482 (2011).

11. *N-type doping of poly(p-phenylene vinylene) with air-stable dopants*,
M. Lu, H. T. Nicolai, G. J. A. H. Wetzelaer, and P. W. M. Blom, *Appl. Phys. Lett.* **99**, 173302 (2011).

12. *Quantitative analysis of the guest-concentration dependence of the mobility in a disordered fluorene-arylamine host-guest system in the guest-to-guest regime*,
H. T. Nicolai, A. J. Hof, M. Lu, P. W. M. Blom, R. J. de Vries, and R. Coehoorn, *Appl. Phys. Lett.* **99**, 203303 (2011).

13. *The Effect of Ketone Defects on the Charge Transport and Charge Recombination in Polyfluorenes*,
M. Kuik, G. A. H. Wetzelaer, J. G. Laddé, H. T. Nicolai, J. Wildeman, J. Sweelssen, and P. W. M. Blom, *Adv. Funct. Mater.* **21**, 4502 (2011).

14. *Effect of n-type doping on the hole transport in poly(p-phenylene vinylene)*,
M. Lu, H. T. Nicolai, G. J. A. H. Wetzelaer, and P. W. M. Blom, *J. Polym. Sci. Part B: Polym. Phys.* **49**, 1745 (2011).

15. *Device physics of white polymer light-emitting diodes*,
H. T. Nicolai, A. J. Hof, and P. W. M. Blom, *Adv. Funct. Mater.* accepted for publication (2012).

16. *Unification of trap-limited electron transport in semiconducting polymers*,
H. T. Nicolai, M. Kuik, G. A. H. Wetzelaer, B. de Boer, P. W. M. Blom, C. Campbell, C. Risko, and J. L. Brédas, Submitted for publication.

Acknowledgements

The completion of this thesis is of course a joyful moment. However, at the same time, it is for me also a bit of a sad moment, as it also marks the end of my time in the MEPOS group, which I have enjoyed thoroughly.

I want to thank Paul Blom for his guidance and support during my PhD, and for giving the MEPOS group the outstanding reputation that it has. It was a privilege to be part of the *Blom-group*. As I had no prior experience in the MEPOS group, I did not know what to expect with regards to your way of working. I have come to really appreciate your pragmatic approach to research, which was always driven by your insight of the bigger picture, without getting lost in the small details. I also appreciate your honesty, and the fact that you did not hide any doubts that you had. It is very reassuring for a PhD student to know that there are also things that your professor doesn't understand. It was always very enlightening to discuss my results with you. At moments when I couldn't see the wood for the trees anymore, you always were able to make sense out of a big collection of data and see the bigger picture. Even years after you officially left the group, you still manage to maintain the high level of the group. I have great respect for the effort and energy that you still invest in the MEPOS group.

I also want to thank my former colleague André Hof. Not many PhD students have the luxury of starting a PhD project along an experience postdoc. I have learned a lot from you. You taught me how to properly perform research and to always remain critical. Thanks for the fun we had on the many trips we made!

For a beginning PhD student it is difficult to judge how good the facilities in the group are. Only after a few yours one can truly appreciate the excellent condition of the equipment in the lab and the cleanroom. Minte Mulder, Jan Harkema and Frans van de Horst, thank you for building and maintaining such an excellent lab and cleanroom. Jan Harkema, thank you for your active role in the group after the departure of Paul. Your ability to fix virtually anything is indispensable and you are the thriving social heart of the group. Renate, thank you for your help with all the administrative matters. I really appreciate that you were always thinking along and doing more than strictly required. I would also like to thank Jan Anton Koster, for being available for advice during the past year, but more importantly for the contribution that you made to the group during your PhD. The device model that you developed several years ago has become increasingly important for the research performed in the MEPOS group. Without SIMsalabim, the research described in this thesis would not have been possible. Dago, thank you for always being prepared to give advice on anything remotely related to science.

My years in the MEPOS group have been a very happy time for me, and I look back with great pleasure on my time in the group. For this, I want thank all my current and former colleagues of the MEPOS group. Please forgive me that I do not list all your names here, but since I have spent quite some years in the group, it would really be to many to name you all. I truly believe that the MEPOS group is extraordinary in the sense that we are a very social group where people take a genuine interest in each other, and are always willing to cooperate. On the many activities that we had as a group (BBQs, conferences, the ICOE at the Kempervennen, ...), there was never a dull moment. During my PhD I also had the pleasure of guiding several master students. Jasper, Hans, Milo and Gert-Jan, thank you for your valuable contributions.

I would like to thank the reading committee, Reinder Coehoorn, Dago de Leeuw and Dieter Neher. Thank you serving in my reading committee and for taking the time to read the manuscript. I would also like to thank my colleagues in the OLLA project, especially the little subgroup of *WP3 and friends*. I always enjoyed the open discussions that we had at the OLLA meetings. The fun that I had outside the official sessions with my colleagues from Siemens, Philips and VTT always made the OLLA meetings feel like a small holiday. The past years I had the pleasure of working in another European research project. Reinder Coehoorn, thank you for the pleasant collaboration that we had during the AEVIOM project, and for your help with our publication and for the input that you gave me for my thesis. Rein de Vries, thank you for helping me with my measurements at Philips, and for introducing me in your parameter extraction method.

The MEPOS group is also the place where I met a few of people who I'm happy to call friends in the first place, and colleagues in the second place. Lenes, Hylke, Auke, Kuik, Johan, René en Arne. I would not know where to start to describe the fun that we had in Groningen, or other places (Bratislava, San Francisco, Hasselt, ...). I trust we will continue to see each other in the future. *Wat hebben we toch een gezellige groep!* Kriszty and Martijn, thank you for being my paranymphs. It was great having you two as my roomies. We had a lot of fun in the office, and you have greatly contributed to the fact that I (almost) always were happy to go to the university in the morning.

Bert, my time in the MEPOS group will for always be associated with my memory of you. You were a driving force in the group and your enthusiasm in research worked contagious on the rest of the group. Since your tragic passing away, the group has not been the same anymore. I always enjoyed how you had an opinion about everything, and were not remotely reluctant to share it. The way in which you managed to combine hard work with a joyful attitude and *gezelligheid* is an inspiration for me.

Pap, Mam, Bas en Annemiek, bedankt voor jullie voortdurende steun, jullie niet aflatende interesse en bovendien jullie geduld. Bente en Jurre, bedankt voor het bieden van de perfecte afleiding van mijn onderzoek. Als papers afgewezen werden, of als mijn data niet te fitten was, herinnerden jullie mij er altijd weer aan wat echt belangrijk is.

Herman Nicolai